BOOK OF ABSTRACTS

The 3rd International Conference on Nanomaterials: Fundamentals and Applications

October 09-11, 2017, Štrbské Pleso, High Tatras, Hotel Patria, Slovak republic

Organized by:

Department of Physical Chemistry
Faculty of Natural Sciences
Pavol Jozef Safarik University in Kosice
&
Slovak Chemical Society
Bratislava

ISBN: 978-80-8152-530-8

Edited by: **Andrea Straková Fedorková**, Pavol Jozef Šafárik University in Košice, Institute of Chemistry, Moyzesova 11, 040 01 Košice, Slovakia, andrea.fedorkova@upjs.sk

Ondrej Petruš, Pavol Jozef Šafárik University in Košice, Institute of Chemistry, Moyzesova 11, 040 01 Košice, Slovakia, ondrej.petrus@student.upjs.sk

Reviewed by: **Renáta Oriňáková**, Pavol Jozef Šafárik University in Košice, Institute of Chemistry, Moyzesova 11, 040 01 Košice, Slovakia, renata.orinakova@upjs.sk

Andrej Oriňák, Pavol Jozef Šafárik University in Košice, Institute of Chemistry, Moyzesova 11, 040 01 Košice, Slovakia, andrej.orinak@upjs.sk

 ISBN: 978-80-8152-530-8

LIST OF CONTENTS

ISBN: 978-80-8152-530-8

Preface

The decision to hold the 3rd symposium ´NFA - Nanomaterials: Fundamentals and Application´in October 2017 was made because the previous two (2015 and 2012) had proved that there was a real need for giving scientists and engineers a combined forum to discuss the nanomaterials preparation and analysis of materials and associated problems from their various points of view. Another reason was that there have been many advances in chemical and physical analytical technology, vital to the discovery, production and characterization of materials. A discussion forum could be of great importance to this region of Slovakia.

As with the past two symposia in the series the Slovak Chemical Society again agreed that the symposium could be held under its aegis. This organization has always supported the principle of free communication among bona fide scientists, but for the time in many years, nearly every country in the world allowed their scientists to travel to Slovakia.

The enthusiastic discussions, the constructive arguments and suggestions and the establishment of friendship ties between delegates from all corners of the globe, were proof indeed of the success of the meetings and the symposium generally.

This volume of the keynote speakers´ papers will serve to remind the delegates of a sound and much enjoyed symposium. It should also bring to those who could not attend, an indication of how important the chemical analysis and characterization of nanomaterials has become in virtually all spheres of life, especially those related to the production and improvement of materials. The papers provide an excellent overview of the fields of importance in the ever changing, ever emerging analytical techniques and the areas of application. Now we know how to do research “on top tip” and use interfacial reaction in nanostructure matter. Scientist prepared novel graphene electroactive nanofluids as liquid electrodes applied in flow cells. Very interesting to me creation patterned surfaces (superhydrophobic – superhydrophillic) that can be used as adhesive patterns for cells….. Anyway, book of abstracts contains next very interesting presentation: formation of nanointerface with layer by layer assemblies, how to use nonocomposite film as an antimicrobial surface, how to prepare flexible solar cells; and self-assembly of emitting bone –shaped colloidal nanocrystals. But I was much more fascinated that exist chiral plasmonic helicene nanoassemblies.

The organizers are most grateful, not only to SCHS for its unfailing support over the years, but also to those people, authorities, and organizations that made it possible to hold this symposium.

I wish all participants pleasant stay in High Tatra and Slovakia, enjoy this meeting to collect new information form nanoscience!

The symposium was opened and the technical and scientific discussions followed.

Andrej Oriňak

 ISBN: 978-80-8152-530-8

Research on top of the tip: Interfaces and reactions in nanostructured matter

Guido Schmitz*, Rüya Duran, Sebastian Eich and Patrick Stender

Institute of Materials Science, University of Stuttgart, Germany

**guido.schmitz@imw.uni-stuttgart.de*

Nanostructured materials naturally comprise interfaces in high density, which motivates to investigate their chemical structure in detail. For the microscopic chemical analysis of interfaces, state-of-the-art atom probe tomography is performed. This technique delivers chemical maps of single-atom-sensitivity and outstanding spatial resolution. Due to its direct 3D information, it is especially suited to the investigation of complex morphologies distinguished by curved and rough interfaces. By recent extension with laser-assisted evaporation modes, also the investigation of semiconductors, ceramics, and even polymers became possible.

First, the talk introduces the experimental technique of atom probe tomography including its extension by laser-assisted evaporation modes. The physical principle, example measurements, and their quantitative interpretation will be discussed. In the second part, recent physical studies focussed on nanoscale mechanisms that control stability, transport and reaction at interfaces in metal and semiconductor thin film structures will be presented. What is the natural thickness of interphase boundaries, how does nucleation at reactive interfaces take place, what are the dominating paths of atomic transport in nanocrystalline matter?

Based on local chemical analysis with single atom sensitivity, it can be shown that (i) the thickness of interphase boundaries is clearly temperature dependent, that (ii) segregation and transport rate along triple lines in the grain boundary structure exceeds that of other short circuit paths, that (iii) the nucleation of intermetallic compounds or silicides is controlled by the concentration gradient at the initial reactive interface.

 ISBN: 978-80-8152-530-8

What could be better than graphene for energy storage?

P. Gomez-Romero

Institut Catala de Nanociencia I Nanotecnologia, ICN2 (CSIC-BIST) Campus UAB. 08193 Bellaterra(Barcelona) Spain

** pedro.gomez@icn2.cat*

Graphene will be the advanced material of choice for many applications in years to come. Its unique combination of mechanical, electrical, optical and chemical properties add to its chemical simplicity to spur potential applications in a wide variety of fields from flexible electronics to biomedicine to energy.

In the field of energy, and in particular for energy storage, graphene is no exception and it has already been claimed as a champion material for supercapacitors providing large active area for capacitive double-layer storage. What then could be better than graphene for energy storage?

Hybrid materials offer the opportunity of building synergies thus leading to improved performance over their individual components.[1] In that way, hybrids based on graphene and a variety of molecular species[2.3] or extended phases[4] have been used to design materials with enhanced activity. A wise choice of electroactive species can for instance improve the energy density of graphene-based supercapacitors through hybridization. Furthermore, in our group we have gone beyond the conventional solid state electrode format and have developed graphene electroactive nanofluids as liquid electrodes for flow cells. This novel electrode format is also prone to the development of hybrid materials. In this conference this general hybrid approach, with some emphasis on our own group results will be presented in relation to graphene-based materials for energy storage and illustrative examples discussed.

References

[1] D.P. Dubal, O. Ayyad, V. Ruiz, P. Gomez-Romero* Chemical Society Reviews, 44 (2015) 1777.
[2] J. Suárez-Guevara, V. Ruiz and P. Gomez-Romero*, Phys. Chem. Chem. Phys., 2014, 16 (38), 20411-20414.
[3] DP Dubal, J Suarez-Guevara, D Tonti, E Enciso, P Gomez-Romero. Journal of Materials Chemistry A: Materials for Energy and Sustainability 2015, 3(46), 23483-23492
[4] Deepak P. Dubal*, Rudolf Holze, Pedro Gomez-Romero*. Scientific Reports 2014, 4 : 7349
[5] Electroactive Graphene Nanofluids for Fast Energy Storage. Deepak P. Dubal and Pedro Gomez-Romero. 2D-Materials 2016, 3, 031004

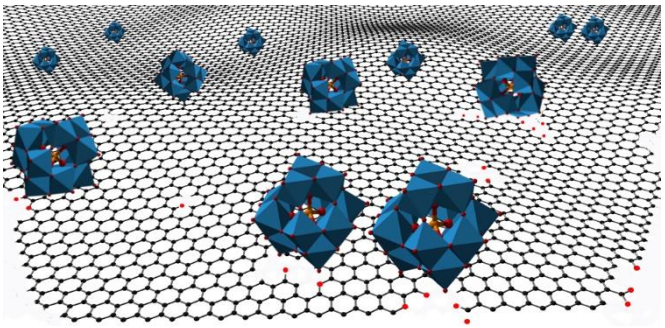

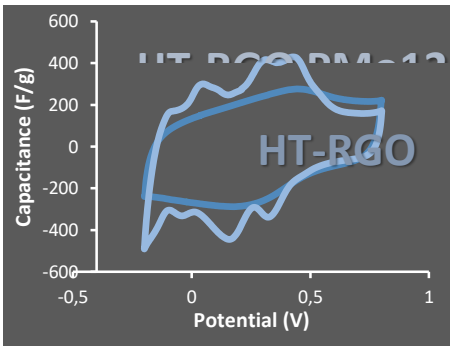

Figure 1. Reduced graphene oxide modified with polyoxometalates (left) lead to hybrid (faradaic + capacitive) energy storage as shown on the Cyclic Voltammogram on the right

 ISBN: 978-80-8152-530-8

Designing Biofunctional Interfaces with Special Wettabilities

Pavel A. Levkin*

Institute of Toxicology and Genetics, Institute of Organic Chemistry,
Karlsruhe Institute of Technology (KIT), Karlsruhe, Germany

levkin@kit.edu; www.levkingroup.com

Patterns of different surface properties are ubiquitous in nature and serve various important purposes. Desert beetles exploit superhydrophilic spots on their superhydrophobic back to collect water from the morning mist in the desert. Hydrophilic spots on a superhydrophobic surface of lichen plants allow them to uptake water, but also prevent the formation of water layers on the surface that could interfere with the discharge of lichen spores into the air. Superhydrophobic and omniphobic surfaces possess various unique properties including self-cleaning, liquid repellent and cell repellent properties. A special type of an omniphobic surface, slippery lubricant-infused porous surface (SLIPS), shows robust antibiofouling, anti-icing, self-healing and cell repellent properties. On the other hand, superhydrophilic and oleophilic surfaces usually show strong adhesive properties towards liquids, cells and particles.

We are interested in creating precise two-dimensional micropatterns of apparently incompatible and opposite properties such as superhydrophobicity and superhydrophilicity or slippery and adhesive properties. To create such patterns we develop novel surface coatings with special wettabilities and novel photochemical surface functionalization strategies. Combining seemingly opposite properties in micropatterns leads to completely new advanced functionalities non-existent on the original homogeneous interfaces. Thus, we showed that superhydrophobic-superhydrophilic patterned surfaces could be used to create patterns of cells, arrays of microdroplets suitable for ultra high-throughput cell screenings, formation of arrays of hydrogel micropads or free-standing hydrogel particles with defined shapes for 3D cell culture. Defect-free hydrophilic-hydrophobic patterns can form arrays of microdroplets of low-surface tension organic solvents, arrays of polymer microlenses or patterns of hydrophobic nanoparticles. Patterned SLIPS could be used to form cell microarrays and arrays of isolated biofilm colonies for biofilm screenings. We anticipate that micropatterns of superhydrophobic, omniphobic or other surface properties can lead to novel advanced functional interfaces and can find important applications in biotechnology, microfabrication, cell biology, sensing and diagnostics.

 ISBN: 978-80-8152-530-8

Current Trends in Nanostructured Materials

Antonios Kelarakis

University of Central Lancashire, School of Physical Sciences and Computing, Preston PR12HE, U.K

akelarakis@uclan.ac.uk

As the early excess of enthusiasm on the promise of nanotechnology gives its place to a mature understanding about its realistic potential, important applications of nanomaterials are becoming parts of our every day live. In this presentation we will describe concepts and engineering principles that are central for the development of functional nanostructured materials.

Well-dispersed polymer nanocomposites, are typically synthesized in the presence of favorable particle-matrix interactions that greatly depend upon the chemical nature of the nanoparticle surface. The polymer chains in the vicinity of the nanofiller interphase exhibit restricted mobility that is considered to be associated with a number of nanoscale effects such as mechanical reinforcement, enhanced barrier properties, ionic conductivity, fire retardancy, etc. In certain systems, nanoparticles are known to preferentially stabilize one crystaline phase at the expense of another. For example, incorporation of clay layers, CNT, graphene, etc tend to promote the evolution of the piezoelectric vita phase of poly(vinylidene fluoride) instead of the common, albeit inert, alpha phase (1). At the same time the dielectric permittivity of the hybrid systems is substantial higher over a wide temperature range, while they exhibit significant mechanical enhancements compared to the neat copolymer.

Layer by layer assemblies rely on the successive deposition of opposing charged nanoparticles where strong electrostatic and hydrophobic interactions allow the build-up of stable coatings that resist detachment even under harsh conditions. Systematic investigations focus on the incorporation of nanoparticles to ultrathin formulations to afford mechanical, scratch and crack resistance, protection against corrosion and photodegradation, antimicrobial and biocatalytic properties, stimuli responsive wetting behavior, improved color retention, self-cleaning, fire retardancy, antireflection and antifogging performance. For example, deposition of positively charged silica nanoparticles to negatively charged plasma treated polypropylene reduces the water contact angle from 71° to virtually zero (2) .

Mesoporous naonocomposite aerogels prepared by ice-templating possess high surface area coupled with additional functionalities such as catalytic activity, ionic or electronic conductivity and are ideal candidates for catalysis, energy and biomedical applications (3).

Referrences

1. Kelarakis, A.; Hayrapetyan, S.; Ansari, S.; Fang, J.; Estevez, L.; Giannelis, E.P. Polymer 2010,51,469
2. Fang, J. ; Kelarakis, A.; Estevez, L.; Wang, Y.; Rodriguez, R. ; Giannelis, E. P. Journal of Materials Chemistry,2010, 20,1651
3. Estevez, L.; Kelarakis, A.; Gong, Q.; Da'as, E.H.; Giannelis, E.P., Journal of the American Chemical Society, 2011, 133,6122

 ISBN: 978-80-8152-530-8

Conduction band engineering in semiconducting oxides: Fundamentals and applications

L. Kavan*

J. Heyrovský Institute of Physical Chemistry, v.v.i., Academy of Sciences of the Czech Republic, Dolejškova 3, CZ-18223 Prague 8, Czech Republic

**kavan@jh-inst.cas.cz*

Conduction band position: properties and applications

The electronic band structure of semiconducting oxides, like TiO_2 or SnO_2 is of fundamental implication for variety of applications in electrochemistry, photoelectrochemistry and photocatalysis [1]. The position of conduction band (CB) edge controls the reductive photocatalytic reactions (e.g. hydrogen evolution from water or CO_2 reduction) [1,2], Li-insertion electrochemistry [1], potential of dye-sensitized solar cell (DSC) [3] and recombination blocking in perovskite solar cells [4]. However, there is a considerable controversy about the position of CB in TiO_2 (anatase, rutile, including the crystals with distinguished facets) [1]. Long-time debate concerns the fact that the CB edge of rutile (in contrast to anatase) is not sufficiently upshifted compared to the energy equivalent to the H^+/H_2 reduction potential [5,6]. Though the photoelectrochemical electrolysis of water was discovered in 1967 (i.e. exactly 50 years ago) many basic questions still remain to be addressed.

Conduction band and flatband potential

A standard electrochemical tool for monitoring of the CB edge position is the flatband potential. It provides the information about CB position, though accurate measurement and correct interrelation of both quantities is a complex issue. Flatband potential is usually obtained from Mott-Schottky plots by electrochemical impedance spectroscopy. Other techniques are: onset of anodic photocurrent of water oxidation or dark H^+ reduction, cyclic voltammetric mapping of DOS including the electron trap states and spectroelectrochemical determination of optical absorbance of CB electrons. The staggered alignment in mixed phases, such as in anatase/rutile, is assumed to enhance photocatalytic activity of titania, but it is widely disputed whether the conduction band edge of rutile or that of anatase is higher. Photoelectron spectroscopy (PES) and most DFT simulations support the former, but the flatband potential measurements provide just opposite results. The controversy can be explained by taking into account the adsorption of OH^- and H^+ ions from the electrolyte solution on the electrode surface [5,6]. Furthermore, PES indicates that the CB edge of (001)-anatase is upshifted by 0.1 eV referenced to (101)-anatase in agreement with the DFT calculation [5,6] and with the electrochemical flatband potentials (upshift of CB by 60 meV) but there are again some conflicting works claiming the opposite (see Ref. [1] for discussion).

Photoelectrochemical reactions on nanocrystalline anatase

Nanocrystalline anatase terminated by various facets, such as {110}, {101} and {001} exhibits different activity for photoelectrochemical water splitting [2]. Although the anodic half-reaction of water splitting and oxygen evolution dominates the overall photo-electrochemical behavior of the photoexcited anatase, simultaneous reduction under photoelectrochemical conditions is also observed on some anatase faces. The activity of individual facets in anodic half-reaction of water splitting (oxygen evolution) increases in the order {101} < {110} < {001}. The increasing oxidation activity tracks the tendency of the surface to generate the $OH^{\cdot}$ radical producing intermediates (H_2O_2, ozone) on the trapped hole states. The activity in reduction processes increases in the reverse order. The reduction activity of the {101} oriented anatase can be attributed to pronounced hydrogen evolution by a charge transfer of photo-generated electrons. The observed trends agree with DFT based models which confirm the possibility of a rational design of the photocatalysts. Theoretically constructed volcano plot of the hydrogen evolution activity pinpoints the {101} face of anatase as the primary site for water reduction, and in-situ differential electrochemical mass spectroscopy confirms selective formation of H_2 at this face [2]. In turn, the water oxidation to O_2 and H_2O_2 is favored on the {110} and {001)} faces, as confirmed by the analysis using rotating ring/disc electrode (Pt-ring/photoexcited-TiO_2-disc) [2].

 ISBN: 978-80-8152-530-8

Electron-specific layers in perovskite photovoltaics

The electron collecting electrodes in perovskite solar cells, with both planar and mesoscopic architectures, require the development of nanometer-thin blocking layers. They selectively transport electrons from the photabsorber to the back contact, but at the same time prevent recombination of these electrons with hole conductor. The latter is either a molecular conductor like *spiro*-OMeTAD or the perovskite itself. The low-temperature ALD-grown TiO_2 and SnO_2 layers are of particular interest for electron selective contacts in these solar cells [4]. Amorphous SnO_2 films are pinhole-free for thicknesses down to 2 nm. Their excellent blocking behavior allows photoelectrode designs with even thinner electron selective layers; thus minimizing resistance losses. The compact nature and blocking function of thin SnO_2 films is not perturbed by annealing at 450 ^oC, which is a significant benefit compared to TiO_2 and other amorphous ALD oxides [4]. Amorphous and crystalline ALD SnO_2 films substantially differ in their flatband (and conduction band) positions. This needs to be taken into account when considering band alignment engineering in solar devices using these high-quality blocking layers. The low-temperature ALD-grown SnO_2 layers are specifically suited for solar cells using mixed-perovskite, such as $(CH_3NH_3PbBr_3)_{0.15}(NH_2CH{=}NH_2PbI_3)_{0.85}$ [4].

Metal-like titania thin films

Oxide materials, like TiO_2 and SnO_2 are traditionally regarded semiconductors. Doping of SnO_2 by fluorine provides the well-known quasi-metallic (degenerate semiconductor) material, but little is known about similar doping-induced metal-like behavior of TiO_2. We have recently succeeded in demonstration of this kind of material [7]. Metal-like electrochemical properties were found for certain Ta-doped, optically transparent thin films of TiO_2 (anatase) made by pulsed-laser deposiiton [7]. The quasi-metallic TiO_2 films surprisingly show significant UV-photocurrent of water oxidation, and rectifying function for redox couples with highly positive electrochemical potentials [4]. Highly conducting, optically transparent Ta-doped TiO_2 (anatase) thin films were deposited on ordinary soda-lime glass substrate. They exhibited quasi-reversible electrochemistry (cyclic voltammograms of $Fe(CN)_6^{3-/4-}$ and dimethylviologen redox couples), mimicking the electrochemical activity of F-doped SnO_2 (FTO). However, these films are idle for the $Ru(bpy)_3^{2+}$ oxidation, which is attributed to a space-charge barrier. Depending on the applied potential, the films show both the metal-like double-layer charging and the semiconductor-like chemical capacitance in pure supporting electrolyte solutions. The flatband potentials are ca. 0.2 V positive compared to values for undoped reference films and/or pristine anatase single-crystal electrode. Photoelectrochemical activity occurs upon irradiation with UV light at potentials positive to flatband, and scales inversely with the Ta-content. The Li-insertion ability analogously decreases with the increasing Ta-content which is attributed to the competition between Ta^{5+} and Li^+ ions in the anatase lattice. Consistent with the quasi-metallic nature of these films, the Li-extraction peak in cyclic voltammograms shows no cut at larger potentials.

Acknowledgement

This work was by the Czech National Science Foundation (contract No. 13-07724S).

References

[1] L. Kavan, *Chem.Rec.* **12,** 131 (2012).

[2] K. Minhova-Macounova, M. Klusackova, R. Nebel, M. Zukalova, M. Klementova, I.E.Castelli, M.D.Spo, J. Rossmeisl, L. Kavan, P. Krtil, *J.Phys.Chem.C* **121**, 6024-6032 (2017).

[3] L. Kavan, *Curr. Opinion Electrochem.* **2**, 88-96 (2017).

[4] L. Kavan, L. Steier, M. Grätzel, *J.Phys.Chem.C* **121**, 342-350 (2017).

[5] J. Kullgren, B. Aradi, T. Frauenheim, L. Kavan, P. Deak, *J.Phys.Chem.C* **119**, 21952-21958 (2015).

[6] P. Deak, J. Kullgren, B. Aradi, T. Frauenheim, L. Kavan, *Electrochim.Acta* **199**, 27-34 (2016).

[7] H. Krysova, P. Mazzolini, C.S. Casari, V. Russo, A. Li Bassi, L. Kavan, *Electrochim.Acta* **232**, 44-53 (2017).

 ISBN: 978-80-8152-530-8

The Role of X- and Q-band EPR Spectroscopy in the Characterization of Titania Nanocrystalline Systems

V. Brezová*, Z. Barbieriková, D. Dvoranová, M. Mazúr

Institute of Physical Chemistry and Chemical Physics, Faculty of Chemical and Food Technology, Slovak University of Technology in Bratislava, Radlinského 9, SK-812 37 Bratislava, Slovak Republic

**vlasta.brezova@stuba.sk*

The investigation of photoinduced reactions on the semiconductor surfaces, *i.e.* photoelectrochemical, photocatalytic reactions, demonstrated extraordinary progress over the last decades [1]. Upon the irradiation of a semiconductor crystal by ultra-band-gap radiation, *i.e.* with the energy sufficient to excite the semiconductor valence electrons, the positive charge centers (holes) in the valence band and the negative charge centers (electrons) in the conduction band are generated, both with the facility to enter the consecutive redox reactions with compounds present in the system [2]. The important criteria for the choice of a suitable semiconductor represent the energy band gap (E_{bg}), which corresponds to the semiconductor excitation wavelength, and its stability upon irradiation [3]. Among the previously-studied prospective photocatalysts, titanium dioxide meets the criteria for wider industrial applications. Stability, low cost, relatively low toxicity and high photocatalytic activity predispose TiO_2 allotropes to the applications in various areas (gas sensors, photocatalysts, solar cells, etc.) [3]. However TiO_2 reveal several limitations as a photocatalyst; the recombination of photogenerated holes and electrons in a nanosecond scale inhibits the desired consecutive reactions of the charge carriers. In addition, the anatase $E_{bg} \sim 3.2$ eV corresponds to UVA light which rules out the visible light photoexcitation [3]. The attempts to overcome these limits are concentrated mainly on the preparation of new types of TiO_2 nanostructures, including titania modified with metal or non-metal elements. The UV- and visible-light activity of metal-modified TiO_2 material is significantly dependent on the synthetic route and reflects the character, concentration and distribution of the dopant, its energy levels within TiO_2 lattice, as well as the absorption properties of the photocatalysts [4]. The metal ions embedded in the TiO_2 lattice generate new energy levels resulting in the visible-light activity and improved trapping of electrons inhibiting the electron-hole recombination. On the other side incorporation of metal ions in TiO_2 leads to the formation of defects and vacancies acting as detrimental recombination centers [5]. As shown in the recent studies the modification of titania nanostructures using anionic doping is a promising method to shift the photoactivity to the visible region [6].

The photoinduced processes on a semiconductor surface are significantly influenced by its crystal structure, particle size, morphology and porosity. The information on the paramagnetic centers present in the structure of a nanocrystaline TiO_2 photocatalyst may bring remarkable insight into the issues of the origin of the photocatalytic activity in the specific structures and may offer an explanation for their increased or decreased activity.

Our contribution illustrates the power of EPR spectroscopy in the characterization of paramagnetic species existing in TiO_2 matrix before exposure, as well as those generated upon *in situ* photoexcitation of pristine or modified TiO_2 nanopowders. In order to obtain more detailed information on the paramagnetic centers found in the studied photocatalysts, EPR experiments in Q-band were also conducted, as the application of higher frequency (~ 34 GHz), provides enhancement of the sensitivity and resolution of the EPR signals compared to the standard EPR in X-band (~ 9.5 GHz). The applications of EPR spin trapping technique to detect radical intermediates upon *in situ* photoactivation of TiO_2 in water and in different organic solvents will be also discussed [7-10].

Acknowledgements

This study was financially supported by Scientific Grant Agency of the Slovak Republic (VEGA Project 1/0041/15).

References

[1] A. Fujishima, X. Zhang, D. Tryk, Surf. Sci. Rep. **63** (2008) 515-582.

[2] O. Carp, C. Huisman, A. Reller, Prog. Solid State Chem. **32** (2004) 33-177.

[3] U. Diebold, Surf. Sci. Rep. **48** (2003) 53-229.

[4] M. Pelaez, N. Nolan, S. Pillai, M. Seery, P. Falaras, A. Kontos, P. Dunlop, J. Hamilton, J. Byrne, K. O'Shea, M. Entezari, D. Dionysiou, Appl. Catal. B **125** (2012) 331-349.

[5] M. Fittipaldi, D. Gatteschi, P. Fornasiero, Catal. Today **206** (2013) 2-11.

[6] E.M.Samsudin, S.B. Abd Hamid, Appl. Surf. Sci. **391** (2017) 326-336.

 ISBN: 978-80-8152-530-8

[7] E. Pližingrová, M. Klementová, P. Bezdička, J. Boháček, Z. Barbieriková, D. Dvoranová, M. Mazúr, J. Krýsa, J. Šubrt, V. Brezová, Catal. Today **281** (2017) 165-180.

[8] Z. Barbieriková, D. Dvoranová, M.-V. Sofianou, C. Trapalis, V. Brezová, J. Catal. **331** (2015) 39-48.

[9] V. Brezová, Z. Barbieriková, M. Zukalová, D. Dvoranová, L. Kavan, Catal. Today **230** (2014) 112-118.

[10] D. Dvoranová, Z. Barbieriková, V. Brezová, Molecules **19** (2014) 17279-17304.

 ISBN: 978-80-8152-530-8

Nanomechanical Testing of Hard Materials

J.Dusza[a]*

[a] *Institute of Materials Research, Slovak Academy of Sciences, Watsonova 47, Košice, Slovak Republic*

**jdusza@imr.saske.sk*

The nano-mechanical characteristics and deformation and damage characteristics of differently oriented WC grains/crystals in WC – Co, Si3N4 grains/crystals in reaction bonded Si3N4 system and ZrB2 grains/crystals in ZrB2 polycrystal were investigated. Depth-sensing nano-indentation and scratch tests of grains and micro-compression tests of micropillars prepared by focused ion beam from oriented facets of grains were studied. Electron backscatter diffraction (EBSD), atomic force microscopy (AFM) and scanning electron microscopy (SEM) investigations were performed to determine the grain orientation and to study the surface morphology and the resulting deformation and damage mechanisms around the indents and in micropillars.

The hardness and scratch resistance of the differently orientated grains showed significant angle dependence from the basal towards the prismatic directions, Fig. 1 and 3. A strong influence of the grains orientation on compressive yield stress and rupture stress values was found during the micropillar test, too, Fig. 2. The active slip systems for individual ceramics have been recognized. The different properties of the basal and prismatic planes was found to be connected with the different deformation mechanisms – slip and dislocation activities.

The elastic and deformation characteristics were modeled using different methods.

References

1. T. Csanádi, M. Bľanda, N.Q. Chinh, P. Hvizdoš, J. Dusza, Orientation-dependent hardness and nanoindentation-induced deformation mechanisms of WC crystals, Acta Mater. 83 (2015) 397-407.
2. T. Csanádi, D. Németh, J. Dusza, Z. Lenčés, P. Šajgalík, Nanoindentation induced deformation anisotropy in β-Si3N4 ceramic crystals, J. Eur. Ceram. Soc. 36 (2016) 3059-3066
3. T. Csanádi, P. Szommer, N.Q. Chinh, S. Grasso, J. Dusza, M. Reece, Plasticity in ZrB2 micropillars induced by anomalous slip activation, J. Eur. Ceram. Soc. 36 (2016) 389-394.

Acknowledgements

This work was realized within the frame of the project „Infrastructure Improving of Centre of Excellence of Advanced Materials with Nano- and Submicron- Structure“, ITMS 26220120035, supported by the Operational Program “Research and Development” financed through European Regional Development Fund.

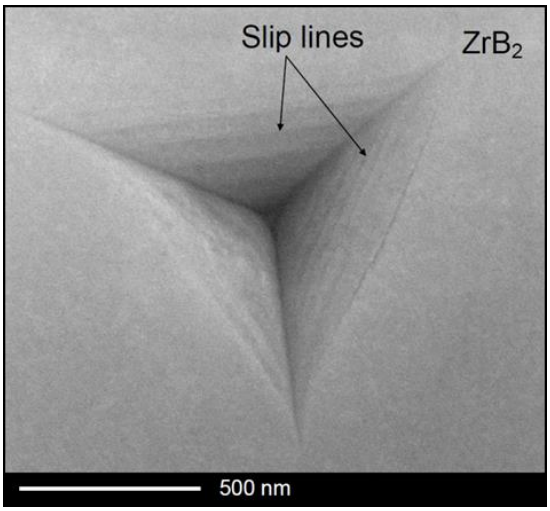

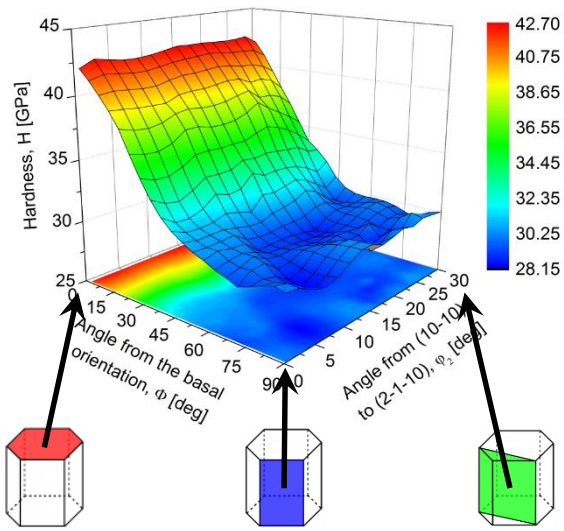

 ISBN: 978-80-8152-530-8

Fig. 1 Slip lines in ZrB_2 grains – a and hardness anisotropy in WC grains – b.

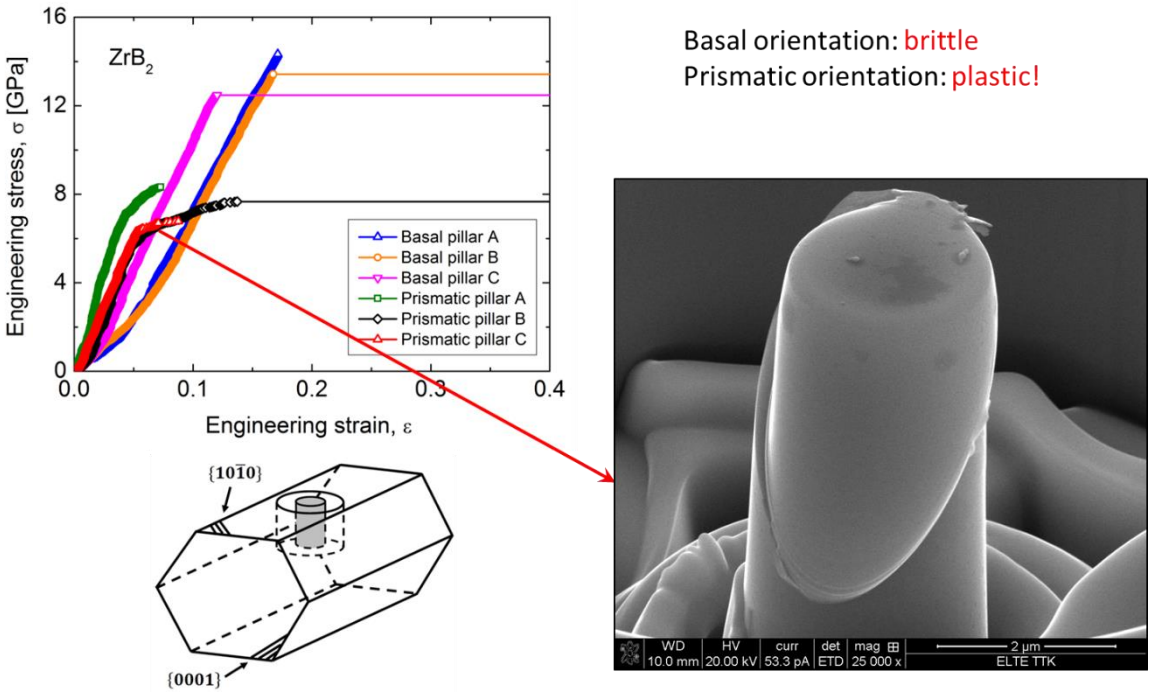

Fig. 2 Anisotropy during the micropillar testing of ZrB_2 grains.

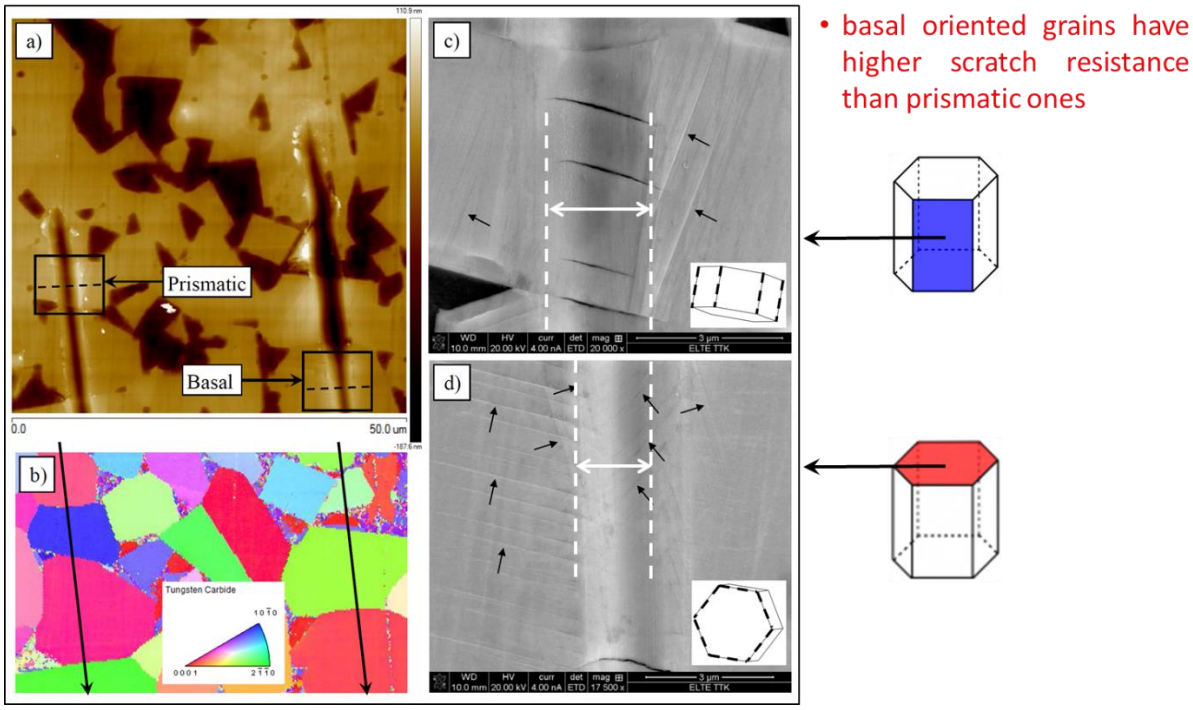

Fig. 3 Anisotropy during the micro/nano sratch testing of ZrB_2 ceramic system.

 ISBN: 978-80-8152-530-8

Relaxation Dynamics of a Multihierarchical Polymer Network Consisting of Dual Sierpinski Gasket and Regular Dendrimer

A.Jurjiu[a]*, T. Bitera, and F. Turcu[a]

[a] *Faculty of Physics, Babes-Bolyai University, Street Mihail Kogalniceanu 1, 400084 Cluj-Napoca, Romania*

**electronic address: aurel.jurjiu@phys.ubbcluj.ro*

One of the basic challenges in polymer physics is to unveil how the dynamical features of a polymeric material are related to its geometry. Originating from the seminal works of Rouse and Zimm, who focused on the investigation of dilute solutions of linear polymers, the issue of relating the structure of a polymer to its dynamics is becoming of increased importance due to the continuous advances in polymers synthesis. The fast development of modern technologies demands very versatile polymeric materials with continuously changing requirements of the industry. Using modern strategies, such as controlled radical polymerizations, supramolecular polymerizations or stepwise synthesis, new macromolecules or supramolecules with very complex architectures and tunable properties have been synthesized.

The present work extends the theoretical studies on relaxation dynamics of polymers with complex architectures by considering a new multihierarchical polymer network which is built through the replication of the dual Sierpinski gasket in the form of a regular dendrimer. The choice of dendrimer and of dual Sierpinski gasket as constituents of the new multihierarchical polymer network is based on the fact that both are already synthesized experimentally. So that, for a possible future chemical synthesis of the multihierarchical structure the ingredients exist. Another reason is that we wish to link a structure with loops with a loopless structure in order to see if the loops of one component may affect the whole dynamical behavior of the multihierarchical structure, especially when the hydrodynamics interactions are taken into account.

The relaxation dynamics of the multihierarchical structure is investigated in the framework of generalized Gaussian structure model which represents the extensions of the Rouse and Zimm models, developed for linear polymer chains, to polymer systems with arbitrary topologies and which highlight both the connectivity of the molecules under investigation, as well as the influence of hydrodynamic interactions.

In the Rouse model, taking the advantage that the main relaxation patterns depend only on the eigenvalues, we have developed a method whereby the whole eigenvalue spectrum of the connectivity matrix of the multihierarchical structure can be determined iteratively. Based on the eigenvalues obtained in the interative manner we are able to investigate the dynamics of the multihierarchical structure at very large generations, impossible to attain through numerical diagonalizations.

In the Rouse type-approach, where the interactions are considered only between nearest neighbors monomers, the general picture that emerges is that the multihierarchical structure preserves the individual behaviors of its constituents. The intermediate time/frequency domain of the dynamical quantities divides into two regions, each region showing the typical behavior of a component of the multihierarchical structure.

Remarkably, the multihierarchical structure still holds the original individual relaxation behaviors of its components even with the hydrodynamic interactions taken into account. Although the dual Sierpinski gasket was replicated in shape of a dendrimer and in the Zimm type-approach one allows to each monomer to interact with any other, not only with nearest neighbors, the intermediate domain of the dynamical quantities still splits into two independent regions, each highlighting the individual dynamics of a constituent component of the multihierarchical structure. The loops in the multihierarchical structure affects the dynamics in a similar way like they do on the original dual Sierpinski gasket. Their presence leads to lost of scaling of the dual Sierpinski gasket component in the Zimm model, but they do not affect in such a way to interfere with the dendrimer component and to result a mixture-like behavior.

Our theoretical findings with respect to the splitting of the intermediate domain of the relaxation quantities are well supported by experiments performed on associative polymer networks, micelles networks, physical polymer gels, and supramolecular dendritic polymer networks. The present work is part of a very recent publication [1].

 ISBN: 978-80-8152-530-8

Acknowledgements

The authors gratefully acknowledge the financial support of UEFISCDI through Project No. PN-II-RU-TE-2014-4-1957, contract code 234/01.10/2015.

References

[1] A. Jurjiu, T. Biter, F. Turcu, Polymers, 9, (2017) 245.

 ISBN: 978-80-8152-530-8

Quantum-chemical Research of Endohedral Yttrium Metallo-fullerenes

A.S. Kholtobina[a]*, D. Tsyplenkovaa, A. Fedorov[a,b]

[a]*Siberian Federal University,Svobodny 79, Krasnoyarsk, 660041, Russia*
[b]*Kirensky Institute of Physics, 50/38 Akademgorodok, Krasnoyarsk, 660036 Russia*

**akholtobina93@mail.ru*

Introduction

Endohedral metallofullerenes have attracted much attention due to their unique properties that originate from the interactions between the fullerene cage and the encapsulated metal atom [1]. Particularly, endohedral yttrium-fullerenes have been obtained by several research groups [2, 3]. In 1995, Takata and co-workers performed synchrotron X-ray studies on a powder of $Y@C_{82}$ to confirm the endohedral nature of EMFs for the first time [3]. However, it is still not clear whether the sample contained a pure $Y@C_{82}$ isomer or if it was a mixture of two or more regioisomers. The major $Y@C_{82}$ is confirmed to have C_{2v} symmetry and X-ray results of its carbene derivative firmly confirmed the cage connectivity and the metal location [4,5]. Potential applications of endodedral fullerenes were also predicted on the basis of their peculiar electronic, physical and chemical properties, including superconductors [5], metallo-fullerene lasers [5] ferroelectric materials [6, 7], nanomemory devices [5] quantum computers, etc [8].

Methods

The structural and electronic properties of endohedral yttrium-fullerenes were investigated using software package OpenMX (Open source package for Material eXplorer), designed for nano-scale material simulations based on density functional theories (DFT) norm-conserving pseudopotentials, and pseudo-atomic localized basis functions. Simulations of single complex of $Y@C_{82}$, structure, consisting of two complexes of $Y@C_{82}$, and crystal of $Y@C_{82}$ (face centered cubic cell with a=11.457_A) [9] were performed. Potential barriers of yttrium transitions were then calculated using NEB method. To search a minimum energy path (MEP) in geometrical phase space connecting two stable structures, a nudged elastic band (NEB) method based on is supported in OpenMX. The Monkhorst-Pack [10] k-point Brillouin sampling was used. The k-point grid contained 1 _ 1 _ 1 points along a, b and c directions, respectively.

Results and discussion

The first part of this investigation is to find the possible positions of yttrium atom inside the C_{82} fullerene cavity (C_{2v} isomer). So far as this isomer is sufficiently close to the spherical shape, it is not entirely clear that there can be several positions. From the data on the crystal structure of $Y@C_{82}$ (Fig. 1) [4], it can be seen that yttrium atom can occupy at least two positions in the C_{82} fullerene cavity, namely (top_hex) above the center of the hexagon and (bond_hex_penta) over the bond between the hexagon and the pentagon.

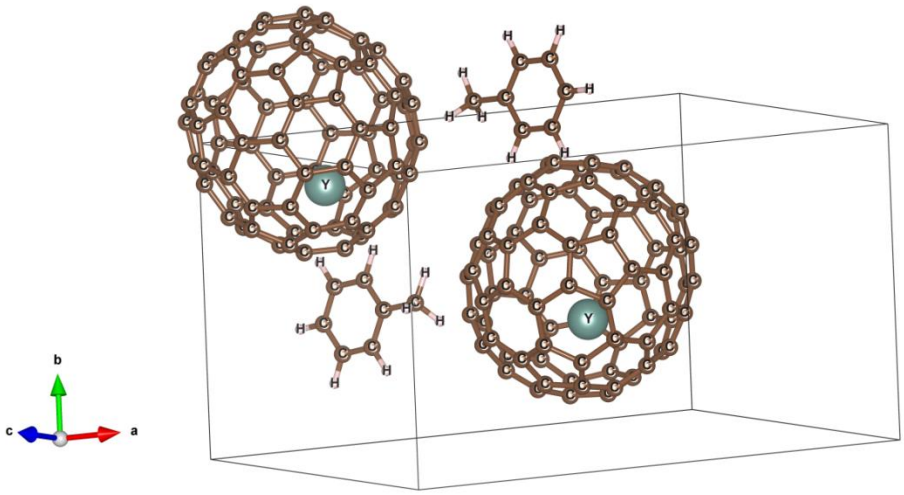

Figure 1 - Crystal structure of $Y@C_{82}$ (C_{2v} isomer). For convenience, there are shown two full fullerene molecules and two toluene molecules obtained by translation of the unit cell.

 ISBN: 978-80-8152-530-8

In addition, from our previous work on endohedral complexes Y@C_{82} [11] it is known that the yttrium atom positions inside the fullerene depend on the surroundings of such a molecule and may not coincide with the crystal structure, dimers and single molecules. Due to this fact, several other possible positions of yttrium atom in a single C_{82} molecule were modeled, besides those found in the crystal structure. Among them it can be noted the yttrium atom (bond_hex_hex) is located above the connection between two hexagons (Figure 2); the yttrium atom (top_c_hex_penta) is located above the carbon atom belonging to both the hexagon and the pentagon, this position is close to (bond_hex_penta); the yttrium atom (top_c_hex_penta) is located above the carbon atom belonging to two hexagons, this position is close to (bond_hex_hex). Table 1 shows the geometries and their energies in the initial stages of optimization and after optimization. From the binding energies calculated by the formula 1 it is clearly seen that there are two the most energetically favorable positions of yttrium atom, namely bond_hex_hex and top_hex, only the second of which was found in the crystal structure.

$$E_{bond}=E_{comlex} - E_{ful} - E_{Y}, \quad (1)$$

Table 1 - The binding energies for various positions of yttrium inside the C_{82} fullerene cavity (C_{2v} isomer)

Name of initial position Y	Name of final position Y	Binding energy, eV
bond_hex_penta	top_hex	-6.368
bond_hex_hex	bond_hex_hex	-5.796
top_c_hex_penta	bond_hex_hex	-5.170
top_c_hex_hex	bond_hex_hex	-5.524
top_hex	top_hex	-6.368
top_penta	top_hex	-6.361

Figure 2 gives detailed illustrations of the data for the arrangement of the yttrium atom inside the C_{82} fullerene molecule.

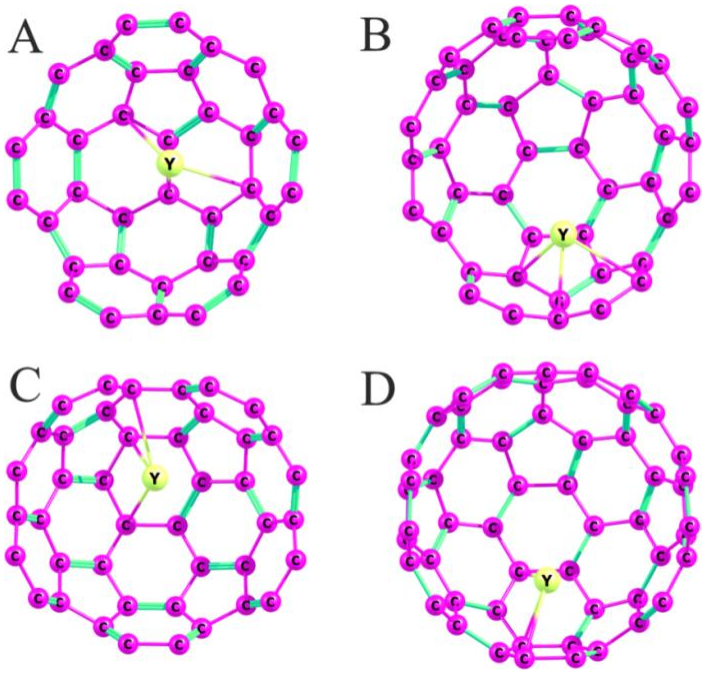

Figure 2 - Positions of the Y atom inside the C_{82} cavity (C_{2v} isomer) : A - bond_hex_hex top view, B - bond_hex_hex side view, C - top_hex top view, D - top_hex side view. For convenience, there are shown only the lower parts of fullerenes for A and C, only the rear walls of fullerenes for B and D, respectively.

References

[1] Yung S and Wang C- R 2014 Word Scientific p 433.
[2] Ross M M, Nelson H H, Callahan J H, McElvany S W 1992 J. Phys. Chem. 96 5231.

 ISBN: 978-80-8152-530-8

[3] McElvany S W 1992 J. Phys. Chem. 96 4935.
[4] Takata M, Umeda B, Nishibori E, Sakata M, Saitot Y, Ohno M, Shinohara H 1995 Nature 377 46-49.
[5] Bao L, Pan C, Slanina Z, Uhlik F, Akasaka T, and Lu X 2016 Angew. Chem. Int. Ed. 55 1-6.
[6] Bethune D S, Johnson R D, Salem J R, Devries M S, Yannoni C S 1993 Nature 366 123.
[7] Cioslowski J J 1992 Am. Chem. Soc. 113 4139.
[8] Popov A A, Yang S, Dunsch L 2013 Chemical reviews 113 5989-6113.
[9] Suematsu H, Murakami Y, Kawata H, Fujii Y, Hamaya N, Shimomura O, Kikuchi K, Achiba Y, Ikemoto I 1994 Mat. Res. Soc. Symp. Proc. 349 01994.
[10] Monkhorst H J and Pack J D 1976 Phys. Rev. B 13 5188.
[11] Kholtobina A S, Tsyplenkova D I, Kuzubov A A, Visotin M A, Fedorov A S 2017 Journal of Siberian Federal University. Mathematics & Physics 4 1–7.

 ISBN: 978-80-8152-530-8

Application perspectives of nanosize composites as the components of polymer compositions

Rahima S. Mammadova

Azerbaijan State Pedagogical University , Az.1000, U. Hajibeyli 68, Baku

(rehime_memmedova@yahoo.com)

Introduction

At present the following factors condition large scale use of polymer compositions in various fields of vital activity [1]:

- lack of natural materials as a result of dynamic increase of population;
- natural materials don't meet the required indices;
- possibility of controlling of the structures and properties of polymer compositions due to the requirements;
- necessity of compensation of human's increasing demands from quantity and quality points of view.

Analyses and synthesis

Various directions components are added to the content of polymer compositions to control their properties due to the requirements of treatment and exploitation condition. These components are classified according to the application direction: stabilizing compositions, antioxidants, plastisizors, blowing agents, fillers, cross-links-consolidators and vulcanizers, dyes, fire retardants, antistatic agents, anti-microbe agents, biological breakdown agents and etc[1,2].

The components being added to polymer parent mass and increasing durability to a number of influences of various exploitation conditions have been studied widely and are applied.

Polymer composition materials obtained from the expedient use of these components serve for compensating demands of the various fields of human activity in a large scale. But there are also some disadvantages of the application of these components. Incomplete homogenization of these components in polymer parent mass, their extraction out of the composition content, and harmful influences on the environment, reduce of the composition durability to the influences as a result, extraction and etc. are shown as an example.

The abovementioned can cause sharp weakening of polymer compositions indices, sometimes increase of risks for human activity. For example, in 2016 polymer compositions materials used as coating for some buildings caused self-ingnition because of sharp decrease of durability to sun beams, heat, *increase* of risks for humans and loss of life. It is true, such *tragedic* events can take place very seldom. But possibility of risks in this field isn't excluded, there is probability of material loss, harmful influences for human health and etc. It should be noted that influences of a number of factors must be considered. For example, use of the items not according to their direct application and negative influence which can take place are not excluded.

Currently, development of Nanochemistry and Nanothechology, synthesis of nanocomposites the use of which is expedient as polymer composition component, have opened wide perspectives in front the researchers of the corresponding field for successful study of the above mentioned. Possibilities to increase the durability of exploitation condition of polymers to various harmful influences have been created because of the less addition of high activity nanocomposites to the content. Analyses of the researches carried out in this direction testify obtaining of polymer compositions with high exploitation indices.

Conclusion and Discussion

While controlling content and properties of new polymer compositions, the component having expedient use of nanosize compositions as corresponding application can bring to the increase of exploitation indices of polymer – based nanomaterials and providing of human activity safety. The researches carried out in this direction can be evaluated from ecological and economic points of view. Researches carried out in the secondary treatment of LDPE based items which are once in the direction of modification with nanosize biologically active compounds has scientific – practical significance[3] .

 ISBN: 978-80-8152-530-8

References

[1] R.S.Məmmədova. “Polietilenin müxtəlif iqlim şəraitlərində qocalmasının tədqiqi və təkrar emal zamanı modifikasiyası”. Namizədlik dissertasiyası. Bakı, 2001, 133 s.

[2] Rahima S. Mammadova. Expediency of biology activity providing during the modification at the process of secondary treatment of polymers. “ Ecological & environmental chemistry 2017”(Moldaviya) The 6th International Conference, p/89-90

[3] Rahima S. Mammadova ,Oktay H. Akperov. Advantages of modification of exploited LDPE with nanosize biologically active substances. “Ecological & environmental chemistry 2017” (Moldaviya) The 6th International Conference, p.93-94

 ISBN: 978-80-8152-530-8

Structural evaluation of antimicrobial nanocomposite films

Ilie- Daniel Timpu[a*], Bianca-Ioana Dogaru[a], Maria-Cristina Popescu[a], Flavia Burlec[b], Cristina Tuchilus[b]

[a] *"Petru Poni" Institute of Macromolecular Chemistry of Romanian Academy, Iasi, Romania*
[b] *Gr. T. Popa Medicine and Farmacy University, Faculty of Farmacy, Iasi, Romania*

**dtimpu@icmpp.ro*

A new trend in agricultural products preservation consists in the use of active coatings in order to enlarge the safety margin and reassure high quality products and the incorporation of antimicrobial agents in films. Films and coatings with antimicrobial properties have innovated the concept of active coatings (packaging), being developed to reduce, inhibit or stop the growth of microorganisms on agricultural products.

In order to obtain antimicrobial films, starch-PVA and starch/PVA/CNC based films with silver nanoparticles (AgNPs) have been developed and characterized as to their physical and antimicrobial properties. The $AgNO_3$ salt was incorporated in different stage of the blend formation and in order to obtain the Ag nanoparticle, the obtained solutions were thermally or UV treated. The cast films obtained were evaluated using FTIR spectroscopy, SPM - Scanning Force Microscopy and WAXD – Wide Angle X-Ray Diffraction.

The antimicrobial activity of the films was tested at *Staphylococcus aureus*, *Bacillus cereus*, *Bacillus subtilis*, *Escherichia coli*, *Candida albicans*, and *Klebsiella*. These were compared with the activity of the reference drugs (chloramphenicol, tetracycline, ofloxacin and nystatin). It has been established that all compounds tested were very active against both Gram-positive and Gram-negative bacteria and the antimicrobial activity remain almost the same after 1 year.

Acknowledgements:

This work was supported by a grant of the Romanian National Authority for Scientific Research and Innovation CCCDI-UEFISCDI, project number COFUND-M-ERA.NET II- COMPIO, within PNCDI III.

 ISBN: 978-80-8152-530-8

Transport Through a Strongly Interacting Quantum Dot Coupled to Graphene Electrodes

Levente Máthé[a]*, Ioan Grosu[a]

[a] *Department of Physics, "Babeș-Bolyai" University, str. M. Kogălniceanu 1, Cluj-Napoca 400084, Romania*

**mathelevente_91@yahoo.com*

Introduction

Graphene is a two-dimensional graphite, where the carbon atoms condense in a hexagonal (honeycomb) lattice due to their sp^2 hybridization creating a non-Bravais lattice. The electrons in graphene behave as relativistic massless 2D fermions therefore their motion is described by a 2D Dirac-like equation. Thus, the graphene has a Dirac-like band structure, where the density of states of conduction electrons is proportional to the absolute value of energy [1]. Many interesting transport properties can be observed in mesoscopic systems [2]. Such a system can be realized from a quantum dot connected to two metallic electrodes, or graphene contacts. The transport properties of quantum dots attached to metallic contacts have been studied both theoretically [3, 4, 5] and experimentally [6]. High thermoelectrical efficiency of a single quantum dot connected to graphene electrodes at low temperatures was theoretically investigated [1]. In quantum dot systems described by Anderson model Kondo effect appears due to the interactions between a localized spin and the free electrons in a continuum of states [7]. Theoretically, the Kondo effect in magnetic adatoms on graphene was investigated in Ref. [8]. Experimental measurements for graphene with defects show high values for the Kondo temperature which provides many applications in the future [9].

In this work we theoretically study the electrical transport properties of an interacting quantum dot connected to two graphene contacts. The considered system is described by the standard Anderson Hamiltonian [1, 8, 10, 11] and the equation of motion method [11] is used for the determination of the dot Green's function.

Model Hamiltonian and Green's function

The total Hamiltonian for the system can be written as:

$$H = \sum_{\alpha,s,\sigma} \int_{-k_c}^{+k_c} dk\, \varepsilon_k\, c^{+}_{\alpha sk\sigma} c_{\alpha sk\sigma} + \sum_{\sigma} \varepsilon_{d\sigma} d^{+}_{\sigma} d_{\sigma} + U n_{\uparrow} n_{\downarrow} + V \sum_{\alpha,s,\sigma} \int_{-k_c}^{+k_c} dk \sqrt{|\mathrm{k}|} \left(c^{+}_{\alpha sk\sigma} d_{\sigma} + d^{+}_{\sigma} c_{\alpha sk\sigma} \right) \tag{1}$$

The first term represents the graphene contacts, where $c_{\alpha sk\sigma}^{+}$ ($c_{\alpha sk\sigma}$) is the creation (annihilation) operator for the Dirac-like electrons with valley index s, momentum k, spin $\sigma = \uparrow,\downarrow$ and energy ε_k in the graphene lead α ($\alpha = L$(left), R (right)). The energy dispersion of electrons in graphene is linear ($\hbar$=1): $\varepsilon_k = v_F \cdot k$, where v_F is the graphene Fermi velocity, k_c is the cutoff momentum with the cutoff energy $D = v_F \cdot k_c$ (D ~ 6 eV). The chemical potential $\mu_\alpha(T) \approx \mu_\alpha$ in the lead α is assumed to be constant. The second and third terms describe the quantum dot, where $\varepsilon_{d\sigma}$ is the energy level of dot and d_σ^{+} (d_σ) denotes the creation (annihilation) operator of electrons in the dot. U represents the strength of the Coulomb interaction and $n_\sigma = d_\sigma^{+} d_\sigma$ is the particle number operator for the dot. The last term models the coupling of the quantum dot to the graphene electrodes, where V is the hybridization strength which characterizes the interaction between free and localized electrons and it is set to be symmetrical ($V_L = V_R = V$). Here, we introduce a dimensionless coupling parameter as $\eta = 2(V/v_F)^2$.

We use the equation-of-motion method (EOM) to determine the Green's function for the dot $G_{dd}(\omega)$ which in the case of a general Anderson model leads to an infinite number of higher order correlation functions. In order to obtain an analytical formula for the Green's function, the Lacroix approximation [11] is applied to truncate these correlation functions by decoupling them. The remaining average values of operators are treated non-self-consistently [4]. These approximations can be used for $T > T_K$ [11], where T_K is the Kondo temperature. Also we consider the limit of strong Coulomb interaction ($U \to \infty$) and expect the non-magnetic solution ($\varepsilon_{d\uparrow} = \varepsilon_{d\downarrow}$), i.e. $\langle n_\uparrow \rangle = \langle n_\downarrow \rangle = 1/2$. We thus obtain an analytical expression of the Green's function for the dot:

$$G_{dd}(\omega) = \frac{1 - \langle n_{\bar{\sigma}} \rangle}{\omega - \varepsilon_{d\sigma} - \Sigma_0(\omega) - \Sigma(\omega)} \tag{2}$$

 ISBN: 978-80-8152-530-8

where the self-energies $\Sigma_0(\omega)$ and $\Sigma(\omega)$ are determined analytically in Ref. [12]. The imaginary part of Green's function gives the density of states (DOS): $\rho_\sigma(\omega) = -\mathrm{Im}\, G_{dd}(\omega)/\pi$. The DOS is connected to the current which flows from the leads to the quantum dot.

Results and Discussions

In Fig. 1. a and b, we plotted the density of states both for equilibrium and for nonequilibrium, for different values of dot energy ($\varepsilon_{d\sigma}$), temperature and coupling constant (η). At equilibrium (red line) there is one Kondo peak in the density of states at the chemical potential (μ_L=μ_R). The amplitude of Kondo peak decreases with increasing temperature and at high temperatures disappears totally. Out of equilibrium (blue line), the two graphene leads have different chemical potentials which causes that the Kondo peak splits into two suppressed peaks. These peaks are located at the chemical potentials. Similar phenomena take place in the case of metallic contacts [3, 5].

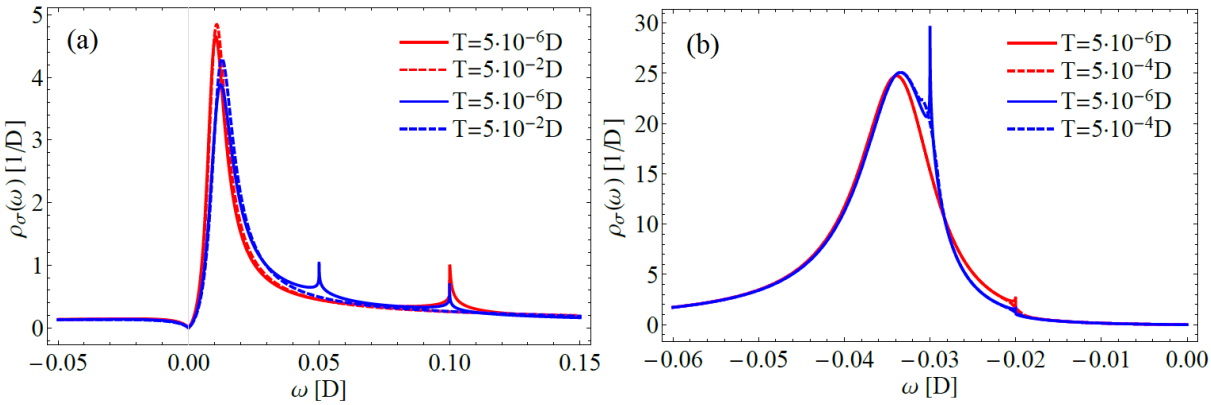

Fig. 1. DOS as a function of energy at different temperatures. The used parameters: (a) $\varepsilon_{d\sigma}$ = -0.35 D, η = 0.25. At equilibrium μ_L=μ_R = 0.1 D and out of equilibrium μ_L= 0.1 D, μ_R = 0.05 D. (b) $\varepsilon_{d\sigma}$ = -0.075 D, η = 0.015. At equilibrium μ_L=μ_R = -0.02 D and out of equilibrium μ_L= -0.02 D, μ_R = -0.03 D. In both figures the red lines indicate the equilibrium cases and the blue lines refer to the nonequilibrium cases.

In Fig. 2. a, we plotted the linear-response conductance as a function of chemical potential at different temperatures for equilibrium. We can observe that the amplitude of conductance peak increases with decreasing temperature and its maximum is shifted to the higher values of chemical potential. At low temperatures the shape of conductance is broadened. Such a conductance peak corresponds to transport through a single level quantum dot. In experiments, usually, the conductance is measured as a function of gate voltage (V_g) at different temperatures. In theoretical models, the gate voltage is related to dot energy via $V_g \sim -\varepsilon_{d\sigma}$ + const. [13]. Fig. 2. b shows the results obtained for the linear-response conductance as a function of gate voltage at different temperatures for equilibrium. The conductance has a minimum which can be due to the Lacroix approximation.

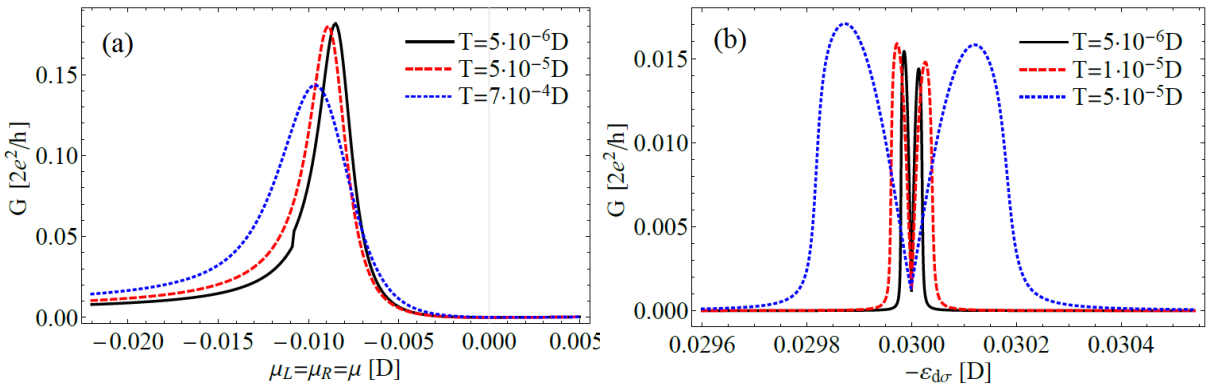

Fig. 2. (a) Conductance as a function of chemical potential at different temperatures for equilibrium. The dot energy is $\varepsilon_{d\sigma}$ = -0.075 D and η = 0.015. (b) Conductance as a function of energy level of dot at different temperatures for equilibrium. The chemical potentials are μ_L=μ_R= 0 D and η = 0.015.

 ISBN: 978-80-8152-530-8

Also, we have calculated the current and the differential conductance as a function of applied bias at finite temperatures for nonequilibrium. In this case we have chosen an asymmetric bias voltage ($eV = \mu_L - \mu_R$), which is also preferred experimentally. Furthermore, we have investigated the current and the differential conductance as a function of gate voltage at different temperatures out of equilibrium.

References

[1] J. R. Isern-Lozano, et al. (2016) arXiv:1601.02255v1.
[2] Y. Imry, *Introduction to Mesoscopic Physics*, Oxford University Press, New York, 1997.
[3] Y. Meir, N. S. Wingreen, P. A. Lee, Phys. Rev. Lett. **70** (1993) 2601-2604.
[4] Y. Meir, N. S. Wingreen, P. A. Lee, Phys. Rev. Lett. **66** (1991) 3048-3051.
[5] N. S. Wingreen, Y. Meir, Phys. Rev. B. **49** (1994) 11040-11052.
[6] A. T. Johnson et al., Phys. Rev. Lett. **69** (1992) 1592-1595.
[7] M. Crișan, I. Grosu, I. Țifrea, Physica E **66** (2015) 245-251.
[8] Z.-G. Zhu, J. Berakdar, Phys. Rev. B **84** (2011) 165105.
[9] J.-H. Chen et al., Nature Phys. **7** (2011) 535–538.
[10] P.W. Anderson, Phys. Rev. 124 (1961) 41-53.
[11] C. Lacroix, J. Phys. F **11** (1981) 2389-2397.
[12] L. Máthé, I. Grosu. In preparation.
[13] R. V. Roermund, Theoretical Study of Non-equilibrium Transport in Kondo Quantum Dots. Strongly Correlated Electrons, PhD Thesis, Université de Grenoble, 2010, pages 47-48.

 ISBN: 978-80-8152-530-8

Nanostructured Transparent Polymer For Encapsulate PV Modules. Replace Glass, Increase Efficiency

E. Shembel[a,b*], V, Redko[a], T. Pastushkin[a], L. Yashchenkoa, N. Yarova[a], A. Markevich[b] .

[a] *Enerize Corporation, Coral Springs, FL, 33067, USA*
[b] *Scientific Research Laboratory of Chemical Power Sources Ukrainian State University of Chemical Technology, Dnipro, 49005, Ukraine*

**eshembel@enerize.com*

Enerize novel materials and technology is a breakthrough based on the patent pending nanostructured transparent polymer (NSTP), which is flexible, durable, has high level of adhesion for various materials, provides high level of hermetic sealing (waterproof) and UV protection, and contains nanostructured clusters with sizes from 20 to 100 nanometers, and micro-domains from 15 to 120 microns. Such composition of nanostructured clusters and micro-domains, located in a certain order in the volume of the polymer, results in micro lensing which increases the concentration of light reaching the semiconductor layer. This novel nanostructured transparent polymer dramatically improves the performance of PV modules encapsulated with one layer of Enerize nanostructured transparent polymer as compared with PV modules laminated with glass or encapsulated with multilayer structure of other polymers.

New design for thin film flexible photovoltaic modules using single layer nanostructured high level transparency polymer for encapsulation, and protective coating of different type of thin film flexible solar cell, such CIGS, organic and DSSC modules. This results in increase efficiency, reduce the weight and manufacturing cost of PV modules. Initial liquid composition of the transparent nanopolymer is applied directly to the PV module surface, where process of polymerization is proceed. Single layer nanopolymer enable to replace the glass and other multilayers polymer barrier structures, which are used for encapsulation solar cells.

The crinkle coat surface morphology covering the surface of the solar cell module with the optically transparent polymer layer (Fig1). Incident light 1; absorbed light 2; reflected light 3 is incident at another point along the surface of the polymer.(Fig.2)

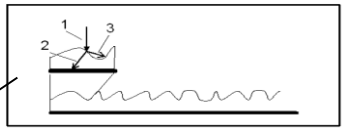

Fig.1 Nanostructure of the volume Enerize transparent polymer has a mosaic structure with nanoscale domane

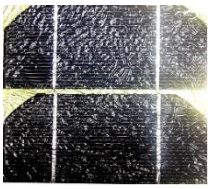

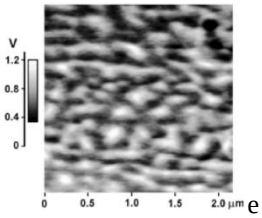

Fig. 2 Images of PV modules safes coated with Enerize transparent polymer

Enerize single film nanostructured transparent polymer materials are coated directly on the surface of solar cells or modules, and do not need any additional lamination with glass or polymer layers to deliver durable encapsulation. This allows simplify the process of PV modules production and reduce their cost.

Non- active materials of PV modules account for 15% to 48% of module manufacturing costs. Demand for new nanostructured transparent polymer technology has average anticipated growth rate of 48% per year. Significant advancement includes Increasing efficiency by 10% -20%; reducing production costs and weight by 30% compared with traditional methods, and increasing durability of thin film PV modules.

 ISBN: 978-80-8152-530-8

Key Elements of Enerize Nanostructured Transparent Polymer

- Enerize's encapsulating polymer layers contain in the structure the nanostructured clusters and micro-domains, which play the role of micro lenses, which results in the concentration of light. As a result, efficiency of PV modules increases.
- Initial liquid composition of the transparent polymer material is applied directly to the PV module surface; Process of polymerization proceed at low temperatures (80*C)
- High transparency (including UV area),
- Flexibility, which is important for thin film flexible solar cells
- High level of adhesion for various materials, which eliminates the need for the adhesives required with glass and some other polymers.
- Waterproof, and UV protection.
- Elimination the multi-layer structure including the reflective surfaces present with glass.
- The transparent polymer can be formed as a flat smooth surface or as a "crinkle coat", which provides additional positive effect for increasing the PV modules efficiency

Example of flexible solar cell encapsulated with Enerize nanopolymer, and flexible solid state Li-ion cell for hybrid system

Fig. 3 Solid state Li-ion cells **with $LiMn_2O_4$** cathode.

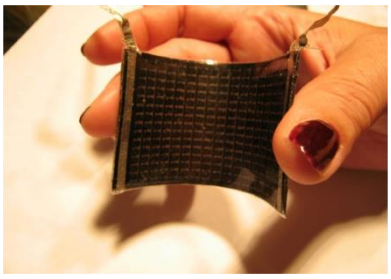

Fig. 4 Flexible solar cell

The key component of the PV modules is a single layer nanostructure optical polymer enabling solar modules of all types to be cheaper, lighter and deliver higher efficiency via encapsulation vs. glass or multilayer polymer coating.

The key components of solid state Li-ion battery: leading-edge cathode, anode based on the composition of graphite and silicon, and solid high ionic conductive electrolyte

 ISBN: 978-80-8152-530-8

Tests Enerize PV modules under artificial hurricane conditions: Florida International University

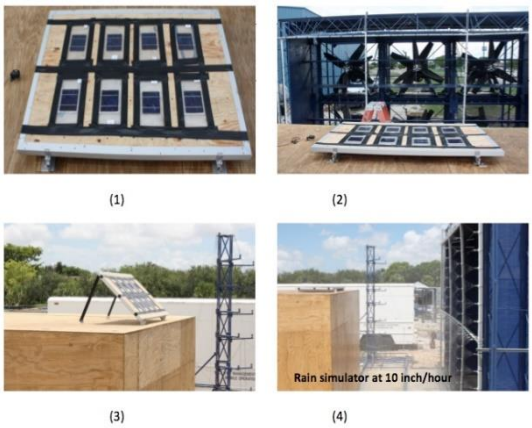

Fig. 5 PV modules which have been tested.

Independent center for testing PV modules at Florida International University tested Enerize PV modules based on mono c-Si encapsulated with NSTP. During tests artificial hurricane conditions were modeled using a special test bench.

During presentation the following results of the testing will be presented

- Short Circuit Current
- Open Circuit Voltage
- PV Efficiency
- Physical Properties – see below and next slide

-Effect of high temperatures (+75^{0}C).
Duration of test: 1200 hours.
Test results: no variations in solar cell parameters.

- Effect of low temperatures (-40^{0}C)
Duration of test: 1200 hours.
Test results: no variations in solar cell parameters.

- Effect of thermal cycling (from -40^{0}C to +75^{0}C).
Duration of each cycle: 3 hours. Number of cycles: 350.
Test results: no variations in solar cell parameters.

Also the following parameters have been tested:

- Single impact testing (number of impacts: 100).
- Repeated impact testing (in a shipping container).
- Electrical strength of the insulation.
- Effect of relative humidity (85±3)%.
- Effect of ultraviolet radiation.

 ISBN: 978-80-8152-530-8

Next steps:

Encapsulate with transparent polymer the solar cells based on CIGS, DSSC and organic solar cells. Test thin film flexible solar cells, encapsulated with transparent nanopolymer. Optimize technology of encapsulation. Provide samples to potential customers and strategic partners for independent test and evaluation.

Major advantages of PV modules encapsulated with Enerize nanostructured transparent polymer

- Increase efficiency by 10% -20% thus allowing higher electrical output under the same illumination.
- Reduce production costs by 30%
- Reduce weight by 30% compared with traditional methods
- Longer durability of thin film PV modules with Enerize coating
- Works with different types of solar cells: monocrystalline, multicrystalline, amorphous silicon photovoltaics and solar cells based on non-silicon systems such as CIGS.
- Effective utilization of shorter wavelength range of the spectrum, including UV, due to the high transparency of the polymeric coating.
- More resistant to degradation by UV and ionizing radiation (so-called photon degradation).
- Stability when exposed to high and low temperatures and thermal-cycling, mechanical impact, and high relative humidity

Acknowledgements

This presentation is connected with the framework of NATO, Science for Peace and Security Programme Project SPS 985148 “Development of New Cathodes for Stable and Safer Lithium-Sulfur Batteries” in the light of the following development the hybrid system: flexible PV modules that encapsulated with Enerize nanostructured transparent polymer, and flexible high energy Lithium-Sulfur Batteries.

 ISBN: 978-80-8152-530-8

Modification of screen-printed electrode by silver nanoparticles for bioapplication

M. Hečková[a]*, R. Oriňaková[a], M. Strečková[b]

[a] *Department of Physical Chemistry, Faculty of Natural Sciences, Pavol Jozef Šafárik University, Moyzesova 11, SK-04154 Košice, Slovakia*

[b] *Institute of Materials Research, Slovak Academy of Science, Watsonova 47, SK-04353 Košice, Slovakia*

**maja.heckova@gmail.com*

Screen-printed electrodes are a suitable alternative to traditional electrodes and show a number of advantages, in particular with respect to their low price, small size, reproducibility, selectivity, accuracy, and sensitivity. In this work, we focused on screen-printed carbon electrodes modified silver nanoparticles [1].

The combination of electrochemically deposited metal nanoparticles and screen-printed electrodes allows the mass production of electrochemical sensors, which have various catalytic effects.

Silver nanoparticles have unique physical, chemical and biological properties compared to their macro-dimensional bulk electrodes. Exceptional properties of silver nanoparticles including high electrical and thermal conductivity, surface-enhanced Raman scattering, chemical stability, catalytic activity, and nonlinear optic behavior enable to these materials potential utilization in microelectronics and biomedical imaging. In addition, silver nanoparticles show antibacterial activity. Significant optical, electrical and thermal properties of Ag nanoparticles predict their use as chemical sensors and biosensors or photovoltaic application [2].

We explored various conditions for the preparation of silver nanoparticles from several working electrolytes. The electrocatalytic activity of modified screen-printed electrodes towards hydrogen evolution reaction was evaluated by linear sweep voltammetry, chronoamperometry, and electrochemical impedance spectroscopy. The surface of screen-printed carbon electrodes modified with Ag nanoparticles was characterized by scanning electron microscopy and the active area of these electrodes was determined by cyclic voltammetry.

In this work, we investigated the most suitable conditions for the preparation of electrode modified with silver nanoparticles usable for determination of cholesterol, glucose and Raman scattering. The highest electrocatalytic activity, electrochemical determination of cholesterol and Raman scattering was observed for the sample where were the silver nanoparticles deposited by potentiostatically method at a constant potential -0,15 V with a deposition time of 10 min. (Fig.1b). On the other hand, the best results for the determination of glucose were obtained on the sample modified by silver nanoparticles electrodeposited by two-step method (Fig 1c).

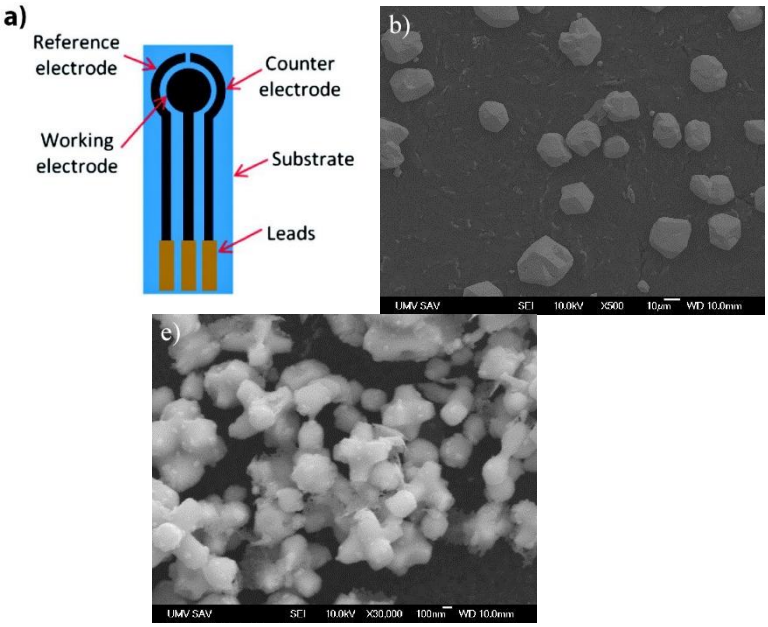

Fig. 1. a) Scheme of unmodified carbon screen-printed electrode [3] b) SEM image of potentiostatically electrodeposited Ag nanoparticles on screen-printed electrode c) SEM image of Ag nanoparticles electrodeposited by two-step method on screen-printed electrode

 ISBN: 978-80-8152-530-8

Acknowledgements

This work was supported by the Scientific Grant Agency of the Ministry of Education, Science, Research and Sport of the Slovak Republic and the Slovak Academy of Sciences, projects No. VEGA 2/0079/17 and 1/007/17.

References

[1] J. Wang, Analyst 119 (1994) 763.
[2] L. Balan, et al., Silver nanoparticles: New synthesis, characterization and photophysical properties; in: Materials Chemistry and Physics, 2007, vol. 104, p. 417–421.
[3] K. K. Mistry et al., A review on amperometric-type immunosensors based on screen-printed electrodes; in: Analyst, 2014, vol. 139, p. 2289 - 2311.

 ISBN: 978-80-8152-530-8

Ni/Ag nanocavities films as a novel plasmonic substrates for SERS applications

O. Petruš[a]*, A. Oriňak[a],R. Oriňaková[a], Z. Orságová Králová[a], M. Kupková[b], E. Múdra[b]

[a] *Institute of Chemistry, Faculty of Science, P. J. Šafárik University, 040 01 Košice, Slovakia*
[b] *Institute of Materials Research of SAS, Watsonova 47, Košice, Slovakia*

**ondrej.petrus@student.upjs.sk*

In our research were prepared metallic nanocavities films (single and hybrid) by colloid lithography followed by electrochemical deposition of Ni and subsequently Ag layers. Initial Ni nanocavities films is easy to produce with high homogeneity and as a substrate for deposition of plasmonic layer which consist of Ag nanoparticles with ~100 nm in diameter. The plasmonic properties were tested depending on polystyrene spheres diameter (100, 300, 500, 700 and 900 nm), different thickness of Ni layer and depending on the time of Ag deposition. Maximum SERS signal enhancement was observed with use 500 nm colloidal mask, for other sizes of colloidal mask was lower enhancement because of to use excitation laser wavelength (532 nm). Similar trend was observed for testing of dependence for different normalised thickness of Ni layer (0.1 - 0.8) using 500 nm colloidal mask. The highest enhancement was reached for normalised thickness ~0.5. At lower and higher normalised thickness were observed weakness interactions with interaction laser. This results were confirmed by FDTD simulations with similar results for enhancement of electric field near the nanocavities surface. The optimal condition for electrochemical deposition of Ag was set to 200 s with constant current density at 1.10-3 A.cm^{-2}. With this time of deposition, the coverage of Ni nanocavities film by Ag nanoparticles is homogenous with optimal density of coverage. Finally, at the best surface (500 nm colloidal mask, normalised thickness of Ni ~0.5 and 200 s of Ag deposition) was measured the concentration dependence with Rhodamine 6G with concentration from 1.10^{-5} mol.dm-3 to 1.10^{-12} mol.dm-3 with R^2=0.95 for 770 cm^{-1} and with standard deviation less than 18 %. Moreover, the time stability was tested with Rhodamine 6G for 13 weeks, where the decrease of Raman signal was observed after first week to ~50% and then stabilized at approximately constant value during 13 weeks. The analytical enhancement factor was calculated to 1.078 × 10^{10} [1].

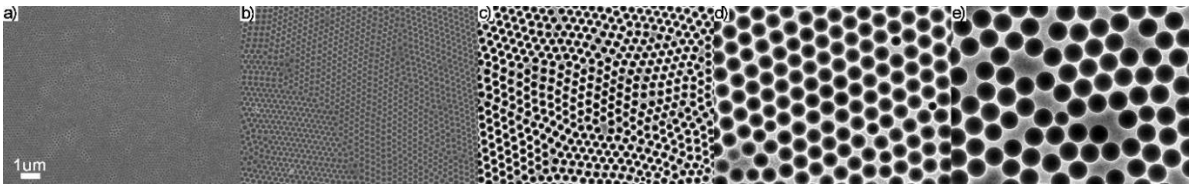

Fig.1 Ni nanocavities films prepared from colloidal mask with different diameter of PS spheres a)100 nm b)300 nm c)500 nm d)700 nm d)900 nm

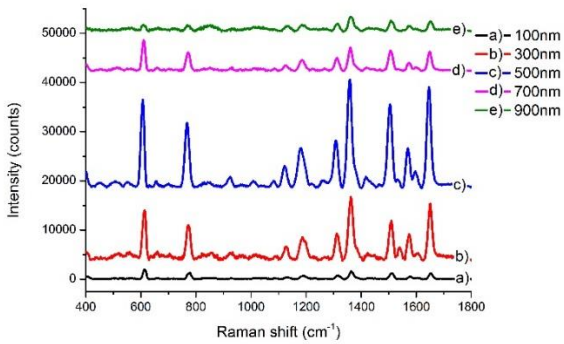

Fig.2 SERS spectra of 1×10^{-6} Rhodamine 6G on Ni/Ag nanocavities films prepared colloidal mask with different diameter of PS spheres corresponding to the Fig.1

Acknowledgements

This research has been financially supported by grant VEGA1/0074/17 of the Slovak Scientific Grant Agency, APVV-16-0029 of the Slovak Research and Development Agency.

References

[1] O. Petruš et.al, Applied Surface Science 423 (2017) 322-330

 ISBN: 978-80-8152-530-8

Silver substrates prepared by pulsed deposition for SERS applications in diagnostics

Zuzana Orságová Králová[a], Andrej Oriňak[a], Renáta Oriňaková[a], Ondrej Petruš[a], Jozef Radoňak[b], Lucia Lakyová[b], Zuzana Jurášeková[c]

[a]*University of P. J.Safarik in Košice, Department of physical chemistry, Moyzesova 2, 04001 Košice, Slovakia*
[b]*Surgical Clinic, Faculty of Medicine, P.J. Safarik University and L. Pausteur Faculty Hospital, Trieda SNP1,Kosice, Slovakia*
[3]*University of P. J.Safarik in Košice Department of biophysics, Jesenná 5, 04001 Košice, Slovakia*

orsagova.kralova@gmail.com

Existing screening techniques such as fecal immunochemical test and colonoscopy are invasive, time consuming methods. Our work is presenting initial experiments for developing a new diagnostic test for early detection of colon cancer by SERS analysis of human blood plasma. Our electrochemically prepared silver surfaces are easily-made, low-cost and rapidly deposited SERS substrates, which can be used for direct diagnostic test in clinical practice. Silver layers were electrochemically deposited onto ITO glass (>7Ω) from solution containing 0.01M $AgNO_3$. For optimization of the most appropriate morphology of SERS substrate we prepared 16 samples by pulsed double potentiostatic method (E_1 = -0,4 V, E_2 = -0,1 V). We modified number of pulses from 10 to 70 and duration time of pulse E_2 from 0,5 s to 2 s. Experiments showed that pulsed deposited silver surface with 70 pulses with E_2= -0,1V for 0,5s had the highest enhanced factor (2.1×10^9) for molecule of Rhodamine 6G. Using this surface, we were able to detect all main components of human blood plasma. Our aim is to collect significant amount of samples of plasma from healthy volunteers and patients with colon cancer. Based on the measured SERS spectra we will be able to find differences between these two observed groups and by principal component analysis (PCA) we will develop reliable diagnostic test for an early detection of colon cancer.

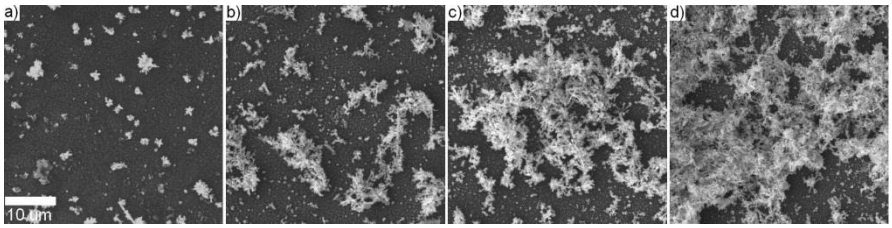

Fig. 1: SEM images of silver dendrites electrodeposited on ITO glass by pulsed double potentiostatic method. Density of the surface coverage density is increasing with number of pulses and time of electrodeposition.

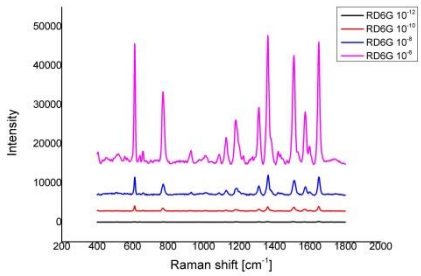

Fig. 2: SERS spectra of Rhodamine 6G of concentration from 1.10^{-6} mol.dm^{-3} to 1.10^{-12} mol.dm^{-3}.

Acknowledgements

This research has been financially supported by grant VEGA 1/0074/17 of the Slovak Scientific Grant Agency and APVV-16-0029 of the Slovak Research and Development Agency.

 ISBN: 978-80-8152-530-8

Unusual Bending Properties of Carbon Nanotubes - a Consequence of Different Stiffness in Tension and Compression?

M. Kupková[a]*, M. Kupka[b]

[a] *Institute of Materials Research of SAS, Watsonova 47, Košice, Slovakia*
[b] *Institute of Experimental Physics of SAS, Watsonova 47, Košice, Slovakia*

**mkupkova@saske.sk*

Introduction

Noteworthy mechanical, thermal and electrical properties of carbon nanotubes open a way to a new generation of high performance nanotube-reinforced polymer coatings and/or bulk composites. Knowledge of the stiffness of carbon nanotubes represents an important step towards the prospective use of such coatings/composites in various applications.

Experimental determination of the elastic modulus relies primarily on measurements of the flexural rigidity of nanotubes. Principles of corresponding procedures more or less resemble those of macroscopic static bending tests and dynamic resonant method. But as the nano-sized samples are used, experiments are based mainly on the techniques of high resolution transmission electron microscopy and atomic force microscopy. To process the data, carbon nanotubes are idealized as continuous elastic tubes.

An interesting result is a trend for higher moduli with smaller tube diameters observed in some experiments [1,2,3].

A true material modulus of elasticity does not depend on the specimen geometry or the method of testing, whereas effective flexural moduli of carbon nanotubes do (e.g. [2,3]).

The dependence of effective flexural modulus on cross sectional dimensions is quite usual for an inhomogeneous tube. But the carbon nanotubes are apparently homogeneous ones.

Here, a model is proposed that combines the properties of both homogeneous and heterogeneous rods in one sample. Namely, a homogeneous continuous tube made of a material with different moduli in tension and compression is considered. When such a tube is bent, it behaves like a “composite beam” consisting of two different materials: one represented by a stretched part of the tube, the other by its compressed part. As a consequence, the dependence of the effective flexural modulus on the inner radius-to-outer radius ratio appears for a homogeneous tube.

Theoretical background and results

Mechanical behaviour of rods made of material with different modulus in tension, E_t, and modulus in compression, E_c. was theoretically studied in papers [4,5,6]. Knowledge of flexural rigidity from [5] is utilized here.

Flexural rigidity, B, is an important integral quantity that characterizes the resistance of the rod against bending. The value of B is obtained experimentally. The ratio B/I, where I is the area moment of inertia of the cross section, is usually called the “effective flexural modulus”, E_{eff}. This modulus is determined by means of bending-based experiments. For homogeneous samples the effective flexural modulus is the same as the Young’s modulus of the sample material [7,8].

For the tube considered here, flexural rigidity was determined theoretically by the method presented in [6]. Once the flexural rigidity is known, the effective flexural modulus is evaluated as $E_{eff}=B/I$. The area moment of inertia of the cross section can be calculated as $\pi(R_o^4-R_i^4)/4$. R_o and R_i are outer and inner tube radii, respectively.

Theoretical results reveal that the dependence of the effective flexural modulus on the cross-sectional dimensions reduces to the dependence of modulus on the inner radius-to-outer radius ratio, and that the effective flexural modulus decreases with increasing R_i/R_o ratio for tubes with E_t different from E_c. Figure 1 presents the effective flexural modulus as a function of R_i/R_o ratio, calculated for various E_t and E_c.

 ISBN: 978-80-8152-530-8

Discussion and conclusions

Size-dependent effective flexural modulus is quite usual for heterogeneous samples, but unexpected for uniform homogeneous ones. Assuming this, the rods that in some sense combine the properties of homogeneous and heterogeneous samples were investigated, namely the uniform homogeneous rods made of material with different moduli in tension and compression. Such samples are homogeneous with respect to their composition, but when they are bent they behave like composite beams consisting of two different materials-compressed and extended parts of the rod.

The principal findings are:

i) The effective flexural modulus can depend on the cross-sectional dimensions when the homogeneous rod/tube material possesses different tensile and compressive moduli.

ii) For tube-shaped samples, the effective flexural modulus is a decreasing function of R_i/R_o ratio.

The results presented in this contribution indicate a possible source of the dependence of effective flexural modulus of carbon nanotubes on their diameters – different tensile and compressive properties of nanotubes. But this hypothesis requires further verification.

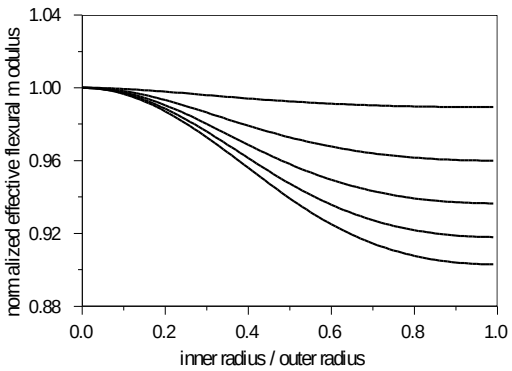

Figure 1. Effective flexural modulus of a tube with different tensile and compressive stiffness. Figure presents modulus of tubes with different E_t/E_c as a function of inner radius / outer radius ratio (from top to bottom, E_t/E_c is 2:1, 4:1, 6:1, 8:1, 10:1).

Acknowledgements
The authors thank for financial support of the research by the Slovak Research and Development Agency under contract APVV No. 0029-16, APVV No. 0677-11 and VEGA grants 2/0100/15, 1/0074/17.

References

[1] H.W. Zhang, J.B. Wang, X. Guo, J. Mech. Phys. Solids **53** (2005) 1929-1950.
[2] M.M.J. Treacy, T.W. Ebbesen, J.M. Gibson, Nature **38** (1996) 678-680.
[3] P. Poncharal, Z.L. Wang, D. Ugarte, W.A. De Heer, Science **283** (1999) 1513-1516.
[4] M. Kupka, M. Kupková, J. Matter Sci Lett. **20** (2001) 445-447.
[5] M. Kupka, M. Kupková, J. Phys. D: Appl. Phys.. **34** (2001) 232-237.
[6] M. Kupka, M. Kupková, J. Phys. D: Appl. Phys.. **39** (2006) 4097-4103.
[7] L.D. Landau, E.M. Lifshitz, Theory of Elasticity, (2nd English edn) (Oxford:Pergamon), 1970.
[8] R.R. Jr. Craig, Structural Dynamics. An Introduction to Computer Methods. (New York: Wiley), 1981.

 ISBN: 978-80-8152-530-8

Chiral Plasmonic Helicene Nanoassemblies

J. Janoušek,[ab*] L. Bednárová,[a] M. Šámal,[a] J. Neburková,a J. Vávra,[a]
J. Rybáček,[a] P. Matějka,[c] P. Cígler,[a] I. G. Stará,[a] I. Starý[a]

[a] *Institute of Organic Chemistry and Biochemistry CAS, Flemingovo n. 2, 166 10 Prague, Czech Republic*
[b] *Department of Analytical Chemistry, UCT Prague, Technicka 5, 166 28 Prague, Czech Republic*
[c] *Department of Physical Chemistry, UCT Prague, Technicka 5, 166 28 Prague, Czech Republic*

* *jiri.janousek@uochb.cas.cz*

Organic field-effect transistors (OFETs) are widely used as logic devices in organic electronics applications because of their low-cost fabrication, energy-efficient production and reliable performance [1]. However, in sharp contrast to an enormous attention being paid to OFETs employing organic semiconductors, organic-inorganic hybrid nanomaterials such as metal nanoparticles functionalized with organic ligands have been less studied in this regard. Moreover, no particular interest was so far given to the OFET device prepared using chiral π-electron containing structures.

Here, we present novel chiral hybrid nanomaterials based on colloidal gold nanoparticles (Au NPs) and colloidal silica nanoparticles with a gold nanoshell (Silica Au NPs) and covalently functionalized with a helicene-like ligand **1** (Scheme 1) with defined chirality. These assemblies were structurally characterized by microscopic and spectroscopic techniques. Preliminary data indicate induction of plasmonic optical activity (Fig. 1) by chiral functionalization of gold nanomaterials. The comparable effect was observed for ligand-coated NPs in solution as well as for NPs deposited on quartz substrates and functionalized afterward.

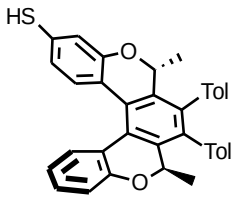

Scheme 1: Structure of a helicene-like ligand (*M*,*R*,*R*)-**1** (>99% *d.e.*) with SH binding group.

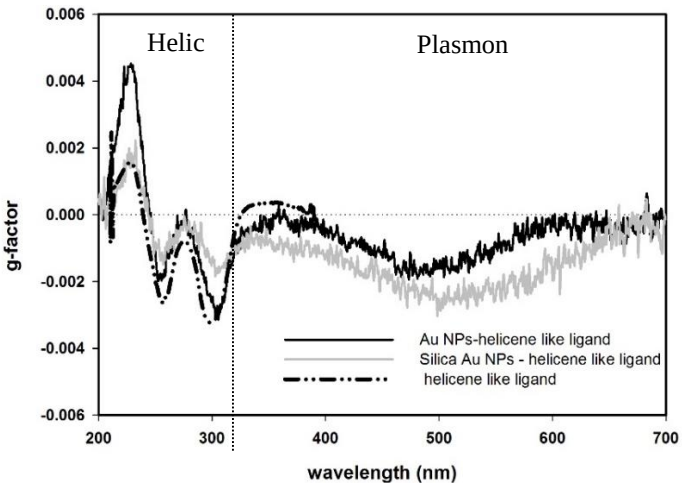

Figure 1: Electronic circular dichroism spectra of Hel-coated NP layers.

 ISBN: 978-80-8152-530-8

Acknowledgements

This work was supported by the Czech Science Foundation (Reg. No. 16-08327S), IOCB CAS (RVO: 61388963), and the specific university research (MSMT No. 20-SVV/2017).

References

[1] (a) Allard, S.; Forster, M.; Souharce, B.; Thiem, H.; Scherf, U. *Angew. Chem. Int. Ed*. **2008**, *47*, 4070; (b) Wang, C.; Dong, H.; Hu, W.; Liu, Y.; Zhu, D. *Chem. Rev*. **2012**, *112*, 2208; (c) *Organic Electronics* (Ed.: H. Klauk), Wiley-VCH, Weinheim, **2006.**

 ISBN: 978-80-8152-530-8

Nanoceramic composites based on organomagnesiumoxanealumoxanes

T. Apukhtina[a]*, G. Shcherbakovaa, M. Varfolomeev[b], A. Rumina[a], N. Krivtsova[a], A. Drachev[a]

[a] *State Research Institute for Chemistry and Technology of Organoelement Compounds, Moscow, Russia*[b] *Moscow aviation institute (National research university), Moscow, Russia*

**tatiana.apukhtina@yandex.ru*

Nanostructured ceramics have unique properties and performance characteristics. However, monolithic nanoceramics are inferior to nanoceramic composite materials, reinforced by continuous or discontinuous ceramic fibers, according to some physical-mechanical parameters, for example, in crack resistance (fracture toughness). The use of discontinuous fibers for reinforcing ceramics has a number of significant advantages, such as precise control of the fiber amount, fabrication cost reduction, and simpler production of irragular shapes. However, a disadvantage of composites reinforced with discontinuous fibers is that they have lower fracture toughness, as compared to composites reinforced with continuous fibers. To improve this parameter, the most uniform mixing of the chopped fibers with the matrix is required.

Another possible method to avoids the problem of homogeneous dispersion of fibers within the matrix is self-reinforcement of the composite [1].

We obtained nanoceramic composites (Fig. 1) from powders of nano-SiC, micro-SiC and a binder based on organomagnesiumoxanealumoxanes [2] (precursors of aluminum-magnesium spinel) first synthesized in the State Research Institute for Chemistry and Technology of Organoelement Compounds, and reinforcing discontinuous spinel fibers of $MgAl_2O_4$ composition. Spinel fibers were obtained by forming polymer fibers from fiber-forming organomagnesiumoxanealumoxanes [2, 3], followed by their pyrolysis (Fig. 2). It is known that due to the high melting point (2135 ºC), hardness, chemical resistance and strength, which remain at high temperatures, aluminum-magnesium spinel is an effective material for high-temperature technology.

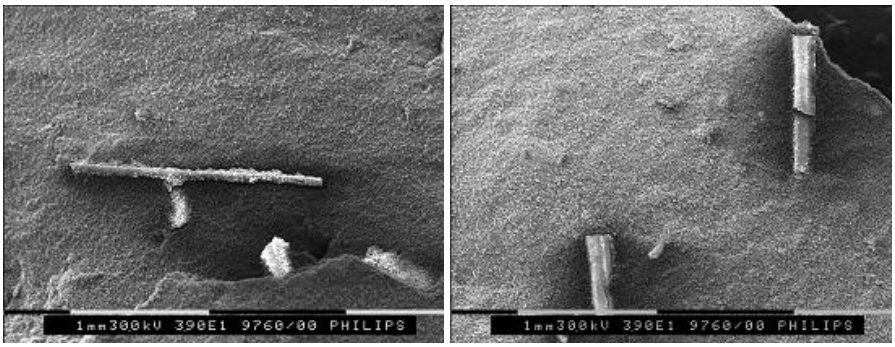

Fig.1 – SEM of the nanoceramic composite

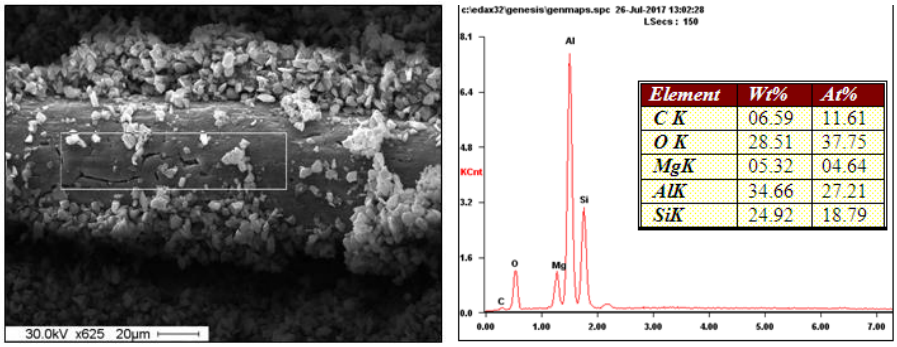

Element	Wt%	At%
C K	06.59	11.61
O K	28.51	37.75
MgK	05.32	04.64
AlK	34.66	27.21
SiK	24.92	18.79

Fig. 2 – SEM and X-ray elemental microanalysis of spinel fiber in a ceramic composite

 ISBN: 978-80-8152-530-8

Moreover, the formation of nanofibers composed of Si_3N_4 was observed. That is, self-reinforcement of the nanoceramic composite occurred (Fig. 3), which positively effected its physical and mechanical properties (density, strength, fracture toughness).

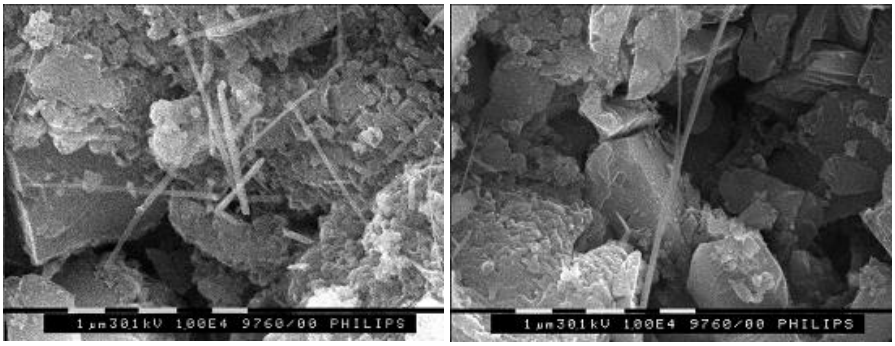

Fig. 2 – SEM of self-reinforced nanoceramic composite

Thus, organomagnesiumoxanealumoxanes can be effectively used as precursors of components (binders, fibers, powders) for high-strength and high-temperature nanoceramic composites.

Acknowledgements

This work was supported by the Russian Foundation for Basic Research, project no. 17-03-00331 A.

References

[1] K. Itatani, S. Yoshiyama, H. Suemasu, et. al. 16th International Conference on Composite Materials.
[2] G.I. Shcherbakova, N.S. Krivtsova, T.L. Apukhtina, et. al. RF Patent 2615147 C1, 2017.
[3] G.I. Shcherbakova, P.A. Storozhenko, T.L. Apukhtina, et. al. Polyhedron **135** (2017) 144–152.

 ISBN: 978-80-8152-530-8

Novel nanocomposites based on epoxy and nano sized phthalocyanine for corrosion protection application

A.M.A. Deyab [a]*

[a] *Egyptian Petroleum Research Institute (EPRI), Nasr City, Cairo, Egypt.*

**hamadadeiab@yahoo.com*

In this study, epoxy/phthalocyanine nanocomposite (H_2Pc/Epoxy) is employed to protect carbon steel corrosion in 3.5% NaCl solution. The performance of the new nanocomposite coatings was evaluated by using electrochemical impedance spectroscopy (EIS), Open circuit potential (OCP), scanning electron microscopy (SEM) measurements. The mechanical property of new nanocomposite coating was investigated using nanoindentation technique. The incorporation of H_2Pc pigments into epoxy resin coating significantly enhances the corrosion resistance as well as the hardness of epoxy coatings. H_2Pc pigment is able to cure the defect in epoxy resin and prevent the diffusion of corrosive electrolyte to carbon steel substrate.

 ISBN: 978-80-8152-530-8

Effect of Anodizing Potentials on Corrosion Behavior of Anodic TiO_2 Nanotubes Grown on Ti6Al4V Substrates

A. Boucheham[a, b] *, A. Karaali[a], A. Manseri[b]

[a]*Laboratoire de Thermodynamique et Traitement de Surfaces des Matériaux, Département de Physique, Faculté des Sciences Exactes, Université des Frères Mentouri- Constantine1, 25000 Constantine, Algeria*
[b]*Centre de Recherche en Technologie des Semi-conducteurs pour l'Energétique, 02, Bd Dr Frantz Fanon, les 07 merveilles, BP : 140, 16038 Algiers, Algeria*

**aghani.boucheham@gmail.com*

In this work, TiO_2 nanotubes were grown by anodic oxidation on Ti6Al4V substrates in organic solution containing ethylene glycol and Ammonium fluoride at several applied potentials varied between 20 and 70V followed by thermal annealing at 450°C for 2h. Different nanotubes diameters and lengths were obtained as revealed by scanning electron microscope. X-ray diffraction exhibits amorphous structure for all as-anodized nanotubes, it transforms to anatase after the annealing. Corrosion behavior was evaluated in artificial saliva at 37 °C with neutral pH of 7.4 by using open circuit potential, cyclic polarization and electrochemical impedance spectroscopy techniques.

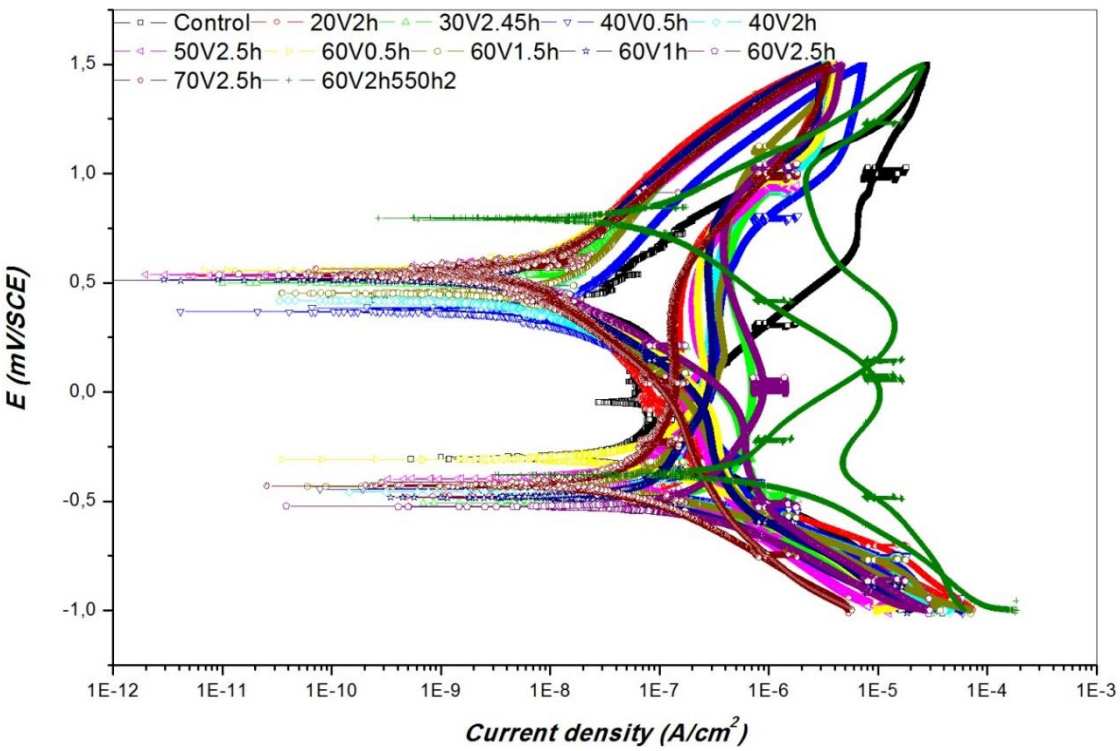

fig.1: Cyclic polarization curves recorded for all studied samples

References

[1] J. Kapusta-Kołodziej, K. Syrek, A. Pawlik, M. Jarosz, O. Tynkevych, G. D.Sulka, Appl. Surf. Sci., 396, 1119 (2016).
[2] J. Grotberg, A. Hamlekhan, A. Butt, S. Patel, D. Royhman, T. Shokuhfar, C. Sukotjob, C. Takoudis, M.T. Mathew, Mater. Sci. Eng., C, 59, 677 (2016).

 ISBN: 978-80-8152-530-8

Synthesis, Structural, and Transport Properties Of Chemically Deposited Nanostructured CdMnS Thin Films

Jaiprakash S Dargad

Dayanand Science College, Latur-413 531, M.S, India

**jsdargad@rediffmail.com*

$Cd_{1-x}Mn_xS$ thin films with x value ranging between 0 to 0.5 were deposited onto the glass substrates using a chemical deposition process. The composition of the as- grown samples was determined by an EDS technique. The polycrystalline growth resulted over the whole range studied and both CdS and $Cd_{1-x}Mn_xS$ films exhibited hexagonal wurtzite structure with growth orientation along (101) direction. Typically, the lattice parameter 'a' decreased from $4.131A^0$ to $4.110A^0$ for the change of x from 0 to 0.1 and thereafter it returned to its original value. Similar changes in c with x were also observed (6.710 A^0 to 6.688 A^0). Average crystallite size increased with increase in x from 0 to 0.1 and then decreased for further increase in x. The electrical conductivity is found to be enhanced with x upto 0.01 and then decreased with further increase in x. The activation energies were calculated in both the conduction regions. The transport characteristics such as thermoelectric power, carrier concentration (n), mobility (μ), and barrier height (Φ_b) were studied as a function of the working temperature and materials composition and attempted to correlate with the observed changes in structural characteristics.

Keywords: DMS, Chemical growth process, Mn^{2+} magnetic ions, spin-spin exchange, lattice parameters.

 ISBN: 978-80-8152-530-8

Electrochemical Detection of Insulin

I. Sisolakova[a]*, J. Hovancova[a], R. Orinakova[a], A. Orinak[a], O.Petruš[a]

[a] *Pavol Jozef Safarik University of Kosice, Department of Physical Chemistry, Srobarova 2, 040 01, Kosice*

**ivana.smoradova@student.upjs.sk*

Diabetes mellitus (DM) is a heterogeneous metabolic disease characterized by chronic hyperglycemia [1]. Often, the symptoms are not sufficiently observable at early stages and so hyperglycemia causes that pathological and functional changes take place in advance, before the diagnosis of the disease [2]. Therefore, the development of sensors that are time saving, accurate, instrumentally undemanding are currently unavoidable.

This work deals with electrochemical determination of insulin on gold and carbon screen printed electrodes using cyclic voltammetry method. Mentioned electrodes have significantly smaller size compared to classic electrodes, achieving miniaturization of the system. The aim of the work was to find optimal conditions for insulin determination, while impact of pH and scan rate was observed. Based on the execution of measurements, correlation coeficient was determined, increase of which was obtained by modifying the electrodes with nanoparticles. In case of carbon screen printed electrode correlation coeficient was increased form -0,18 (unmodified electrode) to 0,87 (carbon electrode modified with CNTs and NiNPs). The active areas of the electrodes was also determined by the method of cyclic voltammetry. Modification with nanoparticles achieved a rapid increase of the active surfaces compared to the unmodified electrodes. In case of modification of gold screen printed electrode with the combination of CNTs and AuNPs, an increase of active area of the electrode was achieved by up to 183%.

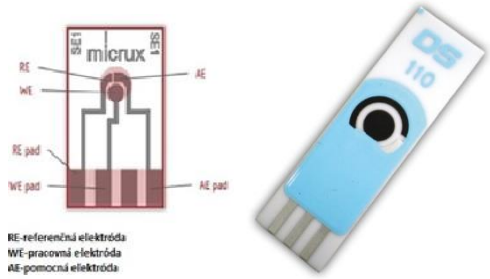

Figure 1 Gold screen printed electrode (left) and carbon screen printed electrode (right)

Acknowledgements

This work was supported by projects VEGA 1/0074/17 and APVV-16-0029

References

[1] S. D. Mathebula, African Vision and Eye Health. Polyol pathway: A possible mechanism of diabetes complications in the eye, **74** (2015) 1-5

[2] X. Bi, J. Lim, C. J. Henry, Food chem. Spices in the management of diabetes mellitus, **217** (2017) 281-293

 ISBN: 978-80-8152-530-8

Deposition of Cobalt Oxide Nanowires and their Possible Use in Electronic

J. Maca[a]*, J. Libich[a], M. Sedlarikova[a], S. Piazza[b], G. Ferrara[b],

[a] *Brno University of Technology, Department of Electrical and Electronic Technology, Technická 10, 616 00 Brno, Czech Republic*

[b] *Laboratorio di Chimica Fisica Applicata, Dipartimento di Ingegneria Chimica Gestionale Informatica Meccanica, Università di Palermo, Viale delle Scienze, 90128 Palermo, Italy*

**macaj@feec.vutbr.cz*

Introduction

The main goal of this paper is to show the manufacturing of nanowires deposition of cobalt oxide by help of anodic aluminium oxide membrane. The possible use in lithium batteries of these nanostructures is discussed. Higher and higher hunger for batteries, with will be lighter, more powerful and with high cycling number increase the pressure on research and development of new concepts and materials. In present time are new concepts like sodium batteries or lithium sulphur researched. Few of the main disadvantages of current most used batteries, lithium ion batteries, used in most of consumer electronics are high price, safety and the relative rarity of lithium in the earth's crust.

New more powerful devices required batteries with big capacity while maintaining present dimensions or smaller and thinner. One of the possible ways to achieve this is to use material with higher theoretical capacity. Possible change may be switching carbon negative electrode with theoretical capacity 372 $mAh \cdot g^{-1}$ by cobalt oxide Co_3O_4 with theoretical capacity of 890 $mAh \cdot g^{-1}$. For using of this material we need to change form current used intercalation principle to conversion principle.

Theoretical analysis

Nanostructured cobalt lure much attention thanks its properties in past. Its potential of use is wide spread in many areas or technology. Cobalt and its oxides can be used as catalyst in fuel cells, no corroding protection layer, in memory media, chemical sensor or batteries. The electro deposition of cobalt was research in different solution like sulphur or chlorine based solvents and others. The base for deposition carbon, cupper of silicon were used[1-3]. The conversion principle, with is needed for using of cobalt oxide in lithium ion batteries was already published for some oxides and sulphides with different degree of reversion like in high temperature cells[4,5]. In present time a few obstacles needed to be solved before of commercial use. To the main obstacles belongs large structural movement with caused the chemical reactions and volume change can cause the decomposition of the material and disallow large number of cycles. Large losses of energy density during charging and discharging. Large hysteresis between charging voltage plate and discharging plate. The last big obstacle is large columbic losses in performing the first cycle[6-8].

Experimental

For creation of nanostructures in form of nanowires was used deposition through membrane. As form for nanowires growth was the filtering membrane Whatman Anodisc 25 used. The diameter of the disc was 25 mm with porous diameter 0.2 µm. It was an anodic aluminium membrane (AAM). The solution form deposition was 0.01M $CoSO_4 \cdot 7\ H_2O$ and 0,1M CH_3COONH_4 (ammonium acetate) dissolved in water. The pH 7 was set by help of ammonium hydroxide dropped into the solution. The deposition took 1 hour at ambient temperature and voltage 1.2 V/SCE. The solution was mixed by help of magnetic stirrer at speed 300 rpm. After deposition the membrane was dissolved in 1M NaOH solution. The result and its EDS spectrum is on figure 1.

 ISBN: 978-80-8152-530-8

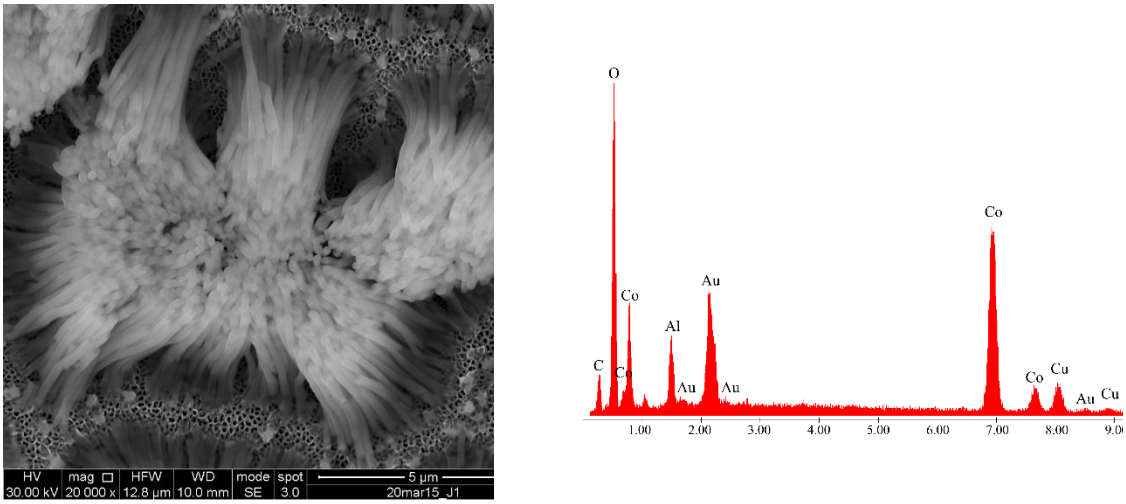

A) B)

Figure 1. A) deposed nanostructure at 20k magnification, B) sample EDS spectrum

Conclusion

On figure 1A is visible the wires structure, the length of the wire is 4.5 µm and diameter of 200 nm. The wires collapsed because of insufficient stability of the base. From the EDS spectrum (figure 1B) is obvious that the material is pure cobalt oxide. Traces of Au, Cu and C are from the background and manipulation support materials. By help of Raman spectroscopy, we determined that the wires are made from Co_3O_4 spinel structure.

Forded investigation of this material is necessary mainly in field of using it as negative electrode materials in lithium ion batteries.

Acknowledgements

This work was supported by project the Centre for Research and Utilization of Renewable Energy under project No. LO1210 – "Energy for Sustainable Development (EN-PUR)".

References

[1] F. Pagnanelli, P. Altimari, M. Bellagamba, G. Granata, E. Moscardini, P. G. Schiavi, L. Toro, *Pulsed electrodeposition of cobalt nanoparticles on copper: influence of the operating parameters on size distribution and morphology*. Electrochimica Acta. **155** (2015) 228-235

[2] E. M. Garcia, J.S. Santos, E. C. Pereira, M.B.J.G. Freitas, E. Moscardini, P. G. Schiavi, L. Toro, J. Power Sour. **185** (2008): 549-553.

[3] G. Ferrara, L. Damen, C. Arbizzani, R. Inguanta, S. Piazza, C. Sunseri, M. Mastragostino. J. Power Sour. **196** (2011) 1469-1473.

[4] J. Cabana, L. Monconduit, D. Larcher, M. R. Palacin, *Beyond Intercalation-Based Li-Ion Batteries: The State of the Art and Challenges of Electrode Materials Reacting Through Conversion Reactions.* Advanced Materials. (2010).

[5] J. Maca, M. Sedlarokova, J. Vondrak, J. Libich, M. Frk, *Metal Oxides use in Lithium Batteries*. In 36. Nekonvenční zdroje elektrické energie. (2015) 100-103.

[6] A. Fert, L. Piraux, E. C. Pereira, M.B.J.G. Freitas, E. Moscardini, P. G. Schiavi, L. Toro. J. Mag. Magnetic Mat. **200** (1998) 338-358.

[7] N. B. Chaure, P. Stamenov, F. M. F. Rhen, J. M. D. Coey, E. Moscardini, P. G. Schiavi, L. Toro, J. Mag. Magnetic Mat.. **290** (2005), 1210-1213.

[8] J. Xu, X. Huang, G. Xie, Y. Fang, D. Liu, P. G. Schiavi, L. Toro, *Fabrication and magnetic property of monocrystalline cobalt nanowire array by direct current electrodeposition: influence of the operating parameters on size distribution and morphology*, Materials Letters. (2005) **59**(8-9) 981-984.

 ISBN: 978-80-8152-530-8

Synthesis and Self-Assembly of Emitting Bone-Shaped Colloidal Nanocrystals

A. Castelli[a,b]*, A. Polovitsyn[a,c], L. Manna[a], M. P. Arciniegas[a]*

[a] *Nanochemistry Department, Istituto Italiano di Tecnologia, Via Morego 30, 16163 Genova, Italy*
[b] *Dipartimento di Chimica e Chimica Industriale, Università degli Studi di Genova, Via Dodecaneso, 31, 16146, Genova, Italy*
[c] *Dipartimento di Fisica, Università degli Studi di Genova, Via Dodecaneso, 33, 16146, Genova, Italy*

**andrea.castelli@iit.it; milena.arciniegas@iit.it*

Introduction

Nanocrystals (NCs) with anisotropic shapes offer versatile functionalities when compared to spherical quantum dots. For instance, polarized light emission arises from the anisotropy of a rod-like shell in CdSe/CdS core/shell dot-in-rods[1], while iron oxide nanocubes show superior heating performances in hyperthermia treatments compared to their spherical homologues[2]. In the field of self-assembled superlattices, anisotropic shapes allow the formation of a variety of unique configurations. This is due to the geometrical restrictions on the NC packing and the preferential interaction between their different facets[3-5]. In the last decade we have witnessed a surge of new synthetic protocols for the fabrication of colloidal NCs with complex shapes[6, 7]. Yet, the seeded growth technique stands as a versatile tool for the synthesis of highly anisotropic NCs, such as rods[8, 9] dumbbells[10], concave cubes[11], tetrapods,[12] and octapods[13]. In such liquid phase processing, pre-synthesized NCs are used (after purification) as seeds to grow further the particles. This strategy has key advantages, as i) it limits the formation of defects, since the seeds serves as heterogeneous nucleation sites for the shell growth[7, 14]; and ii) the seeds and the shell can have different chemical composition, thus creating core/shell nanostructures with unique properties[9, 10]. Importantly, the seed-geometry plays an essential role in regulating the shape of the resulting NCs, thus it can be seen as an interesting route to master highly complex NC morphologies. This is the case, for instance, of branched colloidal NCs (so called octapods) developed by our group[13, 15, 16]. This protocol exploits the {111} facets of $Cu_{2-x}Se$ octahedral or cuboctahedral seeds with cubic lattice to grow eight elongated CdS pods (with hexagonal lattice, h-CdS). In this work we explore the impact of a different shape of the pre-synthesized seeds on the NCs obtained following the octapod's protocol. We used as seeds particles with a platelet shape made of CdSe (with cubic lattice, c-CdSe). We found that the particles obtained preserve the elongated shape of the platelets and exhibit eight CdS pods at their corners, giving an overall bone shape. The pod length can be easily modified varying the amount of seeds employed in the synthesis: the more the seeds the shorter the pods. Interestingly, the platelets undergo anion exchange in the reaction and form cubic CdS (c-CdS). This completely modifies the photoluminescence (PL) spectrum of the resulting nanobones, whose peak shifts from 516 nm (platelets) to 660 nm. Finally, we explore the assembly behaviour of the nanobones in planar superlattices by using an air-liquid interface assembly strategy[17]. Preliminary results show that the nanobones tend to form domains with different translational order, such as shifted side-by-side contact or herringbone friezes. With this, we show the potential of this strategy to create highly anisotropic NCs not observed before with interesting self-assembled superlattices.

Results and discussion

In the present work we followed a protocol already reported by our group for the synthesis of octapods with a pod length of 15 nm to 30 nm[18], and we employed CdSe nanoplatelets with a length of 30 nm and a width of 5.5 nm [19] as seeds (see Figure 1a). Briefly, we injected an aliquot of nanoplatelets together with a mixture of trioctylphosphine (TOP) and sulphur in a reaction flask containing CdO, $CdCl_2$, trioctyphospine oxide (TOPO), hexylphosphonic acid (HPA) and octadecylphosphonic acid (ODPA) at 350°C in inert atmosphere. The reaction was stopped by a fast cooling after 10 min and the solutions were purified via several solvent-antisolvent precipitation steps. We performed the synthesis using three different concentration of nanoplates (2 nmol, to 1.2 nmol to 0.4 nmol) to evidence possible changes in the shape of the synthesized NCs. Figure 1b shows a collection of transmission electron microscopy (TEM) images of the resulting NCs. As it can be seen the resulting particles present an elongated body that preserve the length of the starting platelets but with double of their width, giving an approximate area of 30 x 10 nm^2. They also present eight pods protruding one from each corner of the body. We observed that the pod length changes, from ca. 4 nm to 20 nm, by reducing the amount of injected seeds. From the observation of the final particles morphology, different overgrowth mechanisms seem to take place along the two main directions of the platelets: along their width ($[010]_{c\text{-}CdSe}$ direction[20]) the growth simply extends the size of the particle, while along the length ($[100]_{c\text{-}CdSe}$ [20]) the growth is somehow impeded resulting in pods developing outside the (001) plane that contains the main surface of the platelet. X-ray diffraction from the samples (Figure 1c) shows that the particles are formed only by CdS and both cubic and hexagonal polymorphs are present.

 ISBN: 978-80-8152-530-8

The h-CdS peaks intensity increases with pod length, suggesting that the nano-bones are formed by a flat c-CdS body and h-CdS pods. Inductively coupled plasma analysis on digested samples supports the elimination of Se from the final product. The Se lack from the nanobones and the presence of a flat c-CdS body suggest that the starting c-CdSe platelets undergo anion exchange during the reaction.

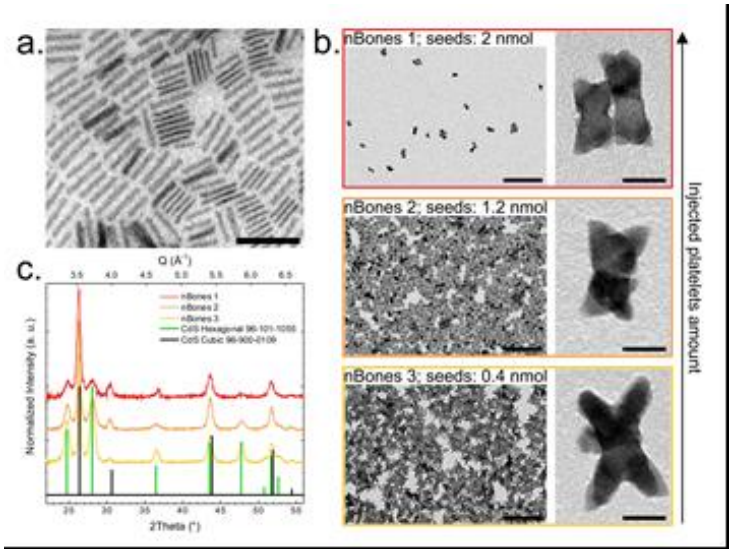

Figure 1: a.b, TEM images of the CdSe platelets employed as seeds in the syntheses (a) and of the resulting nanobones synthesized with different amounts of nanoplatelets (b). Scale bars: (a) 50 nm, (b) 200 nm (left) and 20 nm (right). **c.** Collected XRD patterns of the synthesized NCs. The patterns for h-CdS and c-CdS are used as a reference (solid lines).

This radical structural transformation of the particles is reflected in their optical properties. Under UV irradiation all the nanobones show a saturated red luminescence (Figure 2a) with a peak at 660 nm and a full width at half maximum (FWHM) of ca. 40 nm. Their CIE coordinates are around (0.70; 0.28), as evaluated from the nanobones with shorter pods (Figure 2b). This marks a considerable blueshift and peak broadening compared to the seeds employed, that showed a PL maximum at 516 nm, FWHM of 10 nm and (0.16; 0.72) CIE coordinates. The broadening of the PL peak, in particular, suggests that the exciton in the nanobones is not confined anymore. Absorption measurements (Figure 2a) show that the excitonic features, present at the absorption edge of CdSe seeds, disappear in the nanobones, leaving the bulk CdS absorption around 500 nm. This suggests that the c-CdS body grew not only along the [010] direction, but also along the [001] one. Finally, the remarkable Stokes shift between the absorption edge and the PL maximum (ca. 0.5 eV) is an indication that absorption and emission are spatially separated: the first probably takes place in the h-CdS pods, while the from the c-CdS body.

As demonstrated by our group with octapods[18, 21-23], the strong anisotropy of nanobones makes them appealing for the production of self-assembled, ordered structures. Preliminary results on their behaviour at the liquid-air interface[17, 18] show a tendency to form stripes of particles organized side by side or forming a herringbone pattern (Figure 2c). Obtaining an extended ordered film might show interesting properties of polarized emission, as demonstrated by CdSe/CdS dot-in-rods[24], which, coupled to their saturated red emission and remarkable Stokes shift, could be appealing in light emitting diodes for RGB technology.

 ISBN: 978-80-8152-530-8

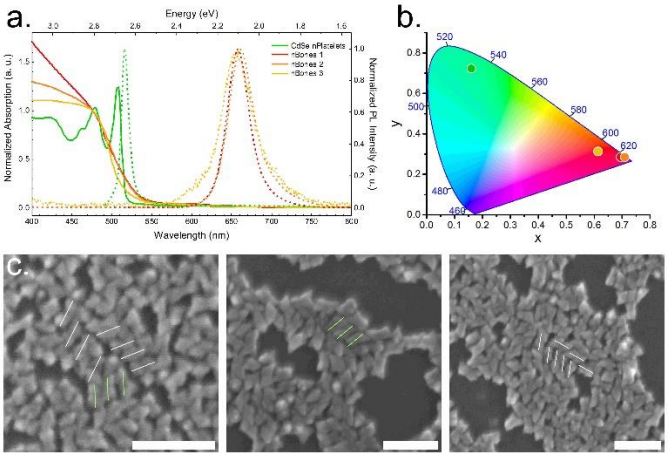

Figure 2: a. Collected absorption (solid lines) and emission (dashed lines) spectra of nanobones reported in Figure 1 and of the platelets employed as seeds in their synthesis. **b.** CIE coordinates of the nanobones and nanoplatelets. **c.** Collection of high resolution SEM images of the self-assembled membranes formed by nanobones at liquid-air interface. Green lines highlight the particles aligned side-by-side and white lines those disposed as a herringbone. Scale bars 100 nm.

Conclusion

We show that, changing the morphology of the seeds from cuboctahedra to platelets in an established protocol for the growth of eight h-CdS pods, we were able to produce highly anisotropic CdS NCs. This was obtained through a controllable "one-pot" synthesis in which an anion exchange takes place. The nanoparticles own a shape that resembles a bone, with a flat and elongated c-CdS central body and one h-CdS pod in each corner. The length of the pods depends on the amount of seeds employed and it varies between 4 nm and 20 nm, while the body sizes are constant at 30 x 10 nm^2. The nanobones, independently from the pod length, exhibit a red emission centred at 660 nm, while the absorption edge is situated at 500 nm. Preliminary results on their 2D self-assembly show a promising ability of the particles to form ordered domains with different geometries, like shifted, side-by-side arrangement and herringbone-like friezes. Their shape with multiple concavity, moreover, makes them appealing for further studies on host-guest binary assemblies with shape complementary particles.

References

1. Pisanello, F., et al., *Dots in rods as polarized single photon sources.* Superlattices and Microstructures, 2010. **47**(1): p. 165-169.
2. Guardia, P., et al., *One pot synthesis of monodisperse water soluble iron oxide nanocrystals with high values of the specific absorption rate.* Journal of Materials Chemistry B, 2014. **2**(28): p. 4426-4434.
3. Quan, Z. and J. Fang, *Superlattices with non-spherical building blocks.* Nano Today, 2010. **5**(5): p. 390-411.
4. Zanella, M., et al., *Assembly of shape-controlled nanocrystals by depletion attraction.* Chemical Communications, 2011. **47**(1): p. 203-205.
5. Ye, X., et al., *Competition of shape and interaction patchiness for self-assembling nanoplates.* Nature Chemistry, 2013. **5**(6): p. 466-473.
6. Peng, X., *Mechanisms for the Shape-Control and Shape-Evolution of Colloidal Semiconductor Nanocrystals.* Advanced Materials, 2003. **15**(5): p. 459-463.
7. Tao, A.R., S. Habas, and P. Yang, *Shape Control of Colloidal Metal Nanocrystals.* Small, 2008. **4**(3): p. 310-325.
8. Jana, N.R., L. Gearheart, and C.J. Murphy, *Seed-Mediated Growth Approach for Shape-Controlled Synthesis of Spheroidal and Rod-like Gold Nanoparticles Using a Surfactant Template.* Advanced Materials, 2001. **13**(18): p. 1389-1393.
9. Carbone, L., et al., *Synthesis and Micrometer-Scale Assembly of Colloidal CdSe/CdS Nanorods Prepared by a Seeded Growth Approach.* Nano Letters, 2007. **7**(10): p. 2942-2950.

 ISBN: 978-80-8152-530-8

10. Najafishirtari, S., et al., *The effect of Au domain size on the CO oxidation catalytic activity of colloidal Au–FeOx dumbbell-like heterodimers.* Journal of Catalysis, 2016. **338**(Supplement C): p. 115-123.

11. Zhang, J., et al., *Concave Cubic Gold Nanocrystals with High-Index Facets.* Journal of the American Chemical Society, 2010. **132**(40): p. 14012-14014.

12. Talapin, D.V., et al., *Seeded Growth of Highly Luminescent CdSe/CdS Nanoheterostructures with Rod and Tetrapod Morphologies.* Nano Letters, 2007. **7**(10): p. 2951-2959.

13. Deka, S., et al., *Octapod-Shaped Colloidal Nanocrystals of Cadmium Chalcogenides via "One-Pot" Cation Exchange and Seeded Growth.* Nano Letters, 2010. **10**(9): p. 3770-3776.

14. Richard, P.S., *Nucleation: theory and applications to protein solutions and colloidal suspensions.* Journal of Physics: Condensed Matter, 2007. **19**(3): p. 033101.

15. Kim, M.R., et al., *Influence of chloride ions on the synthesis of colloidal branched CdSe/CdS nanocrystals by seeded growth.* ACS Nano, 2012. **6**(12): p. 11088-11096.

16. Brescia, R., et al., *Birth and Growth of Octapod-Shaped Colloidal Nanocrystals Studied by Electron Tomography.* The Journal of Physical Chemistry C, 2011. **115**(41): p. 20128-20133.

17. Dong, A., et al., *Binary nanocrystal superlattice membranes self-assembled at the liquid–air interface.* Nature, 2010. **466**(7305): p. 474-477.

18. Castelli, A., et al., *Tic-Tac-Toe Binary Lattices from the Interfacial Self-Assembly of Branched and Spherical Nanocrystals.* ACS Nano, 2016. **10**(4): p. 4345-4353.

19. Bertrand, G.H.V., et al., *Shape control of zincblende CdSe nanoplatelets.* Chemical Communications, 2016. **52**(80): p. 11975-11978.

20. Ithurria, S., G. Bousquet, and B. Dubertret, *Continuous Transition from 3D to 1D Confinement Observed during the Formation of CdSe Nanoplatelets.* Journal of the American Chemical Society, 2011. **133**(9): p. 3070-3077.

21. Miszta, K., et al., *Hierarchical self-assembly of suspended branched colloidal nanocrystals into superlattice structures.* Nature Materials, 2011. **10**(11): p. 872-876.

22. Arciniegas, M.P., et al., *Self-Assembly of Octapod-Shaped Colloidal Nanocrystals into a Hexagonal Ballerina Network Embedded in a Thin Polymer Film.* Nano Letters, 2014. **14**(2): p. 1056-1063.

23. Qi, W., et al., *Ordered Two-Dimensional Superstructures of Colloidal Octapod-Shaped Nanocrystals on Flat Substrates.* Nano Letters, 2012. **12**(10): p. 5299-5303.

24. Rizzo, A., et al., *Polarized Light Emitting Diode by Long-Range Nanorod Self-Assembling on a Water Surface.* ACS Nano, 2009. **3**(6): p. 1506-1512.

 ISBN: 978-80-8152-530-8

Exposure of Primary Human Leukocytes and Hematopoietic Stem Cells to Graphene Quantum Dots

S. Fasbender[a*], S. Allani[a], C. Wimmenauer[a], R.P. Cadeddu[b], K. Raba[c], J. Fischer[c], B. Bulat[d], M. Luysberg[e], C. Seidel[d], T. Heinzel[a] and R. Haas[b]

[a]*Condensed Matter Physics Laboratory, Heinrich-Heine-University, 40204 Düsseldorf, Germany*
[b]*Department of Haematology, Oncology and Clinical Immunology, Heinrich-Heine-University, 40204 Düsseldorf, Germany*
[c]*Institute for Transplantation Diagnostics and Cell Therapeutics, Heinrich-Heine-University, 40204 Düsseldorf, Germany*
[d]*Institute of Molecular Physical Chemistry, Heinrich-Heine-University, 40204 Düsseldorf, Germany*
[e]*Ernst Ruska-Centre, Jülich Research Centre, 52425 Jülich, Germany*

**Stefan.Fasbende@hhu.de*

Graphene quantum dots (GQDs) are often considered as promising candidates for biological applications like long term imaging of cells [1], cancer diagnostics [2] and therapeutic tumor targeting [3] as they are non toxic, chemically stable and inexpensive to prepare. GQDs consist of single or few layer graphene sheets with less than 30 nm diameter and emit a stable photoluminescence due to quantum confinement and edge effects. Nevertheless the reliable preparation is still a challenge and the interaction of GQDs with primary human cells has been scarcely studied.

In the present work primary human leukocytes and hematopoietic stem cells obtained from samples of leukapheresis products of three healthy donors stimulated by granulocyte colony stimulating factor (G-CSF) were exposed to GQDs prepared by the reproducible preparation process of Wu et al. [4]. A time- and concentration dependent uptake was observed with a significantly greater uptake into monocytes and granulocytes in comparison to lymphocytes, suggesting a better incorporation ability of cells with phagocytotic properties. The uptake rates also correlate with the cell membrane area. Looking at the different lymphoid subsets a greater uptake was found into $CD19^+$ B-, $CD56^+$ natural killer cells and $CD34^+$ hematopoietic stem cells in comparison to $CD4^+$ T- and $CD8^+$ T cells. Independent of the cell type studied, the observed uptake dynamics is consistent with a diffusion-driven process, which allows the determination of cell-specific membrane permeabilities for the graphene quantum dots. The toxicity of the quantum dots is relatively low resulting in a 90% viability of the entire leukocyte population after 36 hours of exposure to GQDs at a concentration of 500 $\mu g\ ml^{-1}$.

Acknowledgements

The first author acknowledges financial support of his position by the Düsseldorf School of Oncology (DSO). T.H. acknowledges support by the Betz foundation. Support regarding the XPS analysis by A. Besmehn and H. Hartmann (FZ Jülich), as well as access to the confocal microscope at the Center of Advanced imaging (CAI) of HHU Düsseldorf, is gratefully acknowledged. The authors thank S. Wesselborg for his advice regarding the toxicity studies.

References

[1] J. K. Jaiswal, H. Mattoussi, J. M. Mauro and S. M. Simon, *Nat. Biotechnol.* **21** (2002), 47–51

[2] B. A. Kairdolf, A. M. Smith, T. H. Stokes, M. D. Wang, A. N. Young and S. Nie, *Annu. Rev. Anal. Chem.* **6** (2013), 143

[3] V. Bagalkot, L. Zhang, E. Levy-Nissenbaum, S. Jon, P. W. Kantoff, R. Langer and O. C. Farokhzad, *Nano Lett.* **7** (2007), 3065

[4] Z. L. Wu, M. X. Gao, T. T. Wang, X. Y. Wan, L. L. Zheng and C. Z. Huang, *Nanoscale* **6** (2014), 3868.

 ISBN: 978-80-8152-530-8

Silver nanoparticles and plant extracts complexes as stimulants for the healing process of skin wounds

E. Tomaszewska[1], K. Ranoszek-Soliwoda[1], G. Celichowski[1],
E. Mackiewicz[1], P. Orłowski[2], M. Krzyżowska[2], J. Grobelny[1]

[1] *Department of Materials Technology and Chemistry, Faculty of Chemistry, University of Lodz, Pomorska 163, 90-236 Lodz, Poland*

[2] *Independent Laboratory of Nanobiology and Biomaterials, Military Institute of Hygiene and Epidemiology, Kozielska 4, 01-163 Warsaw*

**etomaszewska@uni.lodz.pl*

Silver nanoparticles (AgNPs) have been widely used as antimicrobial, immunomodulating and pro-regenerative agents. It is well known that the properties of NPs strictly depends on size, shape and surface modification as well as the method of synthesis. Tannins (polyphenols and flavonoids, which are components of plant extracts) that exhibit reducing properties can be used in nanoparticles synthesis, they are produced by plant to protect them from being infected by pathogens. Chemically, tannins are phenolic derivatives. Due to their structure and reactivity they are divided into two groups: hydrolysable and condensed.

The synthesis of AgNPs with plant extracts are known as green synthesis of NPs for many years. The synthesis is based on the reduction of silver ions to AgNPs by compounds present in extract and its further stabilization. However, the use of plant extracts in NPs synthesis leads to particles inhomogeneity in size and shape. This work presents the method of synthesis of monodisperse spherical AgNPs using two plant extracts: i) grape seed (*Vitis vinifera*) and ii) cacao beans (*Theobroma cacao*) along with the additional reducing agent - sodium citrate. The colloids were characterized by UV-Vis spectroscopy and dynamic light scattering technique, while the shape and size of the AgNPs core were determined using scanning transmission electron microscopy. Final conjugated materials containing AgNPs and tannins can be used as potential skin healing aids.

Acknowledgements

This work was co-financed by the NCN project No. UMO 2014/13/B/NZ5/01356 and by University of Lodz, Subsidy for scientific research contributing to the development of young young researchers and PhD students - B1711100001603.02.

 ISBN: 978-80-8152-530-8

Iron based biomaterials with polymer coating

Lucia Markušová-Bučková[a*], Renáta Oriňaková[a], Andrej Oriňak[a], Radka Gorejová[a], Miriam Kupková[b], Monika Hrubovčáková [b], Matej Baláž [c], Petr Vanýsek[d], Pavol Mudroň[e], Karol Kovál'[b]

[a]*Department of Physical Chemistry, Faculty of Science, P. J. Šafárik University, Moyzesova 11, SK-04154 Košice, Slovak Republic*

[b]*Institute of Materials Research, Institute of Material Research, Slovak Academy of Sciences, Watsonova 47, SK-04001 Košice, Slovak Republic*

[c]*Institute of Geotechnics, Slovak Academy of Sciences, Watsonova 45, SK-04001 Košice, Slovak Republic*

[d]*CEITEC-Central European Institute of Technology BUT, Purkyňova 123, CZ-61200 Brno, Czech Republic and Department of Chemistry and Biochemistry, Northern Illinois University, DeKalb, IL, USA*

[e]*Clinic of Ruminants, University of Veterinary Medicine and Pharmacy in Košice,Košice, Slovak Republic*

[*]*markusovabuckova@gmail.com*

Biodegradable implants received increased attention due to their use in various fields of medicine. Iron based materials coated with polyethylene glycol (PEG) were prepared as a potential biodegradable bone implants. Degradation behaviour was studied by anodic polarisation method and immersion test. The degradation rate of open cell materials with polyethylene glycol coating layer was faster compared to uncoated Fe sample. Also the mass losses were higher for samples with PEG coating. The polymer coating brought about the desired increase in degradation rate of porous iron material.

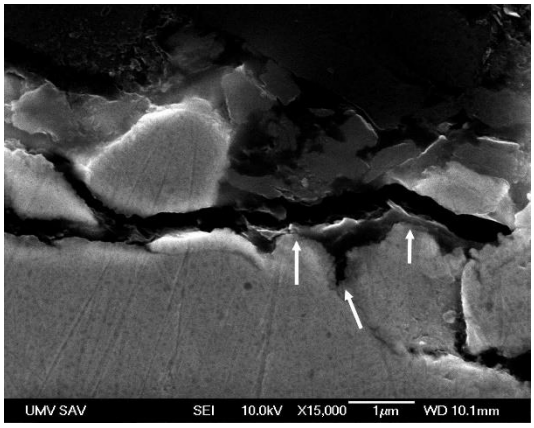

Figure 2 Micrograph of polymer coating layer on the surface of Fe-PEG3 sample (white arrow).

Acknowledgements

This work was supported by projects VEGA 1/0074/17 and APVV-16-0029

 ISBN: 978-80-8152-530-8

Radiobiological Research in Laboratory of Radiation Biology of JINR

M. Lalkovičová [ab]*,

[a] *Laboratory of Radiation Biology, Joint Institute for Nuclear Research, Joliot-Curie 6, 141980, Dubna, Moscow Region, Russia*

[b] *Slovak Academy of Sciences in Košice, Institute of Experimental Physics, Watsonova 47, 04001 Košice, Slovakia*

* *lalkovicova@saske.sk*

The Joint Institute for Nuclear Research (JINR) is a unique international scientific center hosting a diversity of nuclear physics facilities, which generate ionizing radiations with different physical characteristics. For many years, it has attracted specialists from many countries to conduct fundamental research not only in physics, but also in biology. Accelerated charged particles are an efficient tool for solving a lot of urgent problems of modern radiobiology and biophysics.

In Laboratory of radiation biology (LRB) of JINR the investigations were focused on the regularities and mechanisms of molecular disorders in genetic structures of mammalian and human cells, formation of mutations of different types in lower and higher eukaryotes, and radiation damage to eye structures and central nervous system caused by ionizing radiations of different quality. In the course of radiation genetics research, studied in detail were regularities in the formation and repair kinetics of DNA double-strand breaks (DSBs) induced by accelerated heavy ions [1]. It has been shown that in human cell nuclei there are sharp differences in the spatial distribution of damage induced by gamma rays and accelerated heavy ions. After gamma exposure, lesions in cells are distributed randomly; after heavy ion exposure, they are localized along the ion tracks, thus forming "tracks" of clustered DNA DSBs.

In view of the above, the solution of the mentioned fundamental and practical problems, especially in space radiobiology [2], urgently requires. To take into account the high biological effectiveness of high-energy heavy charged particles in radiation risk evaluation for manned interplanetary flights, the concept of "the successful completion of the mission" was introduced by radiobiologist in LRB [3]. Unlike the currently used radiation risk concept, which brings into the foreground the risk of cancer development – the long-term effects of the exposure, the new paradigm is concerned, first of all, with the risk of disorders of higher integrative functions of the crew members' central nervous system. These disorders can impair cosmonauts' operator functions already during the flight and endanger the successful completion of the mission. In many model experiments conducted in LRB biological effects were observed in the central nervous system (CNS) of experimental animals under the influence of heavy carbon ions ^{12}C, γ-rays and protons. It was shown that irradiation of the rodents by charged particles determines the functional, morphological and genetical disorders in CNS structures. The dynamics of formation of changes in the CNS indicates the presence of more pronounced radiation effects in the neurons when irradiated with these particles.

References

[1] Falk, M. Lukasova, E. Falkova, I. Davidkova, M. Bacıkova, A. et al. *Primary and secondary clustering of DSB repair foci and repair kinetics compared for γ-rays, protons of different energies and high-LET 20Ne ions*. Journal of Radiation Research **55** (2014) 79-80.

[2] Parihar, V.K. Allen, B. Tran, K.. et al. *What happens to your brain on the way to Mars*. Sci. Adv. 1. № 4 – 2015 – V.1 - e1400256.

[3] Grigor'ev, A. I. Krasavin, E.A. Ostrovski, M. A. *Assessment of the Risk of the Biological Actions of Galactic Heavy Ions to Interplanetary Flight.* Neuroscience and Behavioral Physiology **45** (2015) 91-95.

 ISBN: 978-80-8152-530-8

Nanomaterials employed for electrochemical sensing, biosensing and energy applications

J. Tkac[a]*, T. Bertok[a], L. Lorencova[a], L. Belickaa, A. Holazova[a], E. Chocholova[a], F. Kveton[a], P. Kasak[b]

[a] *Institute of Chemistry, Slovak academy of Sciences, Dubravska cesta 9, 845 38, Bratislava, Slovakia*
[b] *Qatar University, P.O. Box 2713, Doha, Qatar*

**Jan.Tkac@savba.sk*

Four different types of nanomaterials will be presented including gold nanoparticles, graphene oxide, MXene (2D nanomaterial) and human serum albumin (HSA, as a biocompatible scaffold) for construction of electrochemical sensors, biosensors and bioanodes of biofuel cells.

Gold nanoparticles (AuNPs) were applied for modification of gold electrodes patterned by self-assembled monolayer. Such electrodes were utilised for affinity biosensing using electrochemical impedance spectroscopy (EIS) as a detection platform. AuNPs-modified biosensors (3D configuration) offered much lower limit of detection compared to the biosensor configuration without using AuNPs (2D configuration) [1, 2].

Graphene oxide (GO) was successfully applied for modification of electrodes for construction of affinity-based biosensors and for preparation of a bioanode. EIS-based affinity biosensors with immobilised lectins (carbohydrate binding proteins) were successfully utilised for detection of glycoproteins down to aM level (10^{-18} M) [3, 4]. Protocol of immobilisation of bilirubin oxidase (BOD) on GO affected current density for oxygen reduction significantly from 2.6 μA cm^{-2} to 280 μA cm^{-2} [5]. GO flakes with a tuned density of a negative charge significantly influenced density and orientation of BOD immobilised by a passive physisorption with the highest current density of 597 μA cm^{-2} [6].

Besides GO we applied in our studies another 2D nanomaterial – Mxene. Using this nanomaterial we were able to detect H2O2 down to 0.7 nM with one of the highest sensitivity of H2O2 detection observed so far i.e. 596 mA cm^{-2} mM^{-1} [7].

The last type of nanomaterial HSA was applied in our studies as a scaffold for immobilisation of small glycan antigen. The glycan biosensor was then applied for detection of an antibody, what is an approach applicable for analysis of glycan autoantibodies, which are considered as biomarkers of various types of cancer [8].

Acknowledgements

The research leading to these results has received funding from the European Research Council under the European Union's Seventh Framework Program (FP/2007-2013)/ERC Grant Agreement No. 311532, from the European Union's Seventh Framework Program for research, technological development and demonstration under grant agreement No. 317420, from Slovak Scientific Grant Agency VEGA 2/0162/14 and from Slovak Research and Development Agency APVV-14-0753.

References

[1] T. Bertok, A. Sediva, J. Katrlik, P. Gemeiner, M. Mikula, M. Nosko, J. Tkac, Talanta, **108** (2013) 11-18.
[2] P. Jolly, P. Zhurauski, J.L. Hammond, A. Miodek, S. Liébana, T. Bertok, J. Tkáč, P. Estrela, Sens. Actuat. B: Chem., **251** (2017) 637-643.
[3] L. Klukova, J. Filip, Š. Belický, A. Vikartovska, J. Tkac, Analyst, **141** (2016) 4278-4282.
[4] J. Filip, S. Zavahir, L. Klukova, J. Tkac, P. Kasak, J. Electroanal. Chem., **794** (2017) 156-163.
[5] J. Filip, J. Tkáč, Electrochem. Commun., **49** (2014) 70-74.
[6] J. Filip, A. Andicsová-Eckstein, A. Vikartovská, J. Tkac, Biosens. Bioelectron., 89 (2017) 384-389.
[7] L. Lorencova, T. Bertok, E. Dosekova, A. Holazova, D. Paprckova, A. Vikartovska, V. Sasinkova, J. Filip, P. Kasak, M. Jerigova, Electrochim. Acta, **235** (2017) 471-479.
[8] F. Kveton, A. Blšáková, A. Hushegyi, P. Damborsky, O. Blixt, B. Jansson, J. Tkac, Langmuir, **33** (2017) 2709-2716.

 ISBN: 978-80-8152-530-8

Gel Polymer Electrolytes Modified Nanoparticles

I. Gracheva[a*], M. Jahn[a], M. Sedlaříková[a]

[a] *Department of Electrical and Electronic Technology, The Faculty of Electrical Engineering and Communication Bro University of Technology, Technická 10, Brno 612 00, Czech Republic*

[*] *xgrach00@vutbr.cz*

Introduction

Gel polymer electrolytes have an important role in the transfer of electrones and lithium ions during charging and discharging processes. It is also one of the key factors which influence the effectiveness and efficiency of the battery. The current development of gel polymer electrolytes mainly focuses on increasing of ion conductivity, expanding the potencial window and impoving the chemical and electrochemical stability of the polymer and solvent from the viewpoint of long-term properties. Compared to liquid gel electrolytes have many advantages. Gel electrolytes are more resistant to vibration, mechanical stress and damage, high pressures or temperatures; characterized by great resistance to volume changes and a good adhesion of gel to the surface the electrode. Also eliminate the risk of electrolyte leakage. The research is focused on improving electrical, electrochemical and mechanical properties of gel polymer electrolytes exposure with the addition of nanoparticles [1,4,6,7].

Nanoparticles are characterized by a size from about 1 nm to about 100 nm in at least one direction (10^{-7} to 10^{-9}), and in certain spatial arrangement may create form nanowires, nanotubes, nanocomposites, ceramic or other thin films or layers. Nanoparticles have many useful properties than those given by their chemical composition. These properties may fundamentally differ from the anticipated chemical or physical behavior. And there is a continual discovery of new properties [6,7].

Chemical composition and preparation

The gel electrolyte consists of a conductivity component and a polymer component. In this case the conductivity component was formed by lithium salt $LiPF_6$ and combination of solvents EC/DEC in a weight ratio 1:1. Polymer component was formed by monomer methyl methacrylate, the crosslinking agent – ethylene glycol dimethacrylate and initiator of UV polymerization – benzoin ethyl ether. The molar ratio of monomer to the conductivity component was chosen in ratio of 20 mol% (salt concentration 0,5 mol/l in solvent). The molar proportion of polymerization initiator and crosslinking agent to the monomer was chosen for the initiator 1,0 mol% and for the crosslinking agent 3,5 mol% [2,3,4,5]. Nanoparticiples were added to improve electrical, electrochemical and mechanical properties of gel polymer electrolytes. In this work were selected the following nanoparticles:

- Al_2O_3 – aluminium oxide
- WO_3 – tungsten(VI) oxide
- ZrO_2 – zirconium dioxide
- La_2O_3 – lanthanum oxide

Gel sample is the circular gel with diameter of 16 mm and thickness of 0,9 mm. Preparation of all gel samples and manipulation with them took place in gloverbox with an argon atmosphere. The polymerization process was carried out in a UV chamber for 60 minutes. For all samples electrical and electrochemical properties were investigated.

Experimental part

In the experimental part samples of gel polymer electrolytes with the addition of selected nanoparticles were measured. Quantity, resp. weight of these nanoparticles were added in percentage to the base gel at 0,5% to 15%. The base gel was taken as 100% by weight, which was attributed to the weight percentage of individual nanoparticles [7].

For measuring electrical conductivity was used impedance spectroscopy method. The impedance measuring range was selected from 1 MHz to 0,1 Hz. Measurement results are shown in Table 1 and Picture 1.

Measurement of samples of gel polymer electrolytes modified nanoparticles was performed using TGA and DTA methods, which are call the thermal analyzes. The aim of these analyzes was to determine the influence of nanoparticles on thermal stability and properties of samples. For TGA and DTA were selected gel polymer electrolytes, which contained Al_2O_3 - 7,5%, WO_3 – 5%, ZrO_2 – 1% and La_2O_3 – 1%. Of all samples were cut into small rectangles, which were placed in the device TG-DTA-EGA, which is compose of the TG-DTA part from

 ISBN: 978-80-8152-530-8

TA Instruments Q600 and the THERMO NICOLET IS100 infrared analyzer. This device was used to determine chemical, phase and mass changes during hearting of the prepared sample. For the determination and subsequent comparison of the prepared gel samples, the same parameters were set for all measurements: initial temperature 30˚C, end temperature 600˚C and hearting rate 5˚C/min. Results of thermal analyzes are illustrate in Picture 2 and Picture 3.

Tab. 1: Electrical conductivity of gel polymer electrolytes with nanoparticles [7]

Al_2O_3									
V_N [%]	0,5	1	2,5	5	7,5	10	12,5	15	17,5
γ [mS/cm]	2,69	2,28	4,88	2,27	7,76	4,34	1,65	1,44	3,06
WO_3									
V_N [%]	0,5	2,5	5	7,5	10	12,5	15		
γ [mS/cm]	2,60	2,36	3,23	2,27	2,92	2,29	2,21		
ZrO_2									
V_N [%]	0,5	1	2,5	5	10	12,5	15		
γ [mS/cm]	2,16	5,64	2,31	1,78	3,96	2,44	2,60		
La_2O_3									
V_N [%]	0,5	1	2,5	5	7,5	10	12,5	15	
γ [mS/cm]	2,38	3,64	1,63	3,35	1,78	2,53	1,64	1,18	

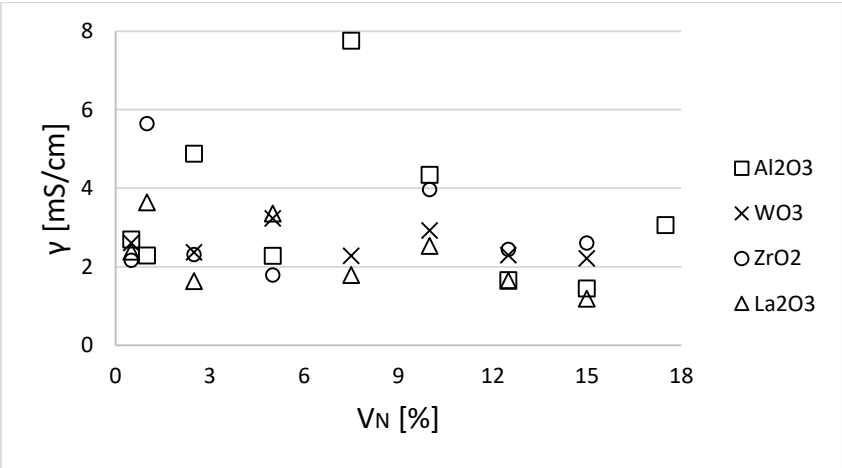

Pic. 1: Graf of electrical conductivity depending on the volume of added nanoparticles

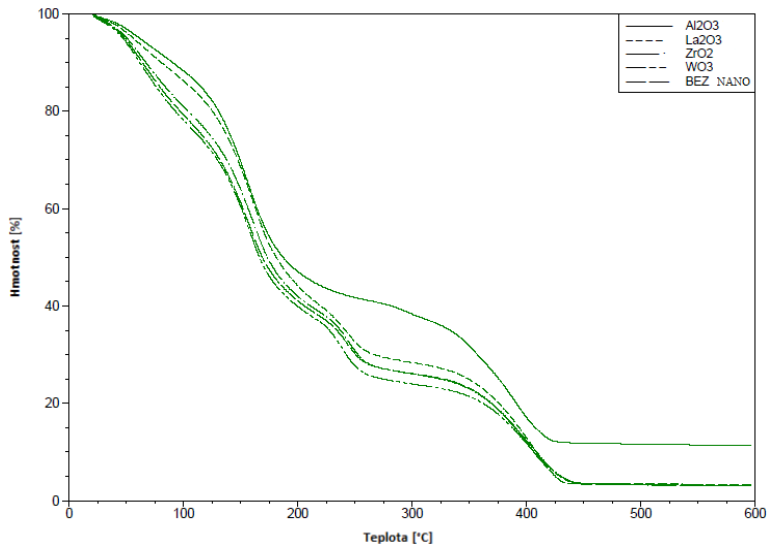

Pic. 2: Comparison weight loss of all prepared samples in percentage [7]

 ISBN: 978-80-8152-530-8

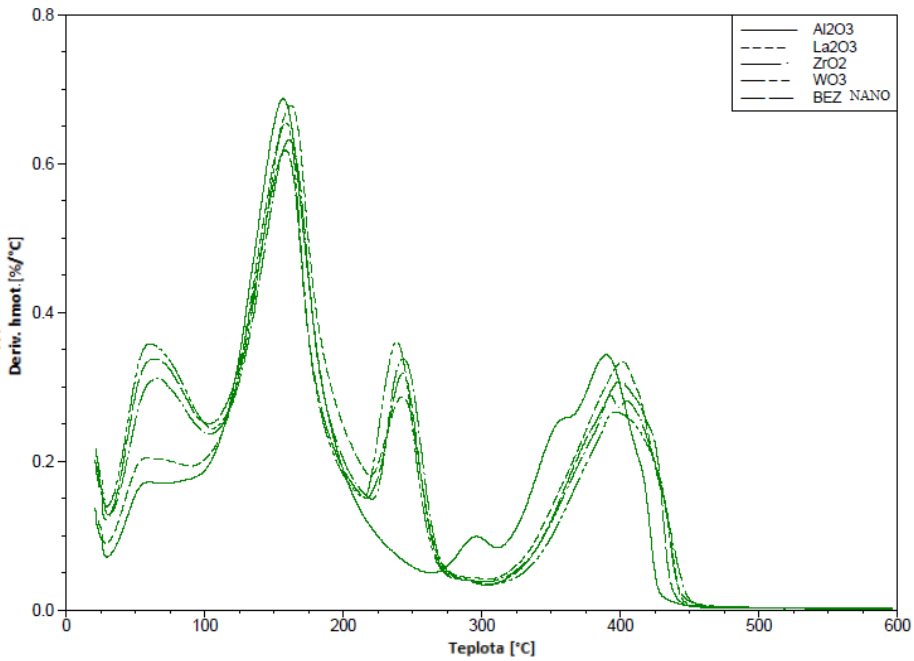

Pic. 3: Differential form of weight loss [7]

Conclusion

The measured and evaluated results show that adding a certain amount of nanoparticles impove the ionic conductivity of gel electrolyte and its electrochemical stability. Graf of electrical conductivity show that the highest values attain samples with the addition of nanoparticles in the range 1-10% weight percentage. The ionic conductivity of most samples ranges between 2-3 mS/cm. The highest value of ionic conductivity 7,76 mS/cm achieved a gel polymer electrolyte with Al_2O_3 percentage volume 7,5%. Regarding thermal analyzes the lowest total weight loss was recorded in the gel sample with nanoparticle Al_2O_3 – 89,17%. The temperature of lowest weight loss was 159˚C. Further research will focus on implementation of thermal analysis on air and comparison results. Other reseach will focus on the using new type of nanoparticles and measuring their electrical, electrochemical and mechanical properties.

References

[1] M. Cafourek, *New polymer gel electrolytes*, The Faculty of Electrical Engineering and Communication Bro University of Technology, Brno (2010).
[2] I. Gracheva, *Gel polymer electrolytes with flame retardants*, The Faculty of Electrical Engineering and Communication Bro University of Technology, Brno (2016).
[3] I. Gracheva, M. Jahn, M. Sedlaříková, J. Vondrák, *Gel polymer electrolytes with fire retardants*, In *38. Nekonvenční zdroje elektrické energie*. 1. Hustopeče: Česká elektrotechnická společnost, (2017), page 145-148.
[4] M. Jahn, *Gel polymer electrolytes for electrochemical power sources*, The Faculty of Electrical Engineering and Communication Bro University of Technology, Brno (2016)
[5] M. Jahn, M. Pospíšilová, M. Sedlaříková, J. Vondrák, *Gel polymer electrolytes modified ionic liquids*, In *38. Nekonvenční zdroje elektrické energie*. 1. Hustopeče: Česká elektrotechnická společnost, (2017), page 27-31.
[6] R. Szotkowski, M. Jahn, M. Sedlaříková, J. Vondrák, *Gel polymer electrolytes with nanoparticles*, In *38. Nekonvenční zdroje elektrické energie*. 1. Hustopeče: Česká elektrotechnická společnost, (2017), page 107-110.
[7] R. Szotkowski, *Gel polymer electrolytes with nanoparticles*, The Faculty of Electrical Engineering and Communication Bro University of Technology, Brno (2016).

 ISBN: 978-80-8152-530-8

Fabrication and Characterisation of Nanocomposites for Post Lithium-ion Batteries

Dominika Capková[a]*, Andrea Straková Fedorková[a], Günter Fafilek[b]

[a] *Faculty of Science, Pavol Jozef Šafárik University, Moyzesova 11, 040 01 Košice, Slovakia*

[b] *Institute of Chemical Technologies and Analytics, Vienna University of Technology, Getreidemarkt 9/164 EC, 1060 Vienna, Austria*

**dcapkova@gmail.com*

Energy storage will play a significant role in future energy systems. Lithium-ion batteries keep many devices and mechanisms in operation. They have a significant impact on information technologies, personal electronic devices and electric vehicles. Today's lithium-ion batteries do not meet the growing requirements for capability and operating life. Therefore, further work on their development is needed. Lithium has small dimensions, the smallest weight of known metals and provides the highest energy density to mass and volume. One of the possible types of the post lithium-ion batteries is lithium-sulfur battery. Lithium-sulfur batteries are being developed for better capability. In theory, Li-S battery has higher energy density and longer life cycle than Li-ion batteries. On the other hand, there are many problems, which are not yet resolved, like the insolation character of sulfur or different density and size of oxidation and reduction products.

In this work, different types of sulfur electrodes were provided. Cells consisted of lithium metal foil as a negative electrode, DME:DOL (2:1) with LiTFSi and $LiNO_3$ as electrolyte, glassy fiber separator and a sulfur positive electrode (80% (sulfur+PPy+MWCNTs) and (sulfur+LFP+MWCNTs) + 10% Super P + 10% PVDF). All cells were fabricated in an argon-filled glove box. We used different electrochemical methods for sample characterization as electrochemical impedance spectroscopy (EIS), cyclic voltammetry (CV) and galvanostatic charge/discharge. The morphology of positive and negative electrodes was investigated by scanning electron microscopy (SEM). Also, we have observed the corrosion processes of lithium anode on our samples after cycling.

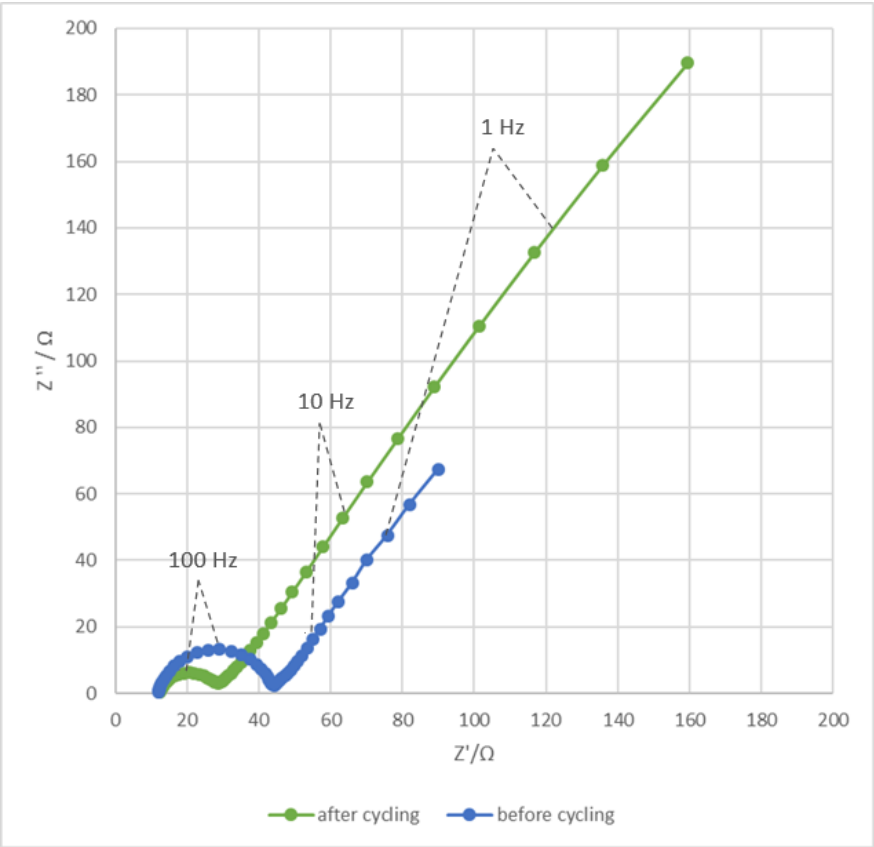

Figure 3 Electrochemical impedance spectra of lithium-sulfur cell before and after cycling

 ISBN: 978-80-8152-530-8

The EIS was measured at open-circuit potential, before charging for the charge state and after charging for the discharge state. Figure 1 shows typical Nyquist plots for our samples. The typical EIS of lithium cell consisted of two partially overlapped semicircles. The intersection of the first semicircle was related to the interfacial of the Li electrode. The interfacial resistance exhibits a continuous decrease trough the cycles. It is probably caused by atomic rearrangement of the exposed surface to the electrolyte to form a stable solid electrolyte interface (SEI) layer. This process is accompanied by the persistent change of SEI layer and/or decomposition of electrolyte. Maybe, in the early stage of cycling the construction of SEI layers takes place to make the ionic diffusion more efficient. The formation of a stable SEI film is not only important for increasing the cell performance but also for reduction of the electrolyte decomposition. [1]

Cyclic voltammograms of sulfur electrodes were measured in an El-cell with lithium as reference electrode at room temperature. Oxidative peaks (corresponding to the charging process) in the cyclic voltammograms are due to oxidation of the polysulfides. It is found that some intermediates (probably they are Li_2S_8 and Li_2S_6) are stable enough to be detected at around 2.7 V upon cycling [2]. Reductive peaks (corresponding to the discharging process) are due to reduction of the polysulfides and they are detected at around 1.5 V – 2.5 V.

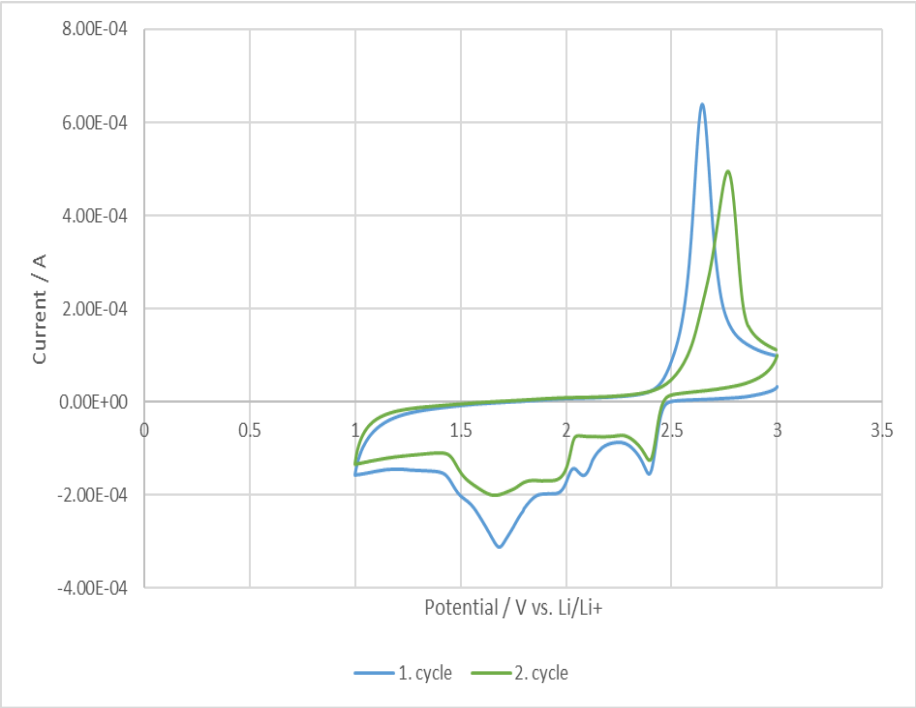

Figure 4 Cyclic voltammetry of Li-S batteries with electrolyte DME:DOL (2:1)

Capability of our cells was dramatically decreased with the number of cycles. Electrochemical impedance spectroscopy of our lithium-sulfur batteries shows, that impedance of Li^+ ions before cycling is higher than impedance after cycling. It is due to formation of the stable solid electrolyte interface layer at the beginning of measurement. Cyclic voltammetry confirmed, that the positive electrodes of lithium-sulfur cells are electrochemically active at around 2.7 V as oxidation (charging) and at around 1.5 V – 2.5 V as reduction (discharge). In cyclic voltammograms, current peaks decrease with cycle number.

Acknowledgements

The authors are grateful to the NATO SPS Project No. 985148, Slovak Academic Information Agency (SAIA).

References

[1] H. Liu, R. Kloepsch, J. Wang, *Truncated octahedral LiNi0.5Mn1.5O4 cathode material for ultralong-life lithium-ion battery: Positive (100) surfaces in high-voltage spinel system;* in: *Journal of Power Sources.* 2015. pages 430-437.

[2] M. Barghamadi, A. S. Best, A. I. Bhatt, et al. *Effect of Anion on Behaviour of Li-S Battery Electrolyte Solutions Based on N-Methyl-N-Buthyl-Pyrrolidinium Ionic Liquids;* in: *Electrochimica Acta.* 2015. page 636.

 ISBN: 978-80-8152-530-8

Preparation of carbon fibers with embedded metal and metal/phosphide nanoparticles as favourable electrocatalysts for hydrogen evolution reaction.

M. Streckova [a], R. Orinakova [b], E. Mudra [a], M. Sabalova [b], J. Duzsa [a]

a Institute of Materials Research, Slovak Academy of Sciences, Watsonova 47, 040 01 Kosice, Slovak Republic
b Department of Physical Chemistry, Faculty of Science, P.J. Safarik University , Moyzesova 11, 041 54, Kosice, Slovak Republic

**mstreckova@saske.sk*

Pollution prevention is not just the responsibility of businesses and government agencies. Citizens can help solve environmental problems by reducing pollution at the source, before it is created. We can all apply pollution prevention in our daily lives. Whether in the home and garden, at the supermarket or on the road, we can make pollution prevention choices every day in order to protect the environment, save money and conserve natural resources [1]. The clean power plants goals are based in part on the proven potential for a production of renewable energy with fewer carbon emissions when reducing the utilization of existing sources of carbon pollution. Nowadays it is necessary to ensure sustainable development and fundamental change in the energy system [2]. One of the most perspective sources of energy is hydrogen. Hydrogen is the simplest, plentiful element in the universe with high caloric value, whereas the engine burning pure hydrogen produces almost no pollution. The electrolysis of water is the most promising technology for the hydrogen production. However, the hydrogen production from the electrolysis of water is still at least three times more expensive than steam reforming. The hydrogen evolution reaction (HER) acquired by the electrocatalytic reduction of water may provide a sustainable energy supply for the future, but this technique is currently limited due to a high price and resource scarcity of the used noble metals such as Pt. Therefore, a lot of efforts were aimed at a development and fabrication of efficient, stable and economically viable non-noble metal electrocatalysts for HER.

The hybride materials composed of carbon and different types of nanopowders exhibit an excellent catalytic activity for HER that is comparable with Pt-based electrodes. Moreover, the carbon in the form of nanotubes of fibers exhibit high specific surface area to volume with hierarchically porous structure, flexibility electric and thermal conductivity and excellent chemical resistance. It was found [3] that the fibers with incorporating metal or metal phosphide nanoparticles facilitates the HER process.

The effective hydrogen evolution reaction was found only in the case of the six different transition metals creating phosphides: Fe, Co, Ni, Cu, Mo and W. In this work, three of them: Co, Ni, Cu were prepared in the form of phosphide nanoparticles embedded in the carbon fibers as an electrocatalysts for HER. The crystallinity of incorporated nanoparticles in the final calcined carbon fibers in comparison with amorphous character of pure carbon fibers was studied. The thermal treatment procedure of precursor polymeric PAN/metal chloride fibers were suggested according the previous work, where was described the stabilization, carbonization and subsequent reduction of fibers in hydrogen atmosphere in detail [3]. Due to the author's previous knowledge about influence of used atmosphere on fibril morphology, the hydrogen reduction atmosphere was again applied after carbonization in Ar for individual fibers. The BET analysis was employed to determination of external surface area and volume of microspores. The results were correlated with electrocatalytic activity of individual fibrous sample for HER. The composition and structural changes of individual fibers samples were described according EDX, XRD and TEM analysis. The electrocatalytic activity for hydrogen evolution was determined by linear sweep voltammetry and electrochemical impedance spectroscopy measurements. The new perspective electrode show excellent durability with unchanged structure even after 500 CV scans in the acidic environment.

Acknowledgement

This work was supported by the Scientific Grant Agency of the Ministry of Education, Science, Research and Sport of the Slovak Republic and the Slovak Academy of Sciences, projects No. VEGA 2/0079/17 and 1/007/17.

References

[1] https://www.epa.gov/p2/what-you-can-do-about-pollution-prevention

[2] S. Dunn, Hydrogen futures: toward a sustainable energy system, Inter. J. Hydro. Ener., **27** (2002) 235–264.

[3] M. Streckova, E. Mudra, R. Orinakova, L. Markusova-Buckova, M. Sebek, A. Kovalcikova, T. Sopcak, V. Girman, Z. Dankova, M. Micusik, J. Dusza, Nickel and nickel phosphide nanoparticles embedded in electrospun carbon fibers as favourable electrocatalysts for hydrogen evolution, Chem. Engeen. J., **303** (2016) 167–181.

 ISBN: 978-80-8152-530-8

SESSION III ***Nanomaterials for energy applications***

Characterization of Sulfur Composite Cathodes for High Performance Li-S Batteries

R. Oriňaková[a], A. Straková Fedorková[a*], K. Gavalierová[a], T. Kazda[b], P. Gómez-Romero[c],

[a]*Institute of Chemistry, Faculty of Science, P. J. Šafárik University, 040 01 Košice, Slovakia*
[b]*Department of Electrical and Electronic Technology, Faculty of Electrical Engineering and Communication, Brno University of Technology, Technicka 10, 616 00 Brno, Czech Republic*
[c]*Institut Català de Nanociència i Nanotecnologia, ICN2, CIN2 / Consejo Superior de Investigaciones Científicas (CSIC), Campus UAB, E-08193 Bellaterra, Barcelona, Spain*

**andrea.fedorkova@upjs.sk*

Lithium rechargeable secondary cells are currently being used as energy source in electronic devices, small portable devices and other electronics. Among the high-energy density storage systems, lithium-sulfur batteries, with energy density of 2600 Wh/kg, holds the potential to serve as next generation of high energy battery. Li-S batteries are cheap, environmentally benign and very safe in comparison with Li-ion batteries. Sulfur-carbon (S-C) composites and sulfur-$LiFePO_4$ (S-LFP) composites were prepared with MWCNTs additive by evaporation and solid state reaction. S-LFP cathode with MWCNTs shows improvement of not only discharge capacity but also cycling stability. It exhibits an initial discharge capacity of 1167 mAh/g sulfur, or 70% of theoretical capacity. The capacity of S-LFP-MWCNTs composite after 20 cycles was 80% of the initial value and remained stable.

Fig. 1 shows the first two cyclic voltammograms (CV) of the S-C composite cell. The two separated reduction peaks at 2.4 and 2.0 V correspond to the conversion of high-order lithium polysulfides (Li_2S_8) to low-order lithium polysulfides (Li_2S_x, $8 > x \geq 4$) and lithium polysulfides to solid-state Li_2S_2/Li_2S. However, only one oxidation peak is observed, implying the transformation of all the polysulfides into the intermediate, which is believed to be S_8^{2-} with the most facile oxidation kinetics [1].

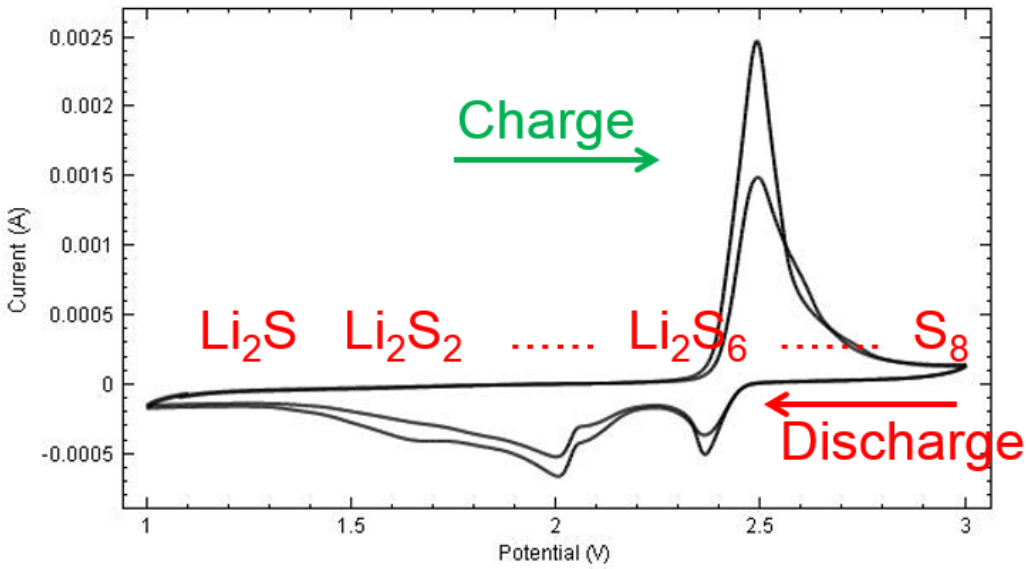

Fig. 1 First two cyclic voltammograms (CV) of the S-C composite at a scan rate of 0.1 mV/s.

Acknowledgement

This research was sponsored by the NATO Science for Peace and Security Programme under grant 985148 and by the project VEGA 1/0074/17.

References

[1] X. Ji and L. F. Nazar, *J. Mater. Chem.* 20 (2010) 9821.

 ISBN: 978-80-8152-530-8

Surface protective layers for the Li-S cathodes

Kazda T[a]*, Sedlaříková M[a], Vondrák J[a], Čech O[a], Čudek P[a]

[a] *Brno University of Technology, Faculty of Electrical Engineering and communication, Department of Electrical and Electronic Technology, Technická 10, 616 00 Brno, Czech Republic*

* *e-mail: kazda@feec.vutbr.cz*

Lithium-ion batteries occupy every year more and more dominant position on the market with batteries. But for further expansion to new fields of use it will be necessary to increase gravimetric and volumetric energy density of current batteries. One of the possibilities is to replace current intercalation cathode materials by conversion materials for example by sulphur. Disadvantage of this new technology is high instability of electrode during cycling due to high volumetric expansion of sulphur during cycling. This paper deals with the influence of used active coating layers to prevent polysulphide shuttle effect.

Introduction

Electromobility undergoes a rapid development in the world nowadays. The problem of current electric vehicles (EV) is the lack of battery capacity which limits their potential range. The solution of this problem could be Li-S batteries with their theoretical capacity of 1675 mAh/g and specific energy of ~ 3200 Wh/kg which greatly exceeds the possibilities of current commercial batteries. [1] [2] Before releasing these batteries into practice, it is necessary to solve a number of problems, such as a very complicated conversion of sulphur to Li_2S and back again without settling soluble polysulfides at the anode during cycling, which leads to a decrease of capacity. Another problem is the expansion of sulphur during cycling, when, during the conversion of sulphur to Li_2S, the volume expansion of about 80 % occurs. This expansion leads to a big stress to the cathode and decreases its capacity. [3] [4] [5] A possible solution of both these problems is the correct choice of carbon which encapsulates sulphur and a binder which can respond to the volume changes without the loss of contact between particles of the electrode. [6] [7] [8] Another possibility is separator coating by active material which prevents migration of polysulphides from cathode side to anode side. Carbons as rGO or Ti_4O_7 can be used as active materials. [9] [10] [11]

Experimental

In the first step, a mixture of sulphur, was Sigma Aldrich Sulphur 99.5 % turned into a mixture consisting of NMP (N-methyl-2-pyrrolidone), binder PVDF (Polyvinylidene fluoride) and Super P carbon. Mixtures were prepared to match the final ratio: 80 % Sulphur, 15 % Super P + 5 % binder. The resulting mixture was applied onto an Al foil using a special coating bar to produce 150 micron layers, which was later dried and pressed using pressure of 3200 kg/cm^2. Other electrod was then covered by disperson of GO (graphene oxide) in ethylalcohol by 12 µm coating bar and again pressed using pressure of 3200 kg/cm^2. A discs of 18mm diameter was punched from the both coated aluminum foils and inserted into the El-Cell © ECC-STD electrochemical cell assembled in an argon atmosphere inside a glove box, pure lithium was used as the anode and electrolyte was a mixture of DME (1,2-Dimethoxyethane):DOL (1,3-Dioxolane) 2:1 (v:v) with 0.7 M LiTFSI + 0.25 M $LiNO_3$ impregnated in a glass fiber separator. Cyclic voltammetry (CV) used to compare properties of the electrodes. Potential window of CV was set at 1.8 to 3.0 V versus lithium and scan rate to 0.1 mV/s.

 ISBN: 978-80-8152-530-8

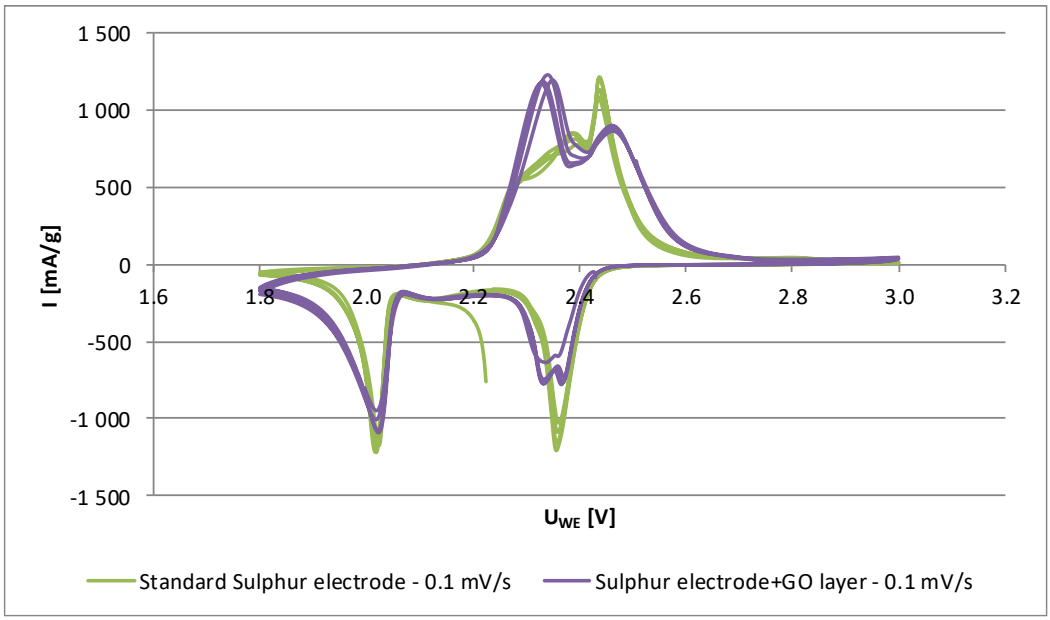

Fig. 1: Comparison of CV for the standard sulphur electrode and Sulphur electrode+GO layer

Conclusion

CV results for the standard sulphur electrode and Sulphur electrode+GO layer are shown in Fig. 1. We can see that GO coating have highly influence to shape and size of the anodic and cathodic peaks. In the case of Sulphur electrode+GO layer we can see two separate anodic peeks the first on the position 2.336 V and second on 2.470 V the second peak is on the same position like peak of the standard sulphur electrode however first peak is shifted to higher potential 2.391 V and is much smaller than in the case of the Sulphur electrode+GO. Cathodic peak at 2.360 V is in the case of Sulphur electrode+GO layer divided to two peaks. Capacity calculated in the last cycle of CV was for the standard sulphur electrode 544 mAh/g and 645 mAh/g for Sulphur electrode+GO layer.

Acknowledgements

This research has been carried out in the Centre for Research and Utilization of Renewable Energy (CVVOZE). Authors gratefully acknowledge the financial support from the Ministry of Education, Youth and Sports of the Czech Republic under NPU I programme (project No. LO1210) and BUT specific research programme (project No. FEKT-S-17-4595).

References

[1] H. Yoo, E. Markevich, G. Salitra, D. Sharon and D. Aurbach, *Materials Today*, **vol. 17**, 110-121 (2014).

[2] Y. Yin, S. Xin, Y. Guo and L. Wan, *Angewandte Chemie International Edition*, **vol. 52**, 13186-13200 (2013).

[3] J. Kim, D. Lee, H. Jung, Y. Sun, J. Hassoun and B. Scrosati, *Advanced Functional Materials*, **vol. 23**, 1076-1080 (2013).

[5] P. Bruce, S. Freunberger, L. Hardwick and J. Tarascon, *Nature Materials*, **vol. 11**, 19-29 (2011).

[6] G. Babu, K. Ababtain, K. Ng and L. Arava, *Scientific Reports*, **vol. 5**, 8763- (2015).

[7] X. Zhao, J. Tu, Y. Lu, J. Cai, Y. Zhang, X. Wang and C. Gu, *Electrochimica Acta*, **vol. 113**, 256-262 (2013).

[8] T. Kazda, P. Cudek, J. Vondrak, M. Sedlarikova, J. Tichy and M. Slavik, *ECS Transactions*, **70**, 121-126 (2015).

[9] J. Wang, Y. Yang and F. Kang, *Electrochimica Acta*, **vol. 168**, 271-276 (2015).

[10] H. Yao, K. Yan, W. Li, G. Zheng, D. Kong, Z. Seh, V. Narasimhan, Z. Liang and Y. Cui, *Energy Environ. Sci*, **vol. 7**, 3381-3390 (2014).

[11] J. Sukac, T. Binar, M. Sedlarikova and K. Silinger, *ECS Transactions*, **70**, 177-185 (2015)

[12] Q. Pang, D. Kundu, M. Cuisinier and L. Nazar, *NATURE COMMUNICATIONS*, **5**, 1-8 (2014)

 ISBN: 978-80-8152-530-8

Reduced graphene oxide / Titanium oxide Nanocomposite Synthesis via Microwave-assisted Method and Supercapacitor behaviors

M.Ates[a,*], Y. Bayrak[b], O. Yoruk, S. Caliskan

[a] *Department of Chemistry, Faculty of Arts and Sciences, Namik Kemal University, Degirmenalti Campus, 59030, Tekirdag, Turkey*

[b] *Department of Chemistry, Faculty of Sciences, Trakya University, Balkan Campus, 22030, Edirne, Turkey*

**mates@nku.edu.tr*

In this paper, graphene oxide (GO) was firstly synthesized by modification of Hummers method from the literature. Secondly, reduced graphene oxide (rGO)/Titanium oxide (TiO_2) nanocomposites were synthesized with different wt/wt % of GO/TiO_2 (1:1; 1:2; 1:5 and 1:10) by microwave- assisted method. By treating GO and GO/TiO_2 nanocomposites in a microwave oven, reduced graphene oxide (rGO) and rGO/TiO_2 materials could be obtained within power of 180 W in 10 min. The weight ratio of rGO and TiO_2 was used to obtain the optimum conditions for nanocomposite materials. The rGO/TiO_2 nanocomposite active materials were characterized by cyclic voltammetry (CV), Fourier-transfrom infrared – Attenuated total reflectance (FTIR-ATR), scanning electron microscopy-energy dispersion X-ray (SEM-EDX), thermogravimetry (TGA), differential thermal analyzer (DTA) and electrochemical impedance spectroscopy (EIS) analysis. Thirdly, supercapacitors were fabricated as a symmetric device with two electrode configuration. The device performances were tested by CV, galvanostatic constant current (CC), and EIS measurements. TGA analysis indicated that the thermal stability of the nanocomposites improved from rGO (40% at 892.8 ^{0}C) to nanocomposite as the initial feed ratio of $[GO]_o/[TiO_2]_o$=1/10 as 94% at 949.3 ^{0}C) increased.

Supercapacitors, also named electrochemical capacitors or ultracapacitors, have attracted more attention over the last years because of their higher energy and power density and longer cycle life than secondary batteries [1-3] . Generally, supercapacitors are divided into two catagories: double layer capacitor electrode and pseudocapacitive electrode materials [4] [43]. In our paper, we used double layer capacitor electrode which is used reduced graphene oxide.

The result show that the as-prepared symmetrical rGO/TiO_2 nanocomposite on the two-electrode system displays very high specific capacitance of 524.02 F/g at 2 mV/s for $[GO]_o/[TiO_2]_o$= 1/5 with a high energy density of E= 50.07 Wh/kg at 2 mV/s for $[GO]_o/[TiO_2]_o$= 1/1 and high power density of P= 58.6 kW/kg at a the scan rate 1000 mV/s for $[GO]_o/[TiO_2]_o$= 1/1. Additionally, the symmetric electrode shows good cycling stability with a retention value of 6.6% for $[GO]_o/[TiO_2]_o$= 1/1 after 1000 cycles. These good results suggest us that rGO/TiO_2 nanocomposite which is obtained by microwave-assisted method has a great potential as an electrode material for supercapacitor applications.

The equivalent circuit model of $R_s(C_{dl}(R_{ct}W))$ was used to explain parameters of solution resistance, double layer capacitence (C_{dl}), charge transfer resistance (R_{ct}), Warburg impedance (W). Theoretical and experimental values support with each other.

Keywords: Supercapacitor, reduced graphene oxide, microwave -assisted, capacitance, TiO_2, energy density, power density.

Acknowledgements

We wish thank to Assoc.Prof.Dr. Murat Turkyilmaz (Trakya Uni., Chemistry Dep., Inorganic Chem. Div., for his TGA/DSC measurements.

References

[1] P. Simon, Y. Gogotsi, Nat, Mater **7** (2008) 845-854.

[2] J.K. Hang, C.H. Huang, W.T. Tsai, M.J. Deng, I.W. Sun, J. Power Sources **179** (2008) 435-440.

[3] C. Xiong, T. Li, Y. Zhu, T. Zhao, A. dang, H. Li, X. Ji, Y. Shang, M. Khan, J. Alloys Compd **695** (2017) 1248-1259.

[4] P.M. Kulal, D.P. Dubal, C.D. Lokhande, V.J. Fulari, J. Alloys Compd., **509** (2011) 2567-2571.

 ISBN: 978-80-8152-530-8

Polypyrrole/Ag nanoparticle/graphene nanocomposites as a symmetric device for supercapacitors

M.Ates[a, *], S. Caliskana, E.Ozten[a]

[a] *Department of Chemistry, Faculty of Arts and Sciences, Namik Kemal University, Degirmenalti Campus, 59030, Tekirdag, Turkey*

**mates@nku.edu.tr*

Improvement in charge storage has been obtained by exfoliation of reduced graphene oxide sheets via intercalation of Ag nanoparticle and polypyrrole. The synthesis procedure of composite is simple, inexpensive and ecofriendly. The formation of composite has been shown by the analysis of Fourier transform infrared-Attenuated transmission reflectance (FTIR-ATR), scanning electron microscopy-Energy dispersion X-ray analysis (SEM-EDX).

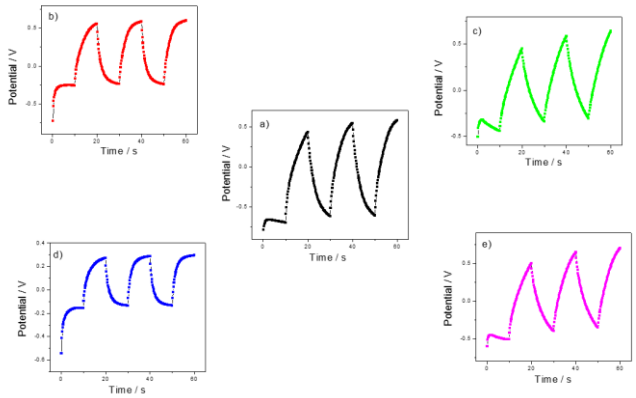

Figure 1. Galvanostatic charge-discharge (GCD) curves of an **a)** rGO, and rGO/PPy nanocomposites with different feed ratios**, b)** $[rGO]_0/]Py]_0$= 1/1, **c)** $[rGO]_0/]Py]_0$= ½, **d)** $[rGO]_0/]Py]_0$= 1/5, **e)** $[rGO]_0/]Py]_0$= 1/10. Electrode active materials were taken at a constant current density of 0.1 mA/g in two-electrode configuration.

Polypyrrole (PPy) is one of the most important active material amongst to conducting polymers due to high charge density, easy preparation, low cost, its relatively high conductivity, good stability within ambient air exposure and environment friendship [1-3].

The ternary reduced graphene oxide (rGO) / Ag nanoparticle / polypyrrole (PPy) (rGO/Ag/PPy) nanocomposites has been developed as the electrode materials for supercapacitors. Under the optimized preparation conditions in different initial feed ratios ($[rGO]_0/[Py]_0$= 1/1, ½, 1/5 and 1/10) were possessed a relatively high Coulombic efficiencies. The highest specific capacitance of was obtained as C_{sp}= 1085.22 F/g at a scan rate of 4 mV/s tested by CV method in 1 M H_2SO_4 aqueous electrolyte with a corresponding specific energy density of E= 36.92 Wh/kg, as well as a retention of 65.30% of its original capacitance after 1000 cycles for [rGO]/[Py]o= 1/5. Noticeable improvements in other electrochemical properties give permission its possible application as electrode active material for supercapacitors.

Keywords: Ag nanoparticle, symmetric supercapacitor, energy density, reduced graphene oxide, polypyrrole, power density.

Acknowledgements

The financial support of Namik Kemal University, Tekirdag, Turkey, project number: NKUBAP.01.GA.16.076 is gratefully ackmowledged. Authors also thank to Expert Muhammet Aydın (Namik Kemal Uni., NABILTEM, Tekirdag, Turkey) for recording SEM-EDX and FTIR-ATR measurements.

References

[1] J. Wang, Y. Xu, J. Wang, X. Du, Synth. Met., **161** (2011) 1141-1144.
[2] H.C. Kang, K. K. Geckeler, Polymer, **41** (2000) 6931-6934.
[3] C. Bora, S. Dolui, Polymer, **53** (2012) 923-932.

 ISBN: 978-80-8152-530-8

Synthesis of rGO/nanoclay/PVCz Nanocomposites and Supercapacitor Applications

M. Ates[a, *], E. Ozten[a]

[a] *Department of Chemistry, Faculty of Arts and Sciences, Namik Kemal University, Degirmenalti Campus, 59030, Tekirdag, Turkey*

**mates@nku.edu.tr*

In this study, graphene oxide (GO) was chemically reacted with sodium borohydride ($NaBH_4$) to form reduced graphene oxide (rGO). rGO, and rGO/nanoclay/PVCz nanocomposite were synthesized by chemical reactions. These nanocomposite active materials were characterized by Fourier-transform infrared spectroscopy-Attenuated transmission reflectance (FTIR-ATR), scanning electron microscopy (SEM), and energy-dispersive X-ray analysis (EDX).

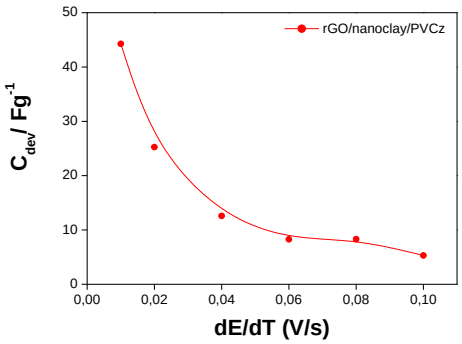

Figure 1. Specific capacitance of rGO/nanoclay/PVCz nanocomposite with scan rates, as determined by CV measurements.

rGO-based nanocomposites have been used for supercapacitor electrochemical performances [1,2]. In literature, many carbon based materials, such as activated carbon electrodes from biomass [3-4], carbon nanotubes [5], graphene [6] and graphite-like carbon nitrite [7], etc.

Supercapacitor device performances were taken by cyclic voltammetry (CV), galvanostatic charge-discharge (CC), and electrochemical impedance spectroscopy (EIS) as two electrode configuration. The rGO/nanoclay/PVCz nanocomposite shows significantly improved capacitance (C_{sp}= 44.27 Fg^{-1}) compared to that of rGO (C_{sp}= 20.78 Fg^{-1}) at the scan rate of 10 mVs^{-1} by CV method. The enhanced capacitance results in high power (P= 483.75 Wkg^{-1}) and energy-storage (E= 0.3 $Whkg^{-1}$) capabilities of the rGO/nanoclay/PVCz nanocomposite material. Ragone plots were drawn to observe energy and power density of supercapacitor devices. Stability tests were examined by CV method for 1000 cycle.

Keywords: Polyvinylcarbazole, nanoclay, reduced graphene oxide, energy storage, charge/discharge.

Acknowledgements

The financial support from Namik Kemal University, Tekirdag, Turkey, project number: NKUBAP. 01.YL.17.090 is gratefullfy acknowledged.

References

[1] W. Qin, T.Q. Chen, L.K. Pan, L.Y. Niu, B.W. Hu, D.S. Li, J.L. Li, Z. Sun, Electrochim. Acta **153** (2015) 55-61.

[2] Y.G. Liu, H.Y. Cheng, H.Y. Sun, H. Arandiyan, J.P. Li, M. Ahmad, J. Power Sources, **273** (2015) 878-884.

[3] Y.Q. Qjao, H.P. Wang, X.Y. Zhang, P. Jia, T.D. Shen, X.F. Hao, Y.F. Tang, X.H. Wang, W.M. Gao, I.X. Kong, Mater. Lett. **184** (2016) 252-256.

[4] A.M. Abioye, F.N. Ani, Renew. Sust. Energy Rev. **52** (2015) 1282-1293.

[5] H. Pan, J.Y. Li, Y.P. Feng, Nanoscale Res. Lett. **5** (2010) 654-668.

[6] M.F. El-Kady, V. Strong, S. Dubin, R.B. Kaner, Science **335** (2012) 1326-1330.

[7] L. Shi, J. Zhang, H. Liu, M. Que, X. Cai, S. Tan, L. Huang, Mater. Lett. **145** (2015) 150-153.

 ISBN: 978-80-8152-530-8

Crystal size and morphology of silicoaluminophosphate SAPO – 11: strategy and parameters of synthesis

I.A. Tiuliukova[a,b]*, N.A. Rudina[a], E.V.Parkhomchuk[a,b]

[a]*Boreskov Institute of Catalysis SB RAS, 5 Lavrentieva St., Novosibirsk 630090, Russia*
[b]*Novosibirsk State University, 2 Pirogova St., Novosibirsk 630090, Russia*

**Tiuliukova@catalysis.ru*

Zeolites and zeolite-like materials with different pore opening have been widely studied for applications in various petrochemical and refinery processes [1]. Molecular sieve materials possess large pore volume, high adsorption capacity, and ability to reversibly adsorb molecules showing molecular transfer property. Like zeolites, molecular sieve materials SAPO – m are considered as promising ones for using as catalysts and adsorbents in petrochemical processes such as hydroisomerization and methanol-to-olefin conversion [2]. However, large crystal size and microporosity of these materials cause severe diffusion limitations for reactants and products that often lead to pore blocking and fast catalyst deactivation by coke formation [3]. One of the approaches to solving this problem relies on the shortening of the diffusion way by decreasing the crystal size [3].

We have been studying the effects of different conditions and the strategy of synthesis on the crystal size and morphology of zeolite-like material SAPO – 11. We varied the temperature and time of crystallization, and used two types of pseudoboehmite, as well as aluminum isopropoxide (AIP) as Al source and different solvents as crystallization media.

In the case of zeolites it is known that decreasing the temperature of hydrothermal crystallization results in efficient reducing the size of growing particle [3,4]. But in the case of SAPO – 11 this strategy is not efficient – the desired phase does not formed in a reasonable time. It may be explained by a more rapid drop in nucleation rate at low temperature due to the higher activation energy of nucleation than in case of zeolites. In this connection, we have been using two - stage crystallization method, which implies a separation of nucleation and crystal growth stages. At the first stage, the formation of nuclei proceeded within 3 hours at 200 °C. After that, the temperature was lowered to provide slow growth of crystals. We have carried out a series of experiments with different growth's time of crystals (2-24 h) at low temperature (120 °C) and produced samples hereinafter referred to as SAPO-(3+n), where n is time of crystal growth in hours. The particle morphology of some of these samples is presented in Figure 1.

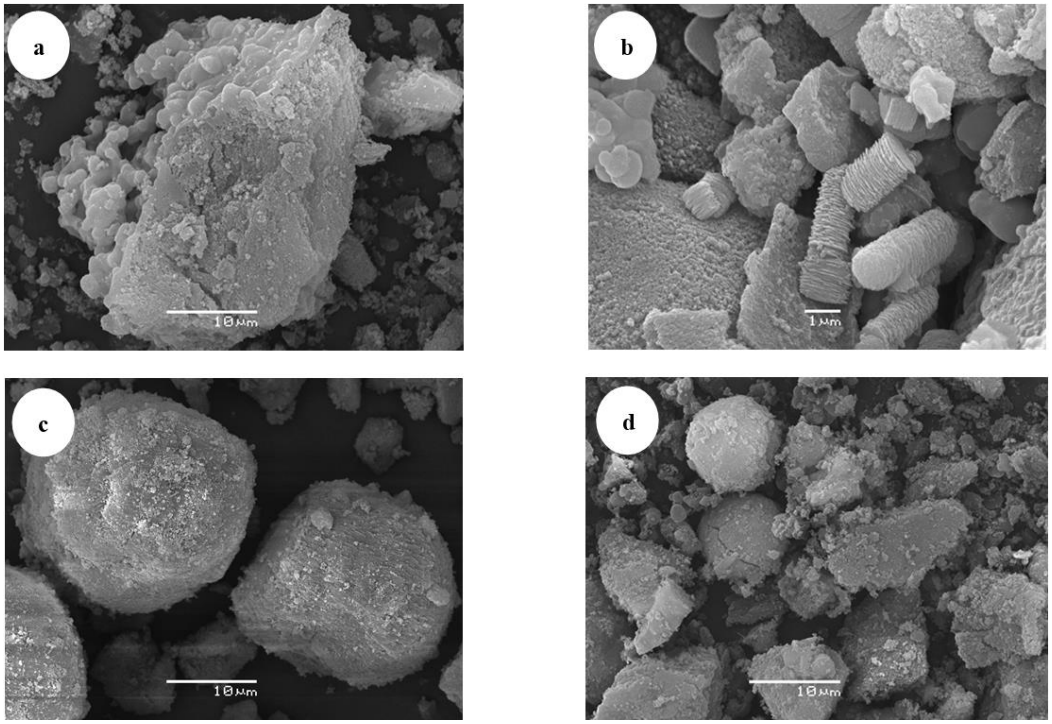

Figure 1. SEM images of materials from a series 1, synthesized by two-stage method with 3 h-nucleation at 200 ºC and different time of crystal growth at 120 ºC: a) 2 h, b) 6 h, c) 12 h, d) 24 h

 ISBN: 978-80-8152-530-8

Figure 2 demonstrates powder X-ray diffraction patterns of SAPO-11 samples synthesized by two-stage method. The identification of AEL-phase was performed by comparison with the corresponding JCPDS card № 42-0428.

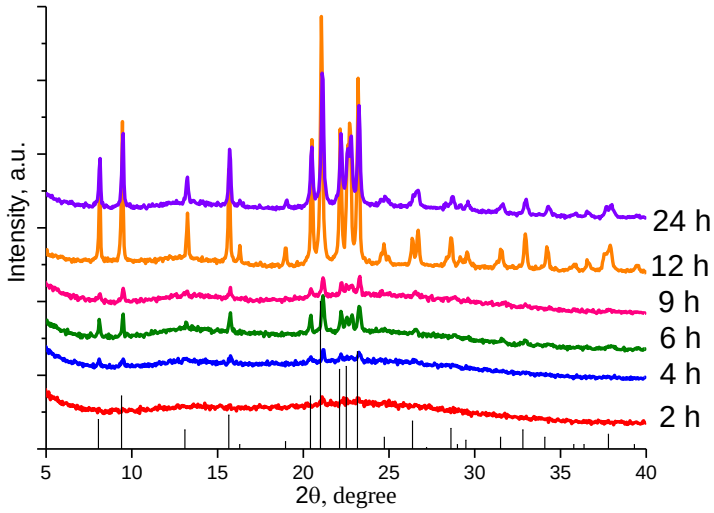

Figure 2. XRD patterns of materials from a series 1, synthesized by two-stage method with 3 h-nucleation at 200 °C and specified time of crystal growth at 120 °C

Particle morphology of the X-ray amorphous sample which grew up during 2 hours (Figure 1a) was bulk and shapeless, but it can be seen that some nuclei are already formed after 3 hours at 200°C: one part of the particle looks like a raw substance of unconverted precursors and another one looks like an aggregate which consists of primary crystallites. These primary particles were also observed in the sample SAPO-(3+6) (Figure1b), besides, cylinder-like particles, which consist of nanoplate crystals, can be seen. In accordance with XRD pattern of SAPO-(3+6) (Figure 2, green line) there are amorphous species too. In the mass the sample SAPO-(3+6) represents large (~10μm) and formless particles. The most crystallized samples: SAPO-(3+12) and SAPO-(3+24) represent the mix of particles with different morphology: the shapeless types and the pseudo-spherical crystals, which are aggregated and giant (>10μm).

Besides, we have been investigating the influence of reaction media on the crystal size and morphology. The samples from above-mentioned series 1 were synthesized in water media, excluding a small amount of iso-propanol which was produced from hydrolyzed AIP, the samples from a series 2 (denoted as Et-SAPO-(5+n), where n is time of crystal growth in hours) were obtained in ethanol media, with AIP as aluminum source by the two-stage crystallization method as well. The sample Et-SAPO-(5+160) (Figure 3a) was obtained with additional ultrasonic (US) pretreatment of precursor suspension before hydrothermal two-stage synthesis. As seen on Figure 3a the crystals have surprising screw-like morphology and evidently were crystallized by another mechanism compared with SAPO-(3+n). The US pretreatment was used to obtain homogeneous mixture of precursors with smaller $AlPO_4$ particles, because we suppose that initial state of aluminium phosphate in mixture plays an important role in AEL phase formation.

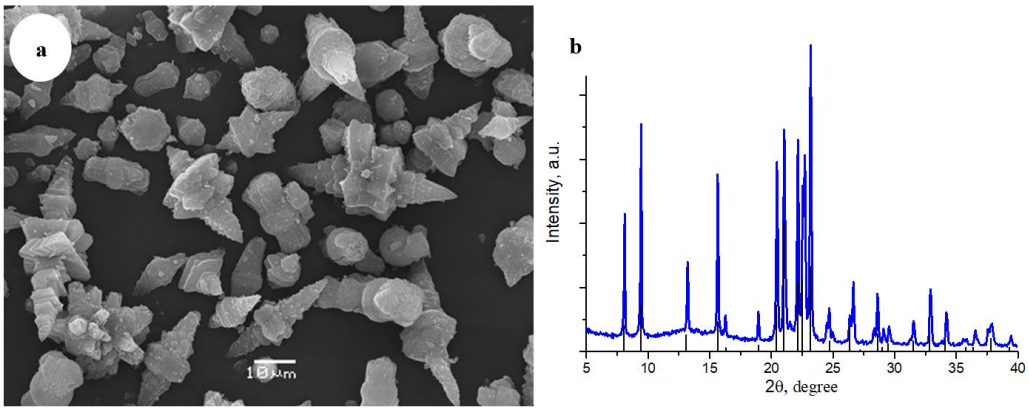

Figure 3. a) SEM image of a sample Et-SAPO-(5+160) from the series 2, synthesized by two-stage method using ethanol as a solvent, b) XRD pattern of the same sample

 ISBN: 978-80-8152-530-8

In summary, we have been developing the synthesis method which allows efficient controlling the crystals size of SAPO – 11 via separation of nucleation and crystal growth stages. Interestingly, morphology of crystals are markedly dependent from the type of a solvent during crystallization. We will investigate and present the results on the role of ethanol on the crystal size, mechanisms of SAPO – 11 formation and influence of Al source, including effect of phase and particle size of $AlPO_4$ on the early stages of the material formation.

Acknowledgements

This work was conducted within the framework of budget project No.0303-2016-0010 for Boreskov Institute of Catalysis, the participation of the author in the Conference was financed by Gasprom Neft.

References

[1] Ono Y. J. Catal. Today, 81 (2003) 3-16

[2] Yadav R., Sakthivel A. J. Appl. Catal. A Gen., 481 (2014) 143–160

[3] Mintova S., Grand J., Valtchev V. J. Comptes Rendus Chim. 19 (2016) 183–191.

[4] Mintova S., Gilson J.-P., Valtchev V. J. Nanoscale, 5 (2013) 6693–6703.

 ISBN: 978-80-8152-530-8

Design of thermal model of supercapacitor

M.Frivaldsky*, P. Drgona

[a] *Department of mechatronics and electronics, Faculty of electrical engineering, University of Zilina*

michal.frivaldsky@fel.uniza.sk

Summary

The paper deals whit the analysis of thermal field in core of supercapacitor. EDLC (Electrochemical double layer capacitor) of macrostructures of supercapacitor we can conclude that its bulk properties represent an anisotropic environment for heat transfer. The structure is geometrically and physically different in axial and radial direction of the body of the thread of EDLC capacitor. The heat transfer this structure is therefore different in axial direction opposite radial direction.

Proposed thermal model of EDLC elaborates the course of the axial and radial components of thermal coefficient of heat transfer by conduction depending on the sequence of the core´s turns.

In second part of paper proposal the graphical results of simulation thermal model of EDLC are shown.

Description of EDLC core and derivation of physical properties

Cylinder interpretation of EDLC consists of 4 layers with different material properties, assembled in sandwich structure in this order:

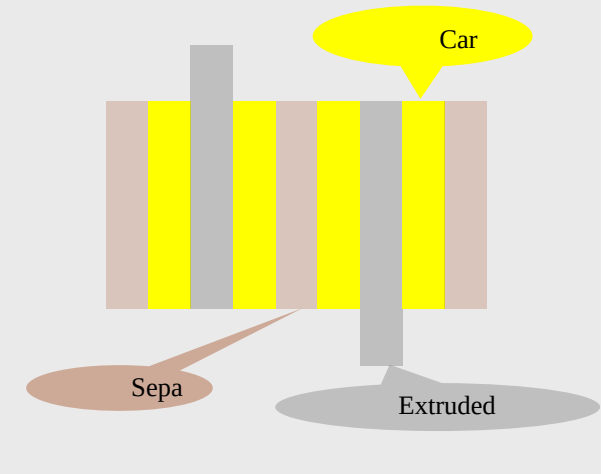

Fig. 1. Cross–section of EDLC structure

- Carbon,
- Extruded aluminum
- Carbon,
- Separator.

Label „n“ as total number of turns in four-layer structure and set $j \in \langle 1, n \rangle$ as order of sandwich turn. The diameter of turn is being changed in dependency on order of turn according to next formula:

$$r(j) = r_0 + (j-1)w \qquad (1)$$

where:

r(j) – is internal diameter of turn in „j - th“ order,

r0 – is diameter of first four-layer structure,

w – is width of one turn:

$$w = w_S + 2w_C + w_{Al} \qquad (2)$$

where:

w_S – is width of separator layer,

w_C – is width of carbon layer,

w_{Al} – is width of extruded aluminum.

The area of bottom turn's side with „j-th“ order is:

$$S(j) = \pi\left(r(j+1)^2 - r(j)^2\right) \qquad j \in \langle 1, n \rangle \qquad (3)$$

Axial part of turn's thermal resistance with „j-th“ order was computed using next formula:

$$R_a(j) = \frac{L}{k_a(j).S(j)} \quad (K/W), \qquad (4)$$

where:

L – is height of turn coil (m), k_a – thermal conductivity in axial direction (W/m.K)

 ISBN: 978-80-8152-530-8

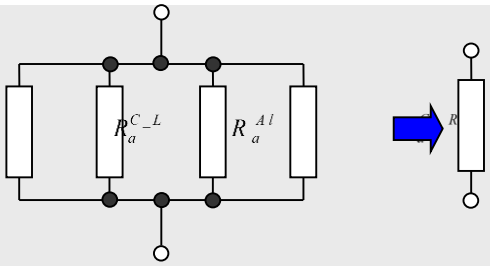

Fig.2. Structure of axial thermal resistances in one turn

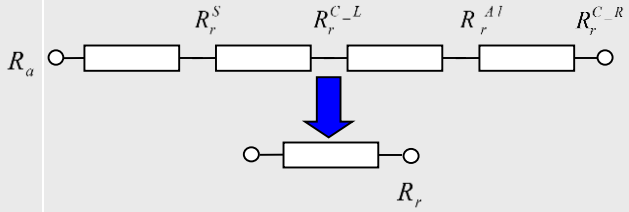

Fig.3. Structure of radial resistances in one turn

Axial thermal resistance of one turn in four-layer sandwich structure consists of four thermal resistances, which are shown on fig.2, whereby:

$R_a^{C\_L}$ - axial thermal resistance of carbon layer on left side,

$R_a^{C\_R}$ - axial thermal resistance of carbon layer on right side,

R_a^{Al} - axial thermal resistance of extruded aluminum layer,

R_a^{S} - axial thermal resistance of separator layer.

For several thermal resistances in axial direction of thermal model shown on fig.2 is valid:

$$R_a^S(j)=\frac{L}{\pi.k_S\left(\left(r(j)+w_s\right)^2-\left(r(j)\right)^2\right)},$$

$$R_a^{C\_L}(j)=\frac{L}{\pi.k_C\left(\left(r(j)+w_s+w_C\right)^2-\left(r(j)+w_s\right)^2\right)},$$

$$R_a^{Al}(j)=\frac{L}{\pi.k_{Al}\left(\left(r(j)+w_s+w_C+w_{Al}\right)^2-\left(r(j)+w_s+w_C\right)^2\right)},$$

$$R_a^{C\_R}(j)=\frac{L}{\pi.k_C\left(\left(r(j)+w_s+2w_C+w_{Al}\right)^2-\left(r(j)+w_s+w_C+w_{Al}\right)^2\right)}, \tag{5}$$

k_S - thermal conductivity of separator,

k_S - thermal conductivity of carbon,

k_{Al} - thermal conductivity of aluminum.

Equivalent axial thermal conductivity of one turn of EDLC shown on fig.2 is given by next equation:

$$\frac{1}{R_a(j)}=\frac{1}{R_a^S(j)}+\frac{1}{R_a^{C\_L}(j)}+\frac{1}{R_a^{Al}(j)}+\frac{1}{R_a^{C\_R}(j)} \tag{6}$$

From equations (4,5,6) we can obtain dependency of thermal coeficient for heat transfer by conduction in one turn of EDLC with „j-th“ order in next formula:

$$k_a(j)=\frac{L}{R_a(j).S(j)}. \tag{7}$$

Waveform of axial part of thermal coeficient in the scale of 100 turns is shown on fig. 4. Total thermal resistance of one turn for „j-th“ order in radial direction could be obtained from fig.3 as:

$$R_r(j)=R_r^S(j)+R_r^{C\_L}(j)+R_r^{Al}(j)+R_r^{C\_R}(j) \tag{8}$$

$R_r^{C\_L}$ - is radial thermal resistance of carbon layer on left side,

$R_r^{C\_R}$ - is radial thermal resistance of carbon layer on right side,

R_r^{Al} - radial thermal resistivity of extruded aluminum layer,

R_r^{S} - radial thermal resistance of separator layer.

 ISBN: 978-80-8152-530-8

After adding several radial resistances we can obtain dependency of equivalent radial thermal conductivity in one turn with „j-th“ order as follows:

$$k_r(j) = \frac{\ln \frac{r_j}{r_{j-1}}}{2\pi L.R_r(j)} \tag{9}$$

Waveform of radial conductivity (9) in scale of 100 turns is shown on fig.5.

Simulation results of thermal distribution

Graphical interpretation of surrounding's thermal distribution computation at the surface of EDLC is shown on fig.6 (left). At the ambient temperature Ta=25° C the maximum temperature on the surface of EDLC is Tmax=35,02° C and minimal temperature Tmin = 34,15° C. Graphical interpretation of internal temperature of EDLC in the direction of y-z axes is shown on fig. 6 (right). At ambient temperature Ta=25° C the maximum temperature inside of EDLC is Tmax=35,14° C and minimal Tmin = 34,16° C.

From attached pictures it can be seen that thermal distribution is influenced by various value of thermal conductivities in axial and radial direction. The gradient of Temperature of heat transfer is different in mentioned direction in the rate of 1/20.

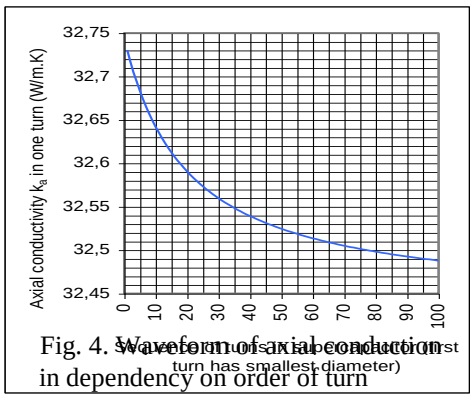

Fig. 4. Waveform of axial conduction in dependency on order of turn

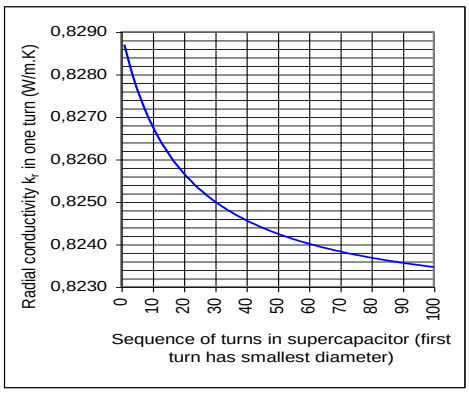

Fig. 5. Waveform of radial conduction in dependency on order of turn

w = 130 μm, L = 125 mm,

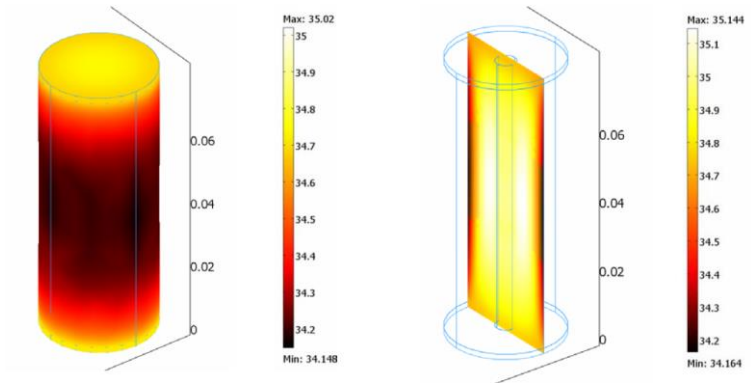

Fig. 6. Temperature distribution of EDLC on the surface (left) and within the core (right)

Acknowledgements

The authors would like to thank to the support within the project VEGA 1/0479/17 granted by VEGA agency

References

[1] Sam G. Parler, Jr., Laird L. Macomber: *Predicting Operating Temperature and Expected Lifetime of Aluminum-Electrolytic Bus Capacitors with Thermal Modeling*, Powersystems World, November 1999

[2] Sam G. Parler, Jr.: *Thermal Modeling of Aluminum Electrolytic Capacitors*,IEEE Industry Applications Society Conference, October 1999

 ISBN: 978-80-8152-530-8

Thin-Layer FeS_2 Electrodes Synthesized by Electrolysis for Li and Li-Ion Batteries

R. Apostolova

Scientific Research Laboratory of Chemical Power Sources of Ukrainian State University of Chemical Technology, Dnipro, 49005, Ukraine

**shembel@onil.dp.ua*

The steadily and rapidly growing miniaturization of electronic technology devices dictates that large-scale production of autonomous miniature power sources is needed. In batteries of this kind the electrodes can be fabricated by electrochemical synthesis that is attractive due to its technical simplicity, ecological safety, high productivity, and low cost. Thin-layer metal-sulfide (MS_x) films of transition metals (M=Fe, Co, Ni, Mo) have been produced from sulfate solutions (M_xSO_4) in the presence of $S_2O_3^{2-}$ [1-6] for lithium autonomous miniature power sources used in micro cards, sensors, micro robots, medical implants, and other devices. M-sulfide deposit films produced by electrolysis present micrometer agglomerates composed of nanometer particles which are perspective for the realization of lithium accumulators. Depending on the synthesis conditions, a number of stoichiometric sulfides with deficiency (MS_{1-x}) or excess (MS_{1+x}) of sulfur can be obtained.

However, it has been impossible to quantitatively produce FeS_2, as the most energy-rich among iron sulfides, by electrolysis from solutions containing $FeSO_4$ and $Na_2S_2O_3$. In the present study it was performed an electrochemical synthesis in order to produce FeS_2 on stainless steel from a solution containing Mohr's salt and $Na_2S_2O_3$, (mole. l^{-1}): $FeSO_4$ $(NH_4)_2SO_4 \cdot 6H_2O$ (1×10^{-2}–1×10^{-3}), $Na_2S_2O_3 \cdot 5H_2O$ (1×10^{-2}–1×10^{-3}), pH 4.7–5.2.

The electrolysis was performed in a 200-cm^3 glass vessel at 295–298 K. A technical-grade VT titanium plate served as the counter electrode; $S_{cathode} : S_{anode} = 1 : 10$. Cyclic voltammograms (CV) were obtained in the working deposition solutions and in solutions of its separate components at potentials in the range from (–1.1 to 0) V relative to the Ag/AgCl reference electrode in order to determine the positions of the redox peaks in the systems under study. The synthesis products were quantitatively deposited potentiostatically at the potentials of CV current peaks, with the phase composition of the deposits determined using a DRON-2 diffract meter with CoK_α radiation. The surface morphology of the deposits was determined with an MBI-6 optical microscope.

The aspects of synthesis of iron sulfides were studied. Based on the obtained results, we assume that separate reactions of the cathode process may correspond to the formation of FeS, H_2S (aq), FeS_2, S^{2-}, Fe, H_2, S. The key role in the formation of sulfide compounds is played by the reaction (1).We believe that formed sulfide ions enter with Fe^{2+} ions from the near-cathode layer into a chemical reaction and Fe-sulfides form (2):

$$S_2O_3^{\,2-} + 2e \rightarrow SO_3^{2-} + S^{2-}. \qquad (1)$$

$$Fe^{2+} + xS^{2-} \rightarrow FeS_x \qquad (2)$$

The main stage transitions successively occur in deposition of iron sulfides at potentials of –0.86, –0.95 V vs. Ag/AgCl-electrode corresponding separate phase formation. The FeS sulfide was identified in the finely crystalline deposit synthesized at a potential of –0.86 V (JCPDS ID 23-1121). The products of synthesis at a potential of –0.95 V are the nanometer FeS_2-crystallites with a marcasite structure (JCPDS ID 37–0475).

The size of FeS_2 crystallites was determined using the Debye–Scherrer formula to be 35.5-38.0 nm.

The optical microscopic images of the surface of synthesized FeS_2 films show thread-like formations. Separate particles are indistinguishable in these formations, which are significantly smaller in size than iron sulfide compounds deposited from the electrolyte containing $FeSO_4 \cdot 6H_2O$–$Na_2S_2O_3 \cdot 5H_2O$ [2]. The latter includes spheroidal agglomerates with sizes of 3–5 μm, composed of nanometer-size particles (200–400 nm).

The electrochemical characteristics of the sulfide compounds in the redox reaction with lithium were studied in an isolated three-electrode cell with a lithium counter electrode and Li/Li^+ reference electrode and also in a prototype coin lithium battery of 2325 configuration with an electrolyte composed of ethylene carbonate (EC, Merck), dimethyl carbonate (DMC, Merck), and 1 mole l^{-1} $LiClO_4$ (Iodobrom) on a testing stand with a software package. The cyclic CV was recorded with a use VoltaLab PGZ 301 analytical radiometer.

The FeS_2 (marcasite) owns the best discharge characteristics in the series of obtained products. Discharge capacity of Li accumulator on the base of FeS_2 (marcasite) achieves of theoretical specific capacity 890 mA h g^{-1} in the first cycle, reversible capacity – 620–800 mA h·g^{-1} (Fig.1).

 ISBN: 978-80-8152-530-8

Synthesized electrochemically FeS_2 with marcasite structure have also the ability for the reversible electrochemical performation in the negative electrodes of Li-ion systems with $LiMn_2O_4$ positive electrode (Fig. 2) ensuring 390-450 mA h g^{-1} FeS_2. The capacity exceeds theoretical capacity of graphite (372 mA h g^{-1}) that uses as the material of the negative electrodes in commercial Li-ion batteries.

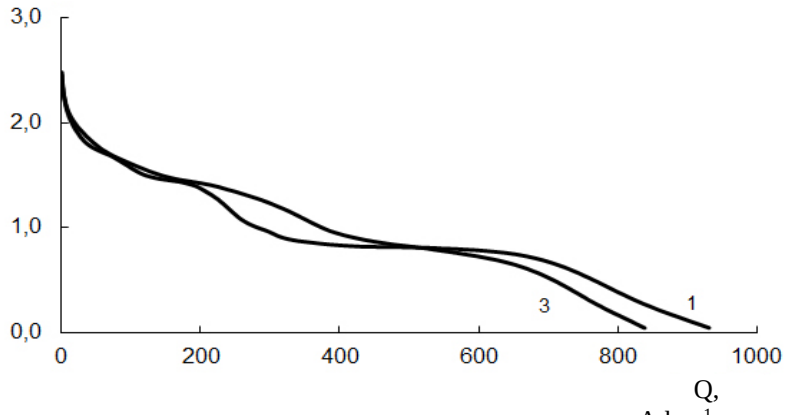

Fig. 1. Discharge curves of the electrochemically obtained FeS_2 in a lithium battery in the first (1) and third (3) cycles. $i_{discharge}$= 0.05 mA cm^{-2}; FeS_2 mass is 0.96 mg cm^{-2}. (*E*) - potential and (Q) - capacity; the same is for Fig. 2.

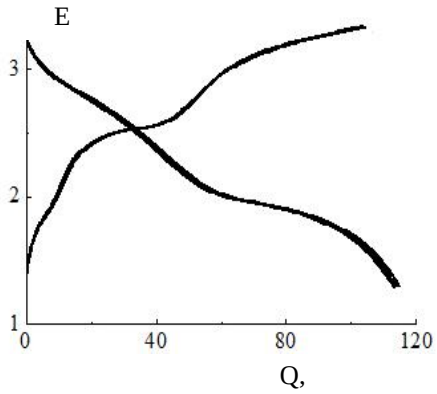

Fig.2**.** Discharge-charge curves of $LiMn_2O_4$ / EC, DMC, 1 mole l^{-1} $LiClO_4$/ FeS_2 (2–6cycles). Mass, mg·cm^{-2}: a) $LiMn_2O_4$ – 4.40; б) FeS_2 – 0.96. $i_{discharge}$= i_{charge}= 0.05 (mA·cm^{-2}). (Q, mg·g^{-1} $LiMn_2O_4$).

Conclusion

In the work the technology of the electrochemical execution of FeS_2 on stainless steel was elaborated. Synthesized FeS_2 with structure of marcasite capable ensure the capacity in thin-layer electrodes of lithium prototype accumulator that equates with high capacity of natural pyrite FeS_2. Obtained electrochemically FeS_2-marcasite may be recommended for 1.5 V- scale lithium miniature accumulators. Suggested 2.0 V Li-ion micro-batteries with FeS_2-marcasite anode and $LiMn_2O_4$ or $LiCoO_2$ cathodes present itself attractive by increased safety.

 ISBN: 978-80-8152-530-8

Acknowledgments

The current presentation has been prepared in the framework of Ministry of Education and Science of Ukraine, №42/150690 project «Development of backup lithium batteries within the temperature range up to minus 25º C with shell-life of 15 years». Head of the project №42/150690, Chief of the NILHIT is prof. E. M. Shembel.

References

[1] R.D.Apostolova, O.V.Kolomoets, O.V.Danilov, E.M.Shembel' // Surf. Engineering and Appl. Electrochem. 50 (2014) 18-25.

[2] E.M.Shembel', R.D.Apostolova., V.M.Nagirnyi et al. // Russ. J. Electrochem. 40 (2004) 843-851.

[3] E.Shembel', R.Apostolova, I.Kirsanova, V.Tysyachny // J. Solid State Electrochem. 12 (2007) 1155-1157.

[4] E.Shembel', R.Apostolova, V.Nagirny, I.Kirsanova, Ph.Grebenkin, P.Lytvyn // J. Solid State Electrochem. 9 (2005) 96-105.

[5] R.Apostolova, V.Tysyachny, E.Shembel' // Russ. J. Electrochem. 46 (2010) 100-106.

[6] E. Shembel', R. Apostolova, D. Aurbach, B. Markovsky // Russ. J. Appl. Chem. 87 (2014) 1260-1267.

 ISBN: 978-80-8152-530-8

Binder free Silicon/Graphite anode: Breakthrough in Li-Ion Batteries.

E. Shembel[a,b], T. Pastushkin[a], V, Redko[a] , O. Markevych[b] , O. Kolomoiets[b]

[a] *Enerize Corporation, Coral Springs, FL, 33067, USA*
[b] *Scientific Research Laboratory of Chemical Power Sources Ukrainian State University of Chemical Technology, Dnipro, 49005, Ukraine*

**eshembel@enerize.com*

Problem: Li-ion batteries based on traditional electrode materials ($LiCoO_2$, etc., graphite) and liquid electrolytes:

1. Safety problems
2. Expensive.
3. Limited energy.
4. Limited operating range of temperatures.
5. Consist of toxic materials

Enerize solution: breakthrough electrode and electrolyte materials, technologies and equipment for production,non-destructive testing during production:

1. Anode based on binder free nano-structured Si-graphite composition.
2. Solid inorganic electrolytes
3. Equipment for high rate thin films depositions which possible for roll-to-roll operation
4. Non-destructive non-contact testing in-line initial materials, semi and final product during batteries production

Key advantages of Li-ion cells based on developed technologies:

1. Energy higher by two times.
2. Price is lower by two times.
3. Increased safety and operating range of temperature up to 250 ^{0}C.
4. Possibility to be used in the existing manufactures of lithium batteries

Current presentation is connected with following solution:

1. Anode based on binder free nano-structured Si-graphite composition.
2. Equipment for high rate thin films depositions which possible for the roll-to-roll operation

Enerize proposes a silicon – graphite composite anode that fabricated via a proprietary method of gas detonation deposition. Results of test reveal >1100mAh/g capacity during cycles, and further improvement are possible.

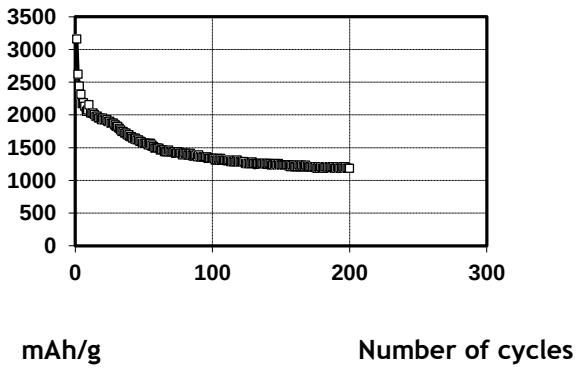

Figure 9. Dynamics of change in discharge capacity of graphite-silicon composite anode prepared by Enerize's gas detonation method. Electrolyte is EC/DMC/$LiClO_4$.

A further benefit is as following: Si - graphite composite electrode that produced using the method of gas detonation deposition do not require a polymer binder. This is because: a) electrodes have high level of the

 ISBN: 978-80-8152-530-8

adhesion between current collector and the composition of Si - graphite; b). particle of Si and graphite have high level of cohesion. These unique properties provide improved stability of the structure of electrodes and as result stability of the energy parameters of the battery during cycling.

Photo and ESM pictures of anode based on the nanostructured Si – graphite composition.

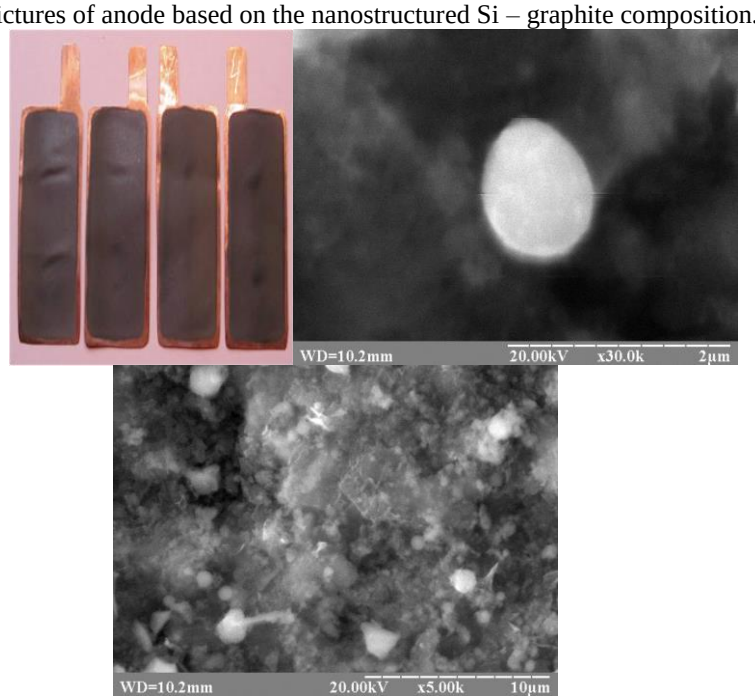

Figure. 2

Summary the benefit of equipment and technology that developed for production electrodes based on the composition of Si and graphite are as following:

- High level of cohesion between particles of the compositions;
- Adhesion of Si composition to substrate of the current collector;
- Strong mechanical strength during cycling without using expensive additives;
- High stable energy of batteries with Si-graphite anode during operation

Important note: the costs in volume production of the Si-graphite composite using the innovative method of gas detonation deposition are calculated to be much lower than alternative approaches such as Si nanowires, Si-graphene composites, etc

During presentation will be presented and described:

- Method and equipment for deposition electrode based on the composition Si and graphite
- Kinetic of electrochemical process on electrode based on Si – graphite composition
- Method of roll-to-roll production Li-ion cells with Si-graphite anode and solid inorganic electrolyte

Acknowledgements

This presentation is connected with the framework of NATO, Science for Peace and Security Programme Project SPS 985148 “Development of New Cathodes for Stable and Safer Lithium-Sulfur Batteries” in the light of development the following innovating batteries with high energy and low self - discharge that are based on Si/graphite anode – Sulfur cathode.

 ISBN: 978-80-8152-530-8

SESSION IV Advanced preparation methods and characterization techniques of nanomaterials

Nanoparticles and UV-C induced DNA damage

J. Labuda[a]*, A. Koutsogiannis[b], J. Sochra, D. Diamantidou[b], J. Blaškovičová[a], V. Svitková[a]

[a] *Institute of Analytical Chemistry, Slovak University of Technology in Bratislava, Radlinského 9, 812 37 Bratislava, Slovakia*

[b] *School of Chemistry, Faculty of Science, Aristotle University of Thessaloniki, University Campus, 54124 Thessaloniki, Greece*

**jan.labuda@stuba.sk*

Introduction

Oxidation stress induced by metallic and other nanoparticles (NPs) is considered to be the main reason of their toxicity. Photoactivated nanoparticles can transfer their energy to proximal molecular oxygen under the formation of singlet oxygen and, consequently, various reactive oxygen species (ROS). Due to the ROS production, NPs stimulated by UV light are considered as materials able to induce structural damage to DNA. Conventional analytical and bioanalytical methods based on the detection of products of the oxidative damage to DNA are often used in studies of toxicity of the nanomaterials [1]. At the same time, DNA-based biosensors have been numerously reported as effective devices for tests of DNA affinity interactions and structural changes [2-4].

The aim of this study was (i) to characterize the ability of gold and silver NPs as well as CdTe and CdS quantum dots (QDs) to generate ROS and (ii) to propose procedures based on the DNA biosensor and biosensing for the assessment of a potential risk of the UV irradiation towards the structure of isolated salmon sperm, calf thymus, and plasmid dsDNA preparatives.

Experimental

Gold NPs (size of app. 10 nm and 30 nm), silver NPs (of app. 12 nm and 65 nm), CdTe (of app. 3.1 nm and 6.2 nm) and CdS QDs (of app. 4.0 to 10.5 nm) have been obtained from the Mendel University in Brno. UV lamp OSRAM PURITEC HNS S 9 W with the working wavelength 253.7 nm and UV-C-radiation power of 2.5 W was used. A time dependent formation of ROS in the presence of individual nanoparticles under the 253.6 nm wavelength (UV-C) treatment was evaluated spectrophotometrically using UV/Vis spectrophotometer Evolution 201 (Thermo Scientific, USA).

Calf thymus double-stranded DNA (ct dsDNA) and low molecular weight salmon sperm dsDNA were obtained from Calbiochem USA/Canada and Sigma–Aldrich, Germany, resp. Electrochemical DNA-based biosensors (NPs/DNA/GCE) were constructed by a surface modification of conventional glassy carbon electrode by the layer of calf thymus, plasmid or salmon sperm dsDNA and the layer of corresponding nanoparticles.

UV lamp OSRAM PURITEC HNS S 9 W with working wavelength 253.6 nm and UV-C-radiation power of 2.5 W was used for the UV radiation. UV/Vis spectrophotometer Evolution 201 (Thermo Scientific, USA) was applied. Cyclic voltammetry (CV) and electrochemical impedance spectroscopy (EIS) in the presence of hexacyanoferrate(III/II), as well as square-wave voltammetry (SWV) of the guanine moiety were performed by AUTOLAB PGSTAT-100 obtained from Metrohm Autolab company (Netherlands) with data treatment using the software NOVA 1.10.23

Results and discussion

Detection of the ROS generation

Under irradiation of the solution of the spectrophotometric indicator 4-chloro-7-nitrobenzo-2-oxa-1,3-diazole (NBD-Cl) and NPs the appearance of new absorption wave of at 470 nm which confirms the presence of superoxide. Similarly, the irradiation of α-diphenyl-β-picrylhydrazyl (DPPH) solution with NPs leads to a decrease in the absorption waves of at 350 nm and 550 nm indicating the degradation of the DPPH radical (Fig. 1). On the other side, trapping of generated O^{2-} by radical scavengers such as quercetin and dsDNA in solution was detected by lower absorbance value of NBD-Cl at 470 nm depending on the scavenger concentration. The generation of ROS becomes limited also under the formation of protein corona at an incubation of metallic nanoparticles with fetal bovine serum.

Detection of damage to DNA using biosensor and biosensing

The NPs/DNA/GCE biosensors were exposed to UV-C radiation by free scattering from 15 cm light source distance for a given time. Then, DNA damage has been evaluated under performance of CV and EIS experiments in 1 mM solution of the $[Fe(CN)_6]^{3-/4-}$ redox indicator. Similarly, the biosensing procedure has been performed

 ISBN: 978-80-8152-530-8

which consisted of an UV-C treatment of the DNA solution in the presence of individual types of NPs followed by an immobilization of damaged DNA onto the bare GCE and electrochemical measurements. Typical records obtained are depicted in Fig. 2.

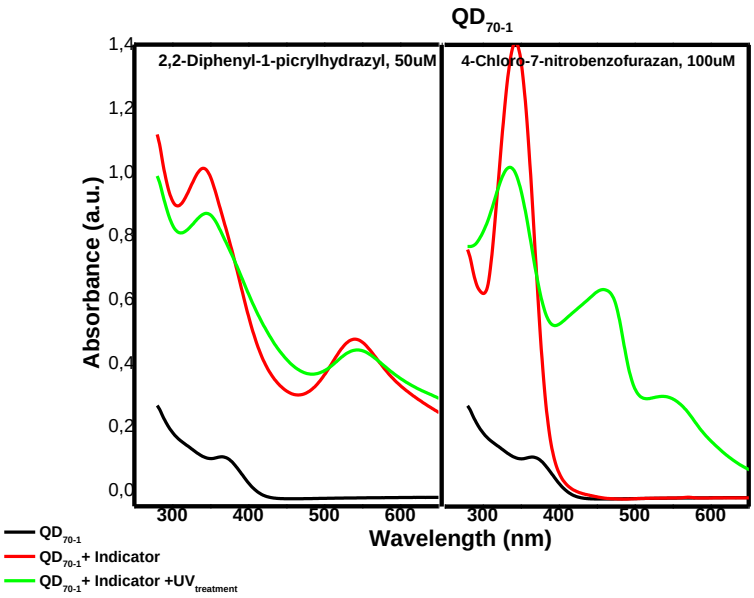

Fig. 1. Spectrometric detection of $OH^{\bullet}$ and $O^{2\bullet-}$ using diphenyl-1-picrylhydrazyl (DPPH) - left and 4-chloro-7-nitrobenzo-2-oxa-1,3-diazole (NBD-Cl) - right, resp.

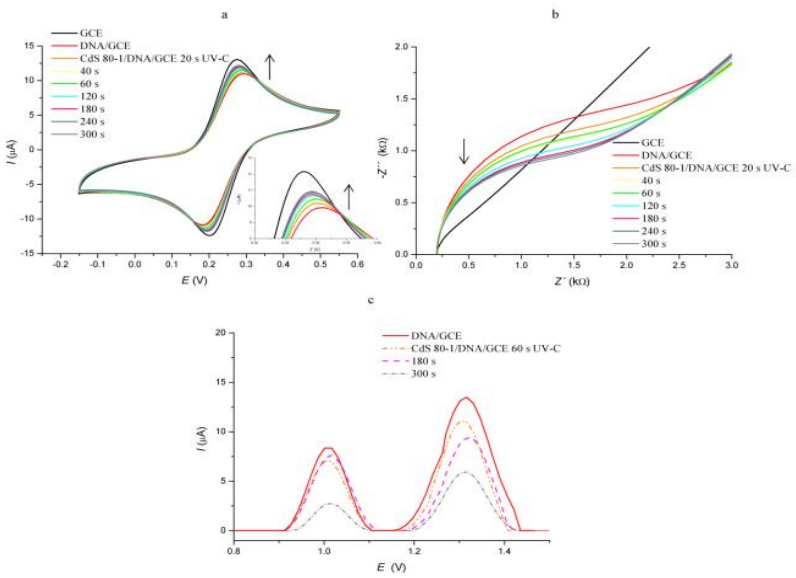

Fig. 2. Electrochemical detection of damage to DNA using DNA-based biosensor: a) CV records and b) Nyquist plots of EIS for 1 mM $[Fe(CN)_6]^{3-/4-}$, c) SWV response of the guanine and adenine moieties after the UV-C irradiation of the biosensor surface for given time [5].

An example of the evaluation of the DNA signals at CV and SWV is shown in Fig. 3. It presents gradual deep structural changes of original DNA which lead to leaching of the DNA rests from the biosensor surface or a formation of poorly covered electrode surface at biosensing [5,6].

 ISBN: 978-80-8152-530-8

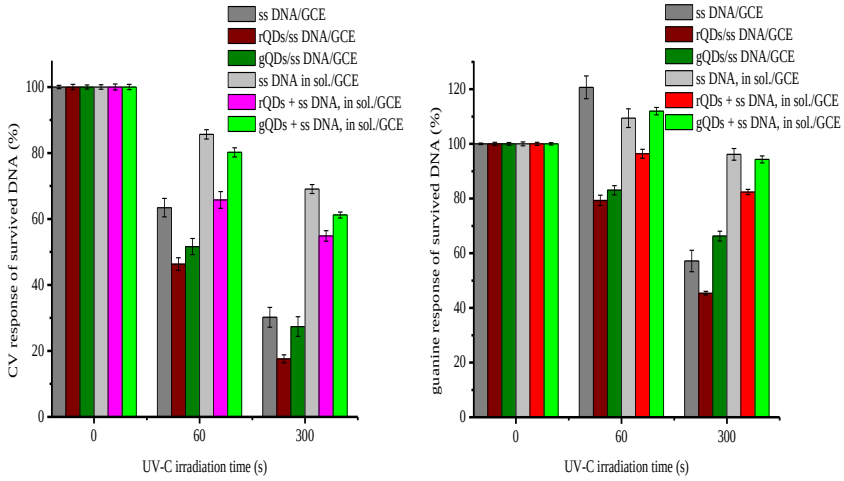

Fig. 3. Evaluation of the DNA signals at CV and SWV measurements using the biosensor and biosensing with salmon sperm DNA. Green emitting CdTe (gQDs) and red emitting CdTe (rQDs) at the biosensor (1st three columns) and in solution - biosensing (2nd three columns) [6].

Conclusion

The degradation of dsDNA by UV-C radiation in the presence of metallic NPs as well as CdTe and CdS quantum dots depends on their fluorescence ability. This study presents the DNA-based biosensor as an effective analytical tool for evaluation of the UV-C degradation of dsDNA structure, i.e. an evaluation of potential risk effect of the nanoparticles towards surface attached DNA.

Acknowledgements

This work was supported by the Scientific Grant Agency VEGA of the Slovak Republic (Project No. 1/0489/16) and by the Competence Center for SMART Technologies for Electronics and Informatics Systems and Services, ITMS 26240220072, funded by the Research&Development Operational Programme from the ERDF.

References

[1] E. J. Petersen, B. C. Nelson, Anal. Bioanal. Chem. **398** (2010) 613–650.

[2] J. Labuda, A. M. O. Brett, G. Evtugyn, M. Fojta, M. Mascini, M. Ozsoz, I. Palchetti, E. Paleček, J. Wang, Pure Appl. Chem. **82** (2010) 1161–1187.

[3] J. Labuda, V. Vyskocil, *DNA/Electrode Interface, Detection of Damage to DNA Using DNA Modified Electrode;* in: *Encyclopedia of Applied Electrochemistry* (G. Kreysa, K. Ota, R.F. Savinell, eds.), Springer, New York, 2014, pp. 346-350.

[4] M. Fojta, A. Daňhel, L. Havran, V. Vyskočil, TrAC - Trends Anal. Chem. **79** (2016) 160–167.

[5] V. Svitková, J. Blaškovičová, M. Tekeľová, B. M. Kallai, T. Ignat, P. Skládal, V. Horňáková, P. Kopel, V. Adam, D. Farkašová, J. Labuda, Sensors Actuat B-Chem **243 (**2017) 435-444.

[6] L. Hlavata, I. Striesova, T. Ignat, J. Blaskovisova, B. Ruttkay-Nedecky, P. Kopel, R. Kizek, J. Labuda, Microchim. Acta **182** (2015) 1715-1722.

 ISBN: 978-80-8152-530-8

SESSION IV Advanced preparation methods and characterization techniques of nanomaterials

Mechanical, thermal, fire resistance and morphological characterizations of surface modified carbon nanotube reinforced thermoplastic polyurethane composites

Y.Kanbur [a]*, U. Tayfun [b]

[a] *Karabuk University, Metallurgical and Materials Engineering, Karabuk, Turkey*
[b] *Inovasens Ltd., Izmir Technopolis, Urla, Izmir, Turkey*

**yasinkanbur@karabuk.edu.tr*

TPU consists of hard and soft segments. Hard segment consists of highly polarized group which is hardened by crosslinking [1] and soft segment consists of polyester phase. Hard segments disperse as micro-domains in the structure and phases are held together by the hydrogen bonds [2]. TPU is a good candidate for broad industrial application area including footswear, automotive, sporting goods, tubes, hoses, wires, cables and medical devices in the form of sheets, films, or profiles [3] due to its easy processibility and fully recyclable nature.

Carbon nanotubes (CNT) have wide application area such as biosensors, solar cells, fuel cells, capacitors, and electromagnetic shielding because of its high aspect ratio, proper electronic and mechanical properties. Agglomeration of CNT inside the polymer matrix is a common problem for the production of suitable CNT/polymer composites. This problem can be overcome by application of different techniques like surface modification of CNT with proper surface groups which are compatible with polymer matrix, melt mixing, solution mixing or addition of compatibilizers.

In this study, thermoplastic polyurethane (TPU) composites containing CNT with the loading ratios of 0.5, 1.0, 1.5 and 2.0 wt% were prepared using melt-compounding process. Surfaces of the CNT particles were treated with sulfuric acid/nitric acid to purify CNT and to achieve compatible surface characteristics between TPU matrix and CNT. Mechanical, thermal, flame retardant, melt flow and morphological properties of TPU/CNT composites were investigated. Carbon nanotube addition to TPU matrix results with prominent increase in tensile strength, percent elongation and modulus of TPU. The mechanical properties are enhanced for lower modified CNT loadings. Carbon nanotube inclusions also improve thermal stability of pristine TPU. Addition of CNT into TPU matrix causes increase in melting and decomposition temperatures of TPU and decrease in glass transition temperature. The UL- 94 rating and LOI of TPU are also shifts to higher values after CNT loadings to matrix. Modified CNT additions at higher concentrations exhibit better fire performance. Additions of m-CNT and pristine CNT show different trends in the case of MFI values. Modified CNTs disperse more homogeneously relative to pristine ones into TPU matrix which is due to improvement in interfacial interactions between carbon nanotube and TPU.

Acknowledgements

This work is supported by Karabuk University Coordinatorship of Research Projects with the project number KBÜBAP-17-YD-393

References

1. A.K. Bhowmick and H.Stephens , Handbook of Elastomers, CRC Press, 2001.

2. T.K.Chen , Y.I. Tien and K.H.Wei, Synthesis and characterization of novel segmented polyurethane/clay nanocomposites. Polymer, 41(2000), 1345–1353.

3. U.Tayfun, Influence of surface treatment of fillers on the mechanical properties of thermoplastic polyurethane composites. Ph.D. Thesis: Middle East Technical University, 2015.

 ISBN: 978-80-8152-530-8

SESSION IV Advanced preparation methods and characterization techniques of nanomaterials

Innovative Non-Destructive Non-Contact Methods for Testing / Evaluation in Nanotechnology

V. Redko[a], E. Shembel[a,b], T. Pastushkin[a], N. Zaderey[b], and O. Markevych[b]

[a] *Enerize Corporation, Coral Springs, FL, 33067, USA*
[b] *Scientific Research Laboratory of Chemical Power Sources Ukrainian State University of Chemical Technology (USUCT), Dnipro, 49005, Ukraine*

**eshembel@enerize.com*

Non-destructive non-contact methods of testing / quality control (NDT) of starting materials, semi- product during the manufacturing process, and the final manufactured product before delivery to customer are ensuring quality, reliability, safety, and reducing cost of product. These issues are very important for number of critical conditions from the space industry to the batteries production; the list of critical examples could be increased.

With growing the nanotechnologies and developing new nanosructured materials the role and benefit of non-contact non-destructive methods of evaluation the properties and defects dramaticaly increases. Non-destructive non-contact methods allow provide quality control of new materials, including nanomaterials and thin-layered materials, which can be sensitive to mechanical contact.

During presentation will be presented non-destructive methods and equipment which developed by Enerize that successfuly used in the area of the Li batteries, solar cell production, and chemical industry.

The safety and reliability of Li battery are determined mainly by its basic design and chemistry. However, without adequate quality control during manufacture, defects in even the best designs can lead to inconsistent performance and early failure. Deployment of automated quality assurance technology at every stage of the manufacturing and assembly process will increase the reliability and safety of batteries while lowering overall manufacturing costs by reducing wastage and preventing defective components from being incorporated into the finished product.

Some examples of innovative equipment for non-destructive testing that are used during Li batteries development and production, are presented below.

Fig 1 and 2. Determination of physical chemical properties, for example conductivity and composition of powdered materials including electrode materials, graphite, and different products in chemical industry

Fig.3. Device for non-destructive non-contact detection of hidden faults of welding in batteries and ultracapacitors

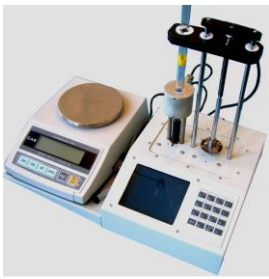

Fig. 1

Fig. 2

Fig. 3

Fig. 4 Holographic interferometry system and optical schematic for detecting hidden defects in electrode structure and batteries. As load the heat as small as 1-2 Celsius degree is used. The sensitivity of the method allows detection of defects even as little as 0.03 microns. Elements of this device include: 1. Laser beam, 2. Optical wedge, 3, 4, and 5. Lenses, 6,7. Mirrors, 8. Recording cell, 9. Test article, and 10. Vibration free table.

 ISBN: 978-80-8152-530-8

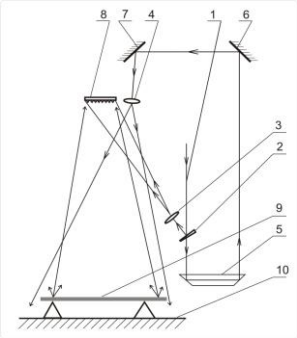

Fig.4

According to Dr. Robert Crawford, Maxwell Technologies Director of Operations (http://www.maxwell.com/) : "Enerize has developed a non-destructive eddy current measurement system for Maxwell that can detect quality problems with our laser welds. This is a proof of concept system that will be used to optimize our laser welding process and ultimately improve our system equivalent series resistance (ESR) as we optimize weld quality. Eventually we would invest in an automated system that will test 100% of our welds".

According to Dr. Dayal T. Meshri, President/CEO of Advance Research Chemicals: (http://www.fluoridearc.com/) "The new method takes advantage of electromagnetic properties of a substance and determines the composition of the powdered materials. It is a novel approach in the chemical industry for monitoring a variety of processes including synthesis, filtration, and drying, etc. especially at high temperatures and pressures and under corrosive conditions. This unique approach improves yields and uncovers hidden problems in manufacturing. It also enables reliable production of quality material to a variety of clients who have different specifications for the same material. In addition it is a very fast and inexpensive method for a quality control. We intend to explore more applications jointly with Enerize Corporation to provide additional benefits to the chemical industry."

Developed equipment based on the following methods

- Electromagnetic eddy-current,
- Electromagnetic capacitance,
- Combined electromagnetic eddy-current & capacitance;
- Holographic Interferometry;
- Gas Discharge Visualization – High Voltage Electric Field method
- Ultrasonic with dry contact

The goals are to conducting the non-destructive non-contact testing & evaluation the following properties (is not limited to):

- Conductivity, composition and purity of the powder materials, liquids, polymer & slurry compositions;
- Interface resistance between current collector and active electrode mass
- Thickness measurement & quality assurance during the electrode coating.
- Hidden defect in electrodes, solid electrolytes and other components.
- Hidden defects in multiple layer structure**,** for examples, Jelly Roll in battery & ultracapacitor
- Weld quality hidden faults in batteries and ultracapacitors

In the light of the framework of NATO, Science for Peace and Security Programme Project SPS 985148 "Development of New Cathodes for Stable and Safer Lithium-Sulfur Batteries" in which Enerize is industrial partner, and USUCT is participant from Ukraine, we will be presenting among other examples the following: how the non-contact testing the conductivity of powdered materials allow optimize the composition of electrode mass. We will also illustrate Other important example will illustrate the test of interface resistance between modified Al current collector and electrode mass based on the sulphur. The value of contact resistance between metallic current lead and electrode mass composite coating is one of the key parameters for determination of performance of energy storage devices, such as batteries, supercapacitors, etc.

 ISBN: 978-80-8152-530-8

Enerize NDT methods are based on the interaction of different vector and scalar fields with the test article

- ✓ Wave acoustic fields of different polarization.
- ✓ Potential electrical and magnetic fields.
- ✓ Vector eddy magnetic fields.
- ✓ Gradient heat fields (infra-red spectrum).
- ✓ Electron emission fields.
- ✓ Glow fields of high voltage pulse discharges.

Non-destructive methods and equipment are innovative tools for successful coordination of R&D, manufacturing, and applications of Li batteries

Major advantages of the Enerize non-destructive non-contact testing methods include the following:

- ✓ Reliability due to non-contact mode of operation.
- ✓ Efficient, fast, simple, and inexpensive to implement.
- ✓ Easy to automate. Results are obtained in real-time.
- ✓ Do not require any special protection for operators and equipment. Safe and less expensive than X-ray methods.
- ✓ Precise determination of specific parameters and defects.
- ✓ **Provide 100% nondestructive control** of the technological operations and the quality of the end product.
- ✓ Provide quality control of material and products **for which contact methods, in principle, cannot provide** reliable information due to extraneous processes at the sensor/test article interface surface.
- ✓ **Provide quality control of new materials, including nanomaterials and thin-layered materials, which can be sensitive to mechanical contact.**

Enerize Non-Destructive Technology Background from Space Systems to Batteries and other industries

History: NDT technologies ensured safety and reliability of Space Systems.

Recent applications: NDT processes have been adapted to new energy storage production.

Hardware: New NDT equipment and new transducers have been designed and delivering to customers.

Areas of applications: Batteries, supercapacitors, solar cells, chemical, construction, petrochemistry industries, etc

Intellectual Property: 15 US patents, 1 UK patent, and 8 US pending patent applications during the last 8 years

Acknowledgements

This presentation is connected with the framework of NATO, Science for Peace and Security Programme Project SPS 985148 “Development of New Cathodes for Stable and Safer Lithium-Sulfur Batteries” in the light of the using the non-destructive non-contact methods and equipment for test and evaluation initial materials and components of batteries for optimize and increasing the energy, stability and safety of Lithium-Sulfur Batteries

References. Enerize Corporation IP in the area of non-destructive testing

1. Method of Non-Contact Measuring Electrical Conductivity of Electrolytes with Using Primary Measuring Transformer. US Patent No. 7,071,684..
2. Method and Apparatus for Measuring Conductivity of Powder Materials Using Eddy Currents. US Patent No. 7,288,941.
3. Method and Apparatus For Eddy Current-Based Quality Inspection of Dry Electrode Structure. US Patent No. 7,355,395 and UK Patent GB No. 2435575
4. Method of Nondestructive Tightness Testing Based on Gas Discharge Visualization. US Patent No. 7,498,817.
5. Integrated Non-destructive Method and Device for Electrochemical Energy System Diagnostics. US Patent No. 7,783,438.
6. Apparatus and Method for Determining Service Life of Chemical Energy Sources Using Combined Ultrasonic and Electromagnetic Testing. US Patent No. 7,845,232.

 ISBN: 978-80-8152-530-8

7. Holographic Interferometry for Non-destructive Testing of Power Sources. US Patent No. 7,911,618.
8. Method and Eddy Current System for Non-Contact Determination of Interface Resistance. US Patent No. 7,982,457.
9. Method and Device for Rapid Non-Destructive Quality Control of Powdered Materials. US Patent No. 8,102,181.
10. Method and Apparatus for Detecting and Inspection Through-Penetrating Defects in Foils and Films. US Patent No. 8,284,247.
11. Methods and Systems for Non-Destructive Determination of Fluorination of Carbon Powders. US Patent No. 8.309,024.

 ISBN: 978-80-8152-530-8

SESSION IV Advanced preparation methods and characterization techniques of nanomaterials

Evaluating the molecular interactions in nanocomposite films using PCA and 2DIR correlation spectroscopy

Maria-Cristina Popescu*, Bianca-Ioana Dogaru, Carmen-Mihaela Popescu

"Petru Poni" Institute of Macromolecular Chemistry of Romanian Academy, Iasi, Romania

cpopescu@icmpp.ro

Two-dimensional infrared (2DIR) spectroscopy was introduced by Isao Noda in 1989 and it is an analytical technique based on time-resolved detection of IR signals [1]. In 2D IR, a spectrum is obtained as a function of two independent wavenumbers. By this method it is possible: the simplification of complex spectra consisting of many overlapped peaks; enhancement of spectral resolution by spreading peaks over the second dimension; and identification of various inter- and intramolecular interactions through selective correlation of IR bands [1]. This method was successfully used by our group for study the interaction in polymeric blends [2], crystallization process [3], and identification of different systems [4] and also was applied to different techniques like MID-IR or NIR spectroscopy.

This method together with principal component analysis (PCA) was used for identification of specific interaction between polyvinyl alcohol/ starch/ cellulose nano-crystals. For this study 90PVA/10/S, 75PVA/25S and 50PVA/50S were used as a polymeric matrix and 5, 10 and 15 % CNC were added as a reinforcing agent. The IR spectra of the pure components and blends with different compositions were investigated in detail. To evaluate the interaction between the blend components, the experimental spectra were compared with the calculated "blends" spectra, constructed using the additivity low from pure components spectra.

After the processing of spectra, the PCA and 2D correlation spectra for experimental and calculated data were constructed and the results were compared.

Thus, PC scores for the two types of spectra established some distinct patterns which clearly expressed their differences. Also, in the 2D correlation spectra different patterns indicate interaction of the components in the blend with the formation of new H-bonds.

Acknowledgements

This work was supported by a grant of the Romanian National Authority for Scientific Research and Innovation CCCDI-UEFISCDI, project number COFUND-M-ERA.NET II- COMPIO, within PNCDI III.

References

[1] I. Noda, Appl. Spec. **44 (4)** (1990) 550-561.

[2] M.C.Popescu, C. Vasile, Spectrochim. Acta - Part A: Molecular and Biomolecular Spectroscopy **79(1)** (2011) 45-50.

[3] M.-C. Popescu, R. Gomez, F.J. De La Mata, B. Rasines, B.C. Simionescu, J. Nanopart. Res. **15(10)** (2013) 2009.

[4] M.-C. Popescu, C. Vasile, O. Craciunescu, Biopolymers **93 (12)** (2010) 1072-1084.

 ISBN: 978-80-8152-530-8

SESSION IV Advanced preparation methods and characterization techniques of nanomaterials

Structure and sorption properties of CNC reinforced PVA films

Bianca-Ioana Dogaru, Maria-Cristina Popescu, Carmen-Mihaela Popescu

"Petru Poni" Institute of Macromolecular Chemistry of Romanian Academy

**dogaru.bianca@icmpp.ro*

The use of biodegradable polymers in different areas of application increased in the last period because producers and consumers value the materials' ability to protect the environment. By replacing fossil fuel-based synthetic plastics (such as polyethylene or polypropylene), with biodegradable polymers reduces consumption of petroleum and natural gas and diminishes the accumulation of persistent waste.

Nanocomposite films were successfully developed using cellulose nano crystals (CNC), as the reinforcing phase, and poly vinyl alcohol (PVA), as the matrix, by solution casting technique. For blend preparation 5, 10, 15 wt % CNC suspensions were incorporated in PVA solution. Structural evaluation was done by Fourier transform infrared spectrometry, 2D IR correlation spectroscopy and X-ray diffraction. IR spectroscopy and 2D correlation spectroscopy evidenced the presence of H-bond interaction between the PVA and CNC and also variation in the conformational rearrangement, while the X-ray diffraction showed that the crystallite size and the degree of crystallinity were strongly affected by the incorporation of CNC in the nanocomposite films. In order to evaluate the interaction of the studied systems with water, contact angle measurement, water vapour sorption and NIR spectroscopy were used. The increase of CNC content induced a reduction in water sorption of the nanocomposite films [1].

Acknowledgements

This work was supported by a grant of the Romanian National Authority for Scientific Research and Innovation CCCDI-UEFISCDI, project number COFUND-M-ERA.NET II- COMPIO, within PNCDI III.

References

[1] M.-C. Popescu, Int. J. Biol. Macromol.**101** (2017) 783-790.

 ISBN: 978-80-8152-530-8

SESSION IV Advanced preparation methods and characterization techniques of nanomaterials

Hydrogenation of carbon dioxide to methanol over catalysts based on silica - alumina modified with Zr-, Pd-salts

Tagiyeva Sh.F., Aliyeva N.M., Mammadov E.E., Ismailov E.H.

Institute of Petrochemical Processes of National Academy of Sciences Azerbaijan, Baku,Azerbaijan, AZ 1025, Baku, 30, Khojaly ave.

**tshaxla@mail.ru*

At present, it can be confidently asserted that the development of technologies for the accumulation of CO_2 and their transformation into various valuable chemicals can effectively contribute both to reducing emissions into the atmosphere and creating new areas of the chemical industry, in related areas. Hydrogenation is one of the effective ways of converting carbon dioxide to important chemical products, for example, methane, methanol or formic acid. Hydrogenation of CO_2 is carried out using both homogeneous and heterogeneous catalysts [1]. Note that the known homogeneous catalysts that are required to convert CO_2 to methanol are destroyed at high temperatures required for the reactions. The search for effective heterogeneous catalytic systems for the hydrogenation of CO_2 into methanol continues to this day. Researches to date are focused on finding mainly selective nanostructured catalysts that can activate carbon dioxide under the mild reaction conditions with high selectivity towards methanol [2].

In the presented report results of research of oxide systems on the basis of silica- alumina with the trade name "SIRAL" of company Sasol, modified by salts of zirconium and palladium, as catalysts of hydrogenation of CO_2 into methanol are given. The influence of the reducing temperature of the samples before catalysis onto the phase composition of the samples, form and distribution of the Pd nanoparticles, obtained after high temperature treatment of the samples with deposited Pd-, Zr-salts in H_2 current is considered. The palladium content in the samples varied in the range 0.1-5.0% by weight, and the zirconium content remained unchanged (10% by mass in terms of ZrO_2). The distribution of the (Pd, Zr) elements of the active component on a carrier was determined using a X-ray fluorescent microscope XGT-7000, Horiba, by scanning a 10-μm beam spot at five randomly chosen points on the sample surface. The phase composition and average size of the crystallites (coherent scattering regions) were estimated using an XRD TD 3500 X-ray diffractometer, China. The JES-PE-3, Jeol radio spectrometer with a working frequency of 9.3 GHz was used to identify the magnetic centers, particles in the catalyst samples before and after the hydrogenation reaction. In the thermal desorption mode, chromatographic analysis of gas phase products was used to study samples of catalysts with adsorbed at room temperature with methanol.

Catalytic tests of the samples, in the hydrogenation of CO_2 at a molar ratio of CO_2 / H_2 of 1: 3, were carried out in a flow-through unit, at atmospheric pressure and at a temperature of 300-500 ° C with chromatographic analysis of gas phase reaction products on-line. Before catalytic measurements, the catalyst samples were subjected to reduction in a stream of hydrogen at a temperature of 350, 450, 550, 650 °C for 1 hour. The effect of preliminary high-temperature reduction of samples with different palladium content on the phase composition of samples, their magnetism, distributions of palladium in the samples, and catalytic properties is discussed.

References

[1] X. Su, J. Xu, B. Liang, H. Duan, B. Hou, Y. Huang // J. Energy Chemistry. **2016**, V. 25, 553–565.
[2] S. Kattel, B. Yan, Y. Yang, Jing G. Chen, and P. Liu. // Journal of the American Chemical Society, **2016,** *138* (38), 12440-12450.

 ISBN: 978-80-8152-530-8

SESSION IV Advanced preparation methods and characterization techniques of nanomaterials

Synthesis and Characterization of Vanadium-Doped Titanium Dioxide Nanotubes

M. Türkay Aytekin Aydın[a*], H. Levent Hoşgün[b]

[a]*Anadolu University, Science Faculty, Department of Physics, 26470 Eskişehir, Turkey*
[b]*Bursa Technical University, Department of Chemical Engineering, Bursa, Turkey*

[*]*maytekin@anadolu.edu.tr*

One-dimensional nanotubes of titanium dioxide (TNTs) doped of vanadium (V) were synthesized via hydrothermal method. Two-step hydrothermal method was developed to prepare V-doped TiO_2 nanotubes (VTNTs). These nanoparticles were characterized by X-ray diffraction (XRD), Fourier transform infrared spectroscopy (FT-IR), Raman spectroscopy, transmission electron microscopy (TEM) and scanning electron microscopy (SEM). BET specific surface areas were determined with N_2 adsorption-desorption isotherms at liquid nitrogen temperature. XRD and FT-IR results showed as-prepared nanotubes were complete anatase phase. The aim of the present VTNTs study was to develop a material that can be investigated the cytotoxic effects of VTNTs on human breast cancer cells.

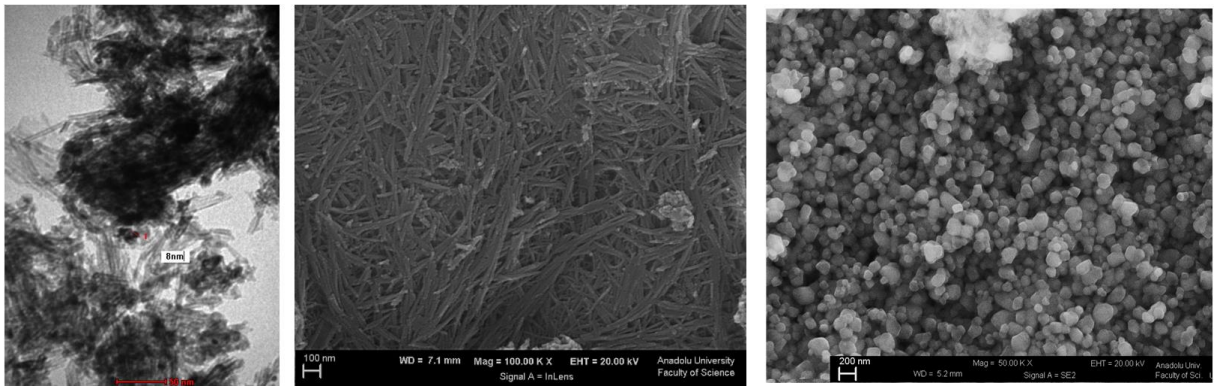

Figure. TEM image of TNT (a), FESEM images of vanadium-doped TNT (b), and TiO_2 (c).

References

[1] C.N.R. Rao, S.R.C. Vivekchand, K. Biswas, A. Govindaraj, Synthesis of inorganic nanomaterials, Dalton Transactions, (2007) 3728–3749.

[2] R.S. Devan, R.A. Patil, J. H. Lin, Y. R. Ma, One–Dimensional Metal–Oxide Nanostructures: Recent Developments in Synthesis, Characterization, and Applications, Advanced Functional Materials, 22 (2012) 3326–3370.

[3] V. Luca, S. Thomson, R. F. Howe, Spectroscopic investigation of vanadium speciation in vanadium-doped nanocrystalline anatase, J. Chem. Soc., Faraday T rans., (1997) 93(12), 2195-2202.

 ISBN: 978-80-8152-530-8

SESSION IV Advanced preparation methods and characterization techniques of nanomaterials

Nano-oxide ceramics based on organoelementoxanes

G. Scherbakova[a*], T. Apukhtina[a], P. Storozhenko[a], M. Varfolomeev[b], A. Ashmarin[c]

[a] *State Research Institute for Chemistry and Technology of Organoelement Compounds, 105118 Moscow, Russia*
[b] *Moscow aviation institute (National research university), 125993 Moscow, Russia*
[c] *Baikov Institute of Metallurgy and Material Science RAS, 119334 Moscow, Russia*

**galina7479@mail.ru*

The ceramic-forming organoelement poly(oligo)mers are a new class of promising precursors for obtaining high-temperature and oxidation-resistant components (ceramic fibers, matrixes, combined protective and barrier coatings, powders) of nanostructured ceramic composites. They allow to apply radically different "polymer technology" for ceramics production through pyrolysis of the ceramic-forming organoelement poly(oligo)mers [1].

On the basis of unstable chemically active organoaluminum compounds we have developed a method for the synthesis of hydrolytically stable in air ceramic-forming organoalumoxane oligomers - chelated alkoxyalumoxanes [2].

It is found that the thermochemical treatment of ceramic-forming organoalumoxanes results in corrundum ceramics α-Al_2O_3 [2].

Based on such ceramic-forming organoalumoxanes, a process for the preparation of a high-purity nanostructured, silica free organoalumoxane binder of corundum composition α-$A1_2O_3$ was developed [3].

The ceramic-forming organoalumoxanes were found to readily interact with metal alkoxides and acetylacetonates and they may comprise a wide range of elements and metals in various combinations and ratios with homogeneous distribution in oligomer matrix on a molecular level. This provides a perfect nanostructure, enhanced physical-mechanical and operational properties of ceramic composites obtained on the basis of ceramic-forming organoelementoxanes. The organometallic synthesis ensures high purity of the starting oligomers. This allows obtaining high-purity oxides of elements of a given composition and producing materials on their base at much lower temperatures as compared with technical-grade oxides use [1].

The hydrolytically stable in air, soluble in organic solvents ceramic-forming organoyttriumoxanealumoxanes having fiber-forming properties were synthesized by the co-condensation of chelated organoalumoxane oligomers and yttrium acetylacetonate [4,5].

Thermochemical transformation (pyrolysis) of ceramic-forming organoyttriumoxanealumoxanes at 1500 °C results in aluminum-yttrium ceramics.

It is found that the pyrolysis of organoyttriumoxanealumoxanes with Al:Y≈1.5-1.7 leads to the formation of an aluminum-yttrium garnet, the samples are a ceramic matrix consisting of globular formations with nanostructured elements whose characteristic dimensions do not exceed 10 nm.

Polymeric organoaluminum-yttrium fibers based on organoyttriumoxanealumoxanes in the pyrolysis process are transformed into ceramic refractory oxide fibers based on alumina, modified with yttrium oxides, including fibers of aluminum-yttrium garnet $Al_5Y_3O_{12}$ composition [5].

The hydrolytically stable in air, soluble in organic solvents ceramic-forming organomagnesiumoxanealumoxanes having fiber-forming properties were synthesized by the chelated alkoxyalumoxane interaction with magnesium acetylacetonate [6].

We found that organomagnesiumoxanealumoxanes pyrolysis with molar ratio of Al:Mg = 2:1 even at 900 ºC results in magnesium-aluminate $MgAl_2O_4$.

Based on ceramic-forming organoelementoxanes (organoalumoxanes, organoyttriumoxanealumoxanes, organomagnesiumoxanealumoxanes) the researchers of SSC RF GNIIChTEOS developed effective method for obtaining components of heat - resistant ceramics and ceramic composites of oxide composition (Al_2O_3, Y_2O_3–Al_2O_3, MgO–Al_2O_3): binders, impregnation compositions, ceramic nanopowders [1,3,6,7].

Acknowledgements

This work was supported by the Russian Foundation for Basic Research, project no. 17-03-00331 A.

References

[1] G.I. Shcherbakova, P.A. Storozhenko, M.S. Varfolomeev et al. *Nanotechnics*. 3(35) (2013) 15-23.

[2] P.A. Storozhenko, G.I. Shcherbakova, A.M. Tsirlin, et. al. *Inorganic Materials*. **43** (2007) 320-382.

 ISBN: 978-80-8152-530-8

[3] M.S. Varfolomeev, V.S. Moiseev, G.I. Shcherbakova, et. al. *Inorganic Materials*. **51** (2015) 76-81.
[4] G.I. Shcherbakova, P.A. Storozhenko, N.B. Kutinova, et. al. *Inorganic Materials*. **48** (2012) 1058-1063.
[5] G.I. Shcherbakova, T.L. Apukhtina, P.A. Storozhenko, *Inorganic Materials*. **51** (2015) 206-214.
[6] G.I. Shcherbakova, N.S. Krivtsova, T.L. Apukhtina, et. al. RF Patent 2615147 C1, 2017.
[7] M.S. Varfolomeev, V.S. Moiseev, G.I. Shcherbakova, et. al. *Inorganic Materials*. **51** (2015) 722-727.

 ISBN: 978-80-8152-530-8

SESSION IV Advanced preparation methods and characterization techniques of nanomaterials

Chemical synthesis and densification of nanocrystalline zirconium diboride powders

Hasan Gocmez[a*], Mustafa Tuncer[a], Iurii Bogomol[b]

[a] *Department of Material Science and Engineering, Dumlupınar University, 43030 Kutahya, Turkey*
[b] *Kiev Polytechnic Institute Department of material and Powder Metallurgy, Kiev, Ukranie*

**hasan.gocmez@dpu.edu.tr*

The scope of this study is to review the synthesis, compaction and sintering of nanocrystalline ZrB_2 powders. ZrB_2 powders were prepared using simple gel method. The characterization of synthesized powders was carried out mainly by X-ray diffraction (XRD), Transmission Electron Microscopy (TEM) and Scanning Electron Microscopy (SEM) and surface area measurement (BET). Samples were densified by pressureless sintering and spark plasma sintering. The XRD results showed that the powders was transformed zirconium diboride phase upon increasing temperature from 1000 to 1500 ^oC. The surface area of the powders heat treated at 1500 ^oC was found to be 1.6 m^2/g. the morphology of the powders at 1500 ^oC were hexagonal rod-like with 60 nm of crystallite size.

ZrB_2 powder with Fe and Ni as a sintering aids was compacted and then pressureless sintered at 1750 ^oC for 5 h. The sintered ZrB_2 + Ni ceramics had a hardness of 15.8 GPa and density of 94.8%, while those was found to be 14.9 GPa and 99.9% for Fe addition. In the SPS processing, ZrB_2 with nickel addition ceramic were densified at 1600 and 1900 ^oC in atmosphere under a pressure of 65 MPa. ZrB_2 sample was sintered to 88 % of relative density at 1300 ^oC, while density of sample sintered at 1600 ^oC was found to be 93 %. The hardness values of the samples were changed from 11 to 13.7 GPa as SPS temperature increase from 1300 to 1600 ^oC. The SPS processing result in homogenous and fine microstructure when compared with conventional one.

Acknowledgements

The financial supports provided by the Scientific Research Project of Dumlupınar University, Project no. BAP 2011-11) and by the National Boron Research Institute of Turkey (BOREN, Project no. 2009- Ç0232) are gratefully acknowledged.

 ISBN: 978-80-8152-530-8

SESSION IV Advanced preparation methods and characterization techniques of nanomaterials

The preparation and characterization of polymer derived nanocrystalline SiOC powders

Sait Altun[a], Hasan Gocmez[a*] , Mustafa Tuncer[a]

[a]*Department of Material Science and Engineering, Dumlupınar University, 43030 Kutahya, Turkey*

**corresponding author: hasan.gocmez@dpu.edu.tr*

The production of advanced ceramics from preceramic polymers offers advantages in terms of simple processing methodology, low processing cost, other properties arising from the composition of the final ceramics. In this study, Silicon oxycarbide (SiOC) powders were prepared by the sol-gel methods using Tetraethylortosilicate/Polydimethylsiloxan (TEOS/PDMS) as organic-inorganic precursors. The gels were pyrolized at 1100 ˚C and were sintered at 1550 ˚C with both He and Ar atmosphere. The obtained powders were characterized by X-Ray Diffractometer (XRD), Scanning Electron Microscopy (SEM), Energy Dispersive X-ray (EDX), Differential Thermal Analyzer (DTA) and Fourier Transform Infrared (FTIR) respectively. The results are compared with literature studies and they showed the SiOC powders were successfully synthesized. The study delivers direction for the systematic design and fabrication of SiOC materials with potential application including catalysis, sorption and membrane separations under extreme conditions, biomedical device and among others.

 ISBN: 978-80-8152-530-8

SESSION IV Advanced preparation methods and characterization techniques of nanomaterials

Isomerization of alpha-pinene over halloysite – the effect of temperature

P.Miądlicki[a]*, A. Wróblewska[a] , M. Malko[a]

[a] *Institute of Organic Chemical Technology, West Pomeranian University of Technology Szczecin,Pulaskiego 10, 70-322 Szczecin, Poland*

* *piotr.miadlicki@zut.edu.pl, agnieszka.wroblewska@zut.edu.pl*

Introduction

During the process of weathering the rocks, also the process of "kaolinization" takes place, in which the sodium feldspar is broken down into minerals of the kaolin group - kaolinite and halloysite. Both materials are hydrated aluminosilicate minerals with the empirical formula of $Al_2Si_2O_5(OH)_4$. Halloysite naturally occurs as small cylinders (nanotubes) that have a wall thickness of 10–15 atomic alumosilicate sheets, an outer diameter of 50–60 nm, an inner diameter of 12–15 nm, and a length of 0.5–10 μm. Its outer surface is mostly composed of SiO_2 and the inner surface is composed of Al_2O_3 - hence these surfaces are oppositely charged [1,2]. The main purpose of this work was to investigate the effect of reaction temperature on the course of the α-pinene isomerization process over natural halloysite.

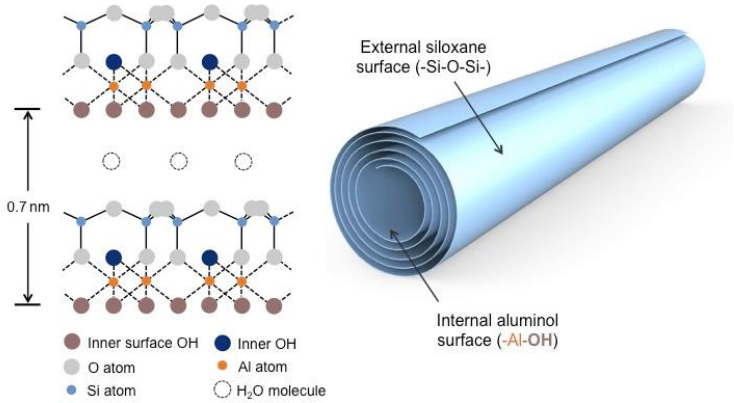

Figure 1. The structure of halloysite [3]

Experimental

In our studies, we used the halloysite obtained from the Dunino mine (Poland). Isomerization tests were carried out in a glass reactor with the capacity of 25 cm^3, equipped with a reflux condenser and magnetic stirrer with heating function. For the isomerization test, 4 g of α-pinene (98%, Aldrich) and a suitable amount of catalyst were put into the reactor which was then placed in an oil bath for 6 hours. The intensity of stirring was constant and amounted to 400 rpm. The quantitative analyses were performed by the gas chromatography method.

Results

During the research the influence of temperature in the range of 80-180°C on the isomerization of α-pinene in the presence of the halloysite was investigated. As the temperature increased, the conversion of alpha-pinene increased to the maximum and amounted to 100 mol% (at the temperature of 140°C). At 140°C, where the conversion of α-pinene reached 100 mol%, the selectivities of the appropriate products were as follows (in mol%): camphene (40.88), limonene (27.76), α-terpinene (3.88), γ-terpinene (2.75), terpinolene (10.54), p-cymene (2.75), and α-phellandrene (0.39). Furthermore, with a total selectivity of 9.94 mol% - fenchene, tricyclene and polymeric products are also formed. Moreover, in the temperature range of 160-180°C, formation of p-cymene is observed.

Conclusion

The current studies have shown that halloysite is an excellent catalyst for alpha-pinene isomerization process. Its use enables obtaining of almost 100 mol% conversion of α-pinene after the reaction time of 6 hours. Compared to the industrially used TiO_2 reaction time can be shortened from 48 to 6 hours. This material, which is of natural origin, is also extremely inexpensive and environmentally friendly.

References

[1] J. W. Anthony, R. A. Bideauxm K. W. Bladh, M. C. Nichols, *Handbook of mineralogy*, Vol. 2. US: Mineralogical Society of America, Chantilly, 2003.

[2] P. Yuan, D. T, F. Annabi-Bergaya, Applied Clay Science, 112-113 (**2015**) 75-79

[3] https://phantomplastics.com/functional-fillers/halloysite/

 ISBN: 978-80-8152-530-8

SESSION IV Advanced preparation methods and characterization techniques of nanomaterials

Isomerization of alpha-pinene over mesoporous Ti-MCM-41 catalyst – the effect of temperature

P.Miądlicki[a]*, A. Wróblewska[a] , M. Malko[a]

[a] *Institute of Organic Chemical Technology, West Pomeranian University of Technology Szczecin, Pulaskiego 10, 70-322 Szczecin, Poland*

* *piotr.miadlicki@zut.edu.pl, agnieszka.wroblewska@zut.edu.pl*

Introduction

Nowadays, carrying out chemical processes that use the waste as a raw material and reduction the emission of pollutants is desirable. An example of this type of process is the isomerization of α-pinene on the Ti-MCM-41 catalyst. The main purpose of this work was to investigate the effect of reaction temperature on the course of the α-pinene isomerization process, mainly taking into account the selectivities of the appropriate products and the conversion of α-pinene. The main reaction products were: camphene, limonene, p-cymene and terpinenes. All from these products are widely used in food, perfumery, and polymer industries and, moreover, in medicine [1].

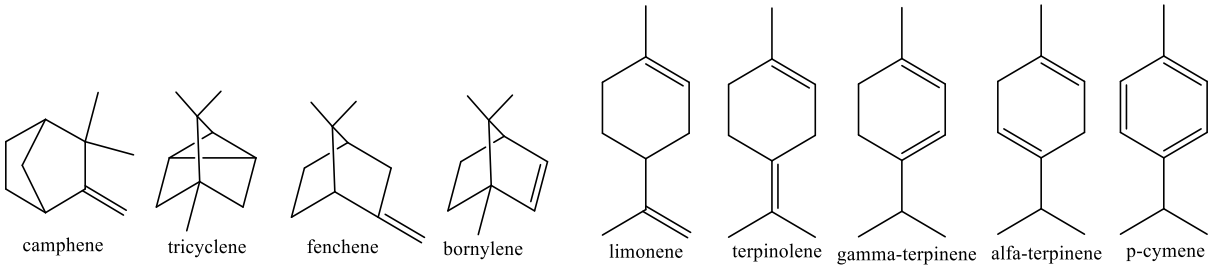

Figure 1. Main products of the alpha-pinene isomerization

Experimental

In these studies we used the Ti-MCM-41 catalyst with high titanium content (molar ratio of Ti:Si in crystallization gel equal to 1:10). Synthesis of this catalyst is described in our previous work [1]. Isomerization tests were carried out in a glass reactor with the capacity of 25 cm^3, equipped with a reflux condenser and magnetic stirrer with heating function. For the isomerization test, 4 g of α-pinene (98%, Aldrich) and a suitable amount of catalyst were put into the reactor which was then placed in an oil bath for 6 hours. The intensity of stirring was constant and amounted to 400 rpm. The quantitative analyses were performed by the gas chromatography method.

Results

During the research the influence of temperature in the range of 80-180°C on the isomerization of α-pinene in the presence of the Ti-MCM-41 catalyst was investigated. As the temperature increased, the conversion of pinene increased to the maximum amounted to 100 mol% (at the temperature of 160°C). Within the temperature range of 100-160°C, the selectivity of camphene and limonene was similar (about 35 mol%). At 160°C, where the conversion of α-pinene reached 100 mol%, the selectivities of the appropriate products were as follows (in mol%): camphene (33.6), limonene (29.9), α-terpinene (7.4), γ-terpinene (4.4), terpinolene (10.8), p-cymene (3.7), and α-phellandrene (1.2). Furthermore, with a total selectivity of 9.0 mol% - fenchene, tricyclene and polymeric products are also formed. However, at the temperature of 180°C, formation of p-cymene is observed.

Conclusion

The current studies show that the Ti-MCM-41 catalyst is the active catalyst in the α-pinene isomerization process. Its use allows to obtain the conversion of α-pinene amounted to 100 mol% after the reaction time of 6 hours. The products obtained in this process are used in many industries and the way of this process performing is easy and environmentally friendly.

References

[1] D. Pybus, C. Sell, *The Chemistry of Fragrances*, The Royal Society of Chemistry, Cambridge, 1999, pages 24-51

[2] A. Wróblewska, E. Makuch, Pol. J Chem. Technol. **15** (2013), 111-115

 ISBN: 978-80-8152-530-8

SESSION IV Advanced preparation methods and characterization techniques of nanomaterials

Doping Concentration in Nano-structures Using X-ray Fluorescence

Jyotsna Sharma[1], Akanksha Tiwari[2] and Shatendra Sharma*[3]

[1] *School of Basic & Applied Sciences KR Mangalam University Gurgaon-122003, India*
[2]*Department of toxicology and Medical Elementology, Jamia Hamdard University New Delhi-110062, India*
[3] *University Science Instrumentation Centre, Jawaharlal Nehru University, New Delhi -110067, India*

**shatendra@gmail.com*

The nano structures are characterized for their properties using several techniques such as SEM, TEM, XRD, Raman, UV-VIS, XPS and PL etc. Being no-destructive and quite accurate, the XRF techniques is also one of the very useful to determine the elemental composition of the material [1]. We have determined the relative doping concentration of Ni in potassium titanate nano-fibres synthesized with hydrothermal method. The chemical doping of Ni was done in potassium titanate sample with expected doping concentrations of 0 to 10 percents. The 22.2 keV photons from x-ray tube with Ag target are used to excite the fluorescence and the emitted x-rays from the sample are detected by an Amptek SDD detector. The spectra of all elements present in the sample are recorded using a multi-channel analyzer in a 90 geometry [2]. Though the absolute production cross-sections of the x-rays can also be detrmined experimentally, but these require the knowledge of absolute incident flux, production cross-sections, and the values of self absorption correction factor and geometry. Due to large uncertainities and errors in these parameters [3,4] the results can not be reliable. Our interest in the experiment is to study the relative change in concentration of nickle as dopant, therefore the simple measurement of relative intensities of nickle x-ray intesities can serve the purpose. Since the measurement of relative concentrations do not require the absolute x-ray intensity, production cross-sections, and the factors like self absorption and geometry are cancelled. As reported earlier [2], we have determined the relative doping concentrations of nickle in potassium titanate structures in a hassel free method by simply measuring the K_α and K_β relative x-ray intensities of nickle. The method of measurement and the results are discussed in this paper.

Keywords: x-ray fluorescence, elemental composition, characterization, relative concentration

References

[1]K. Shatendra, K.L. Allawadhi, B.S. Sood, Phys. Rev. A **31** 5 (1985) 2918-2921
[2]K. Shatendra, K.L. Allawadhi, B.S. Sood, J.Phys. B: At Mol. Phys. **15** 10 (1982) 3377-3382
[3]J.H. Scofield, At. Data Nucl. Data Tables **14** (1974) 121-137
[4]J.L. Campbell, At. Data Nucl. Data Tables **85** (2003) 291-315

 ISBN: 978-80-8152-530-8

SESSION IV Advanced preparation methods and characterization techniques of nanomaterials

Removal of cadmium (Cd^{2+}) from Water using Cellulose Nanofibers and Nano-Clay Composite

Emmanuel Abu-Danso[a]*, Sirpa Peräniemi[b], Jouko Vepsäläinen[b], Sonja Holopainen[b], Amit Bhatnagar[a]

[a] *Department of Environmental and Biological Sciences, University of Eastern Finland, P.O. Box 1627, FI-70211 Kuopio, Finland*

[2] *School of Pharmacy, University of Eastern Finland, P.O. Box 1627, FI70211 Kuopio, Finland*

**emmanuel.abu-danso@uef.fi*

The current focus on naturally abundant nano-sized materials and their applicability in water treatment is increasing due to their unique properties such as high surface area to volume ratio and versatility in the manufacture of composites. This work evaluated the performance of a bio nano composite of cellulose nanofibers synthesized from absorbent cotton and nano-clay to remove cadmium (Cd^{2+}) from water. The composite was synthesized by dissolution with alkali-urea and pressure binding with ethylene glycol under high temperature. The synthesized composite was characterized for functional group analysis by Fourier transform infrared spectroscopy (FTIR) and surface morphology using scanning electron microscope (SEM). From the analyses of functional groups and porous surface, the bio composite showed potential for the removal of metals from water. Batch mode adsorption experiments were conducted to study the effect of different experimental parameters. The results revealed a fast adsorption kinetics and equilibrium was reached in 90 minutes with 90% removal efficiency using an adsorbent dose of 1.0 g L^{-1} and 50 ppm initial cadmium concentration. The adsorption process was assessed with different kinetic models viz. pseudo-first-order, pseudo-second-order and intraparticle diffusion and the results showed that the pseudo-second-order kinetic model best described the adsorption kinetics. The adsorption isotherm fitted with Langnuir model. The regeneration experiments showed that the nano composite material had 90% removal efficiency after four cycles using 0.1 NaOH as an eluent. The results from this study shows the synthesized cellulose nanofibers-clay composite is a potential as heavy metal adsorbent.

Keywords: Cellulose nanofibers; Nano clay; Composite; Cadmium; Adsorption; Kinetics

Acknowledgement

Maj ja Tor nessling säätiö

References

[1] Abu-Danso, E., Srivastava, V., Sillanpää, M., Bhatnagar, Amit Int. J. Biol. Macromol., 2017, 102, 248-257

[2] Hokkanen, S., Repo, E., Lou, S., b, Sillanpää, M. Chem. Eng. J. 260 (2015). Page 886–894

[3] O. Redlich, D.L. Peterson, A useful adsorption isotherm, J. Phys. Chem. 63 (1959), 1024-1024.

 ISBN: 978-80-8152-530-8

SESSION IV Advanced preparation methods and characterization techniques of nanomaterials

Oxidation of R-(+)-limonene over montmorillonite with tert-buthyl hydroperoxide

M.W. Malko[a]*, A. Wróblewska[a], P. Miądlicki[a]

[a] *West Pomeranian University of Technology in Szczecin, Department of Chemical Engineering and Technology, Institute of Organic Chemical Technology, Pulaskiego 10,70-322 Szczecin*

**mariuszmalko@gmail.com, agnieszka.wroblewska@zut.edu.pl*

R-(+)-limonene is found in citrus peels (sweet orange, tangerine, lemon and lime) and has the following physical characteristics: boiling point 176°C (760 mmHg), melting point -74° C; density of 0.94 g/dm^3 and good solubility in methyl alcohol and ethyl alcohol, and also in acetone and benzene. It is the main constituent of oils extracted from citrus fruit waste (biomass). It can be obtained by natural and synthetic methods using, for example, pyrolysis processes. Natural methods (simple distillation or steam distillation of citrus peels) allow to utilize of citrus fruit waste from the food industry and at the same time to obtain pure limonene. Pyrolytic methods require high temperatures and generate significant amounts of wastewater and are very harmful to the environment.

R-(+)-limonene has found mainly applications in cosmetics, in medicine - including natural medicine for aromatherapy (sedative properties, harmonizing and stabilizing nervous system), in perfume industry, in food industry (flavours for food). R-(+)-limonene is also present in carbonated beverages produced by large companies (e.g. Coca Cola Company), in fruit juices, ice creams and candies, where it serves as food flavour and stabilizer [1]. Limonene is used in the synthesis of many useful intermediates for organic industry as well as an alternative solvent for organic synthesis because it is cheap, biodegradable and not toxic. Its disadvantage is that it is easy to oxidize, so it can not be used as a solvent in oxidation reactions. This compound can also be used as a cleaning agent for electronic equipment, due to its degreasing properties. Limonene has also found use as a fragrance component in household chemicals (detergents and air fresheners). R-(+)-limonene is also used in massage and cellulite fighting. In the polymer industry, it is a valuable monomer to produce "fragrant" and biodegradable polymers [2].

Very important processes in which R - (+) - limonene is the raw material are processes of its oxidation. As a result of the oxidation of R-(+)-limonene, we obtained compounds such as carvone, carveol, perillyl alcohol, 1,2-epoxylimonene and 1,2-diol of epoxylimonene.

The literature describes the methods of oxidation with hydrogen peroxide, tert-butyl hydroperoxide, molecular oxygen [3] and ozone [4] in the presence of heterogeneous catalysts, where the catalysts are: titanium-silicate catalysts, porphyrins [5], salts ruthenium [6] and molybdenum [7] and hydrotalcites (synthetic counterparts of natural clayey soil) [8].

One of the most important methods of limonene oxidation is the method which use of titanium-silicate catalysts [9]. In these methods, the advantage is the stability of the catalysts, the easiness f their regeneration, the small number of harmful by-products (mainly water or alcohol). The new method of limonene oxidation is the use of montmorillonite as catalyst in the presence of tert-butyl hydroperoxide for limonene oxidation process.

References

[1] R. Ciriminna, M. Lomeli-Rodriguez, P. D. Cara, J. A. Lopez-Sanchez, M. Pagliaro, Chem. Comm., 97 (2014) 15282-15296.
[2] M. P. Arrieta, J. López, S Ferrándiz., M. A. Peltzer, Polym.Test. 32 (2013) 760-768.
[3] AT. Karlberg, K. Magnusson, U. Nilsson, Contact Dermatitis. 26 (1992) 332-340.
[4] P. A. Clausen, C. K. Wilkins, P. Wolkoff, G.D. Nielsen, Indoor Air. 26 (2001) 511-516.
[5] M. Trytek, J. Fiedurek, S. Radzki, Biotechnol Prog. 23 (2007) 131-137.
[6] A. Feddouli, Y. A. Itto, M.A. Ali, A Hasnaoui., A. Riahi, Synth. Comm., 36 (2006) 3617-3624.
[7] M. Abrantes, S. M. Bruno, C.Tomé, M. Pillinger, I. S. Gonçalves, A. A. Valente, Catal. Comm., 15 (2011) 64-67.
[8] B. Arizaga, A. de Leon , N. Burgueño, López A., Paz D., Martínez N., E. D. Lorenzo, J. Dellacassa, A. Bussi, J. Techn. and Biotech., 82 (2007) 532-538.
[9] A. Wroblewska, Molecules 19 (2014) 19907-19922.
. 145 (1998) 1207-1211.

 ISBN: 978-80-8152-530-8

SESSION IV Advanced preparation methods and characterization techniques of nanomaterials

Process monitoring in Fabrication of Nano Structures by Infrared Spectroscopy: TiO_2 as a Case Study

A.Bagheri Garmarudi*, M. Khanmohammadi, F. Askarian

Chemistry Department, Faculty of Science, Imam Khomeini International University, Qazvin, Iran

**bagheri@sci.ikiu.ac.ir*

Controlling the morphology of nanomaterials via synthesis process modification is an emerging field of research. In particular, there is an emphasis on the development of various nanostructures to be employed in variety of applications as, photo catalysts, sensors, photovoltaics, bio-ceramics, and batteries [1].

Advances in surface chemistry of the growth nuclei are a fundamental concept in development of controlled shaped nanomaterials by promoting or poisoning of growth planes [1]. Sol-gel, hydrothermal, solvothermal, direct oxidation, chemical vapour deposition, microwave, micelle and inverse micelle are the most common procedures for synthesis of nano structures [2,3], among which sol-gel has revealed notabl advantages such as high purity, shape uniformity, low temperature procedure controllable reaction conditions etc. [4]. Investigations on growth mechanism and shape evolution of nano structure would promote both understanding the fundamental phenomena and development of potential industrial scale applications.

Size and morphology of the nano structures are determined by crystal growth mechanism, kinetics, and microstructure development which all let the researcher to control the expected characteristics [6]. Process monitoring and mechanism evaluation has been widely studied by different spectrometric method such as XRD, NMR and FTIR. Synthesis of TiO_2 nanostructures was performed via sol–gel method by adjusting the water to precursor ratio and pH value the hydrolysis and condensation reaction of titanium alkoxide precursor. Mid-infrared spectrometer (Nicolet, Madison, WI, USA) equipped with diffuse reflection sampling cell with a DTGS detector and a CsI beam splitter was used to record spectra during the growth process. The spectral resolution was 8 cm^{-1} and 36scans were accumulated over the range from 400 to 4000 cm^{-1} for each spectrum. Data acquisition was performed every 10 min since the start of synthesis to till the sol preparation step. After sol preparation spectrum recording time intervals was 60 min in the first day and 120 min during the next days.

At the start of reaction TTIP would react violently with water, to be hydrolyzed and from Ti $(OR)_4$-n$(OH)_n$. These species are polymerized to produce water and alcohol and network bonds of Ti-O-Ti. The amount of available water for the hydrolysis process plays an important role in the mechanism. Reaction time is controlled by the amount of water in the reaction. Due to the strong and fast reaction of TTIP with water, the reaction mixture would be diluted by solvent, to reduce its speed. Another key mechanism is to stabilize the solution in the process by settingappropriate pH. Thus, fabrication of TiO_2 nanoparticles was performed in acidic conditions, when the condensation of the half protonated Ti-O-R groups is important. In order to study the spectral variatious along the synthesis process MCR–ALS analysis was performed on the IR absorbance data matrices.The obtained data set from FTIR spectrometry , for different synthesis procces routes were rearranged into a data matrix D(r×c), where the rows of D(r) contain the spectra measured for different samples at and each column "D" (c) provided the wavenumbers monitored. Experimental data matrix (D) was decomposed according to the equation:

$$D = CS^T + E$$

where C (n, q) is the concentration profile describing the evolution of the chemical components (q) $S^T(q,p)$ is the spectral data matrix describing the pure infrared spectra of detected components. **E** contains of residuals (not explained by the model)considered as the experimental error. (ALS) tries to calculate the concentration C and pure spectra S^T using an iterative procedure. Principal component analysis (PCA) as a data compression technique is usually considered as a useful tool to assess the number of effective components using singular value decomposition(SVD).

References

[1] M. H Imanieh, Y. Vahidshad, P. Nour Pour , S. Shakesi, K. Shabani, NANO: Brief Reports and Reviews. 5, 279–285 (2010).

[2] X. Chen, S. Mao, Chemical Reviews. 107 (7), 2891-2959(2007)

[3] J. Zhang, F. Huang, Z. Lin, Nanoscale. 2, 18–34(2010)

[4] C. S. Lim, J. H. Ryu, D. Kim, S.Y. Cho, W.C. Oh, Journal of Ceramic Processing Research, 736~741(2010).

[5] J. Zhang, F. Huang, Z. Lin, Nanoscale. 2, 18–34(2008).

 ISBN: 978-80-8152-530-8

SESSION IV Advanced preparation methods and characterization techniques of nanomaterials

A new double layer epoxy nano composite coating for corrosion protection of Petroleum Equipments

Ashraf M. El-Saeed[a*], Maher A. El Sockary[a], Samya I. El Sherbiny[b], Fatma A. Morsy[b] Mohamed A. ELleithy[b,c]

[a] *Petroleum Applications Department, Egyptian Petroleum Research Institute, Nasr City 11727, Cairo, Egypt*
[b] *Helwan University, Faculty of Science, Chemistry Department, Helwan, Egypt*
[c]*Egyption town gas company, Giza, Egypt*

**ashrfelsaied@yahoo.com*

Homogeneous epoxy coating containing polymer nanocomposite (PNC) was successfully synthesized and applied on carbon steel substrates by room temperature curing of fully mixed epoxy slurry. (PNC) containing both ZNO nanoparticles and epoxy hyper branched polymer (EHBP), a new double layer thin film which comprises ZNO-epoxy as a primer coat and ZNO-EHBP-epoxy as a top coat offers better corrosion protection compared to the purely inorganic ZNO-epoxy coating and hybrid ZNO-EHBP-epoxy coating. Chemical structures of synthesized compounds were confirmed by FTIR, H^1NMR spectroscopy and GPC. The surface morphology and phase structure of the produced Zno nanoparticles were characterized by scanning electron microscopy SEM, transmission electron microscopy TEM and X-ray diffraction. Chemical resistance of theses coatings to NaOH and HCl was investigated. The effect of incorporating polymer nanocomposite and new double layer coating on corrosion resistance of epoxy coated steel was investigated by salt spray test.

Keywords: double layer coating, Epoxy coatings, Hyper branched polymers, polymer nanocomposites, ZNO nanoparticles.

 ISBN: 978-80-8152-530-8

SESSION IV Advanced preparation methods and characterization techniques of nanomaterials

The effect of the perpendicular electric field on structure formation in solution-cast composites of conjugated and dielectric polymers

K.Awsiuk [a]*, J. Rysz[a], M.M. Marzec[b], P. Dabczynski[a], A. Budkowski[a]

[a] *M. Smoluchowski Institute of Physics, Jagiellonian University, Łojasiewicza 11, 30-348 Kraków, Poland*
[b] *Academic Centre for Materials and Nanotechnology, AGH University of Science and Technology, Al. Mickiewicza 30, 30-059 Kraków, Poland*

**kamil.awsiuk@uj.edu.pl*

Large-area polymer composite coatings are fabricated by horizontal dipping, with a horizontally drawn solid substrate wetted by a meniscus of dissolved composite solution, formed between the substrate and a cylindrical bar kept at constant height in the range of a few tens of micrometres[1]. As an extension of this coating technique electric field is applied between the (conducting) substrate and the bar (gold covered) (Fig. 1). Although it is effective only in the beginning part of film structure formation, it has a profound effect on final film morphology. When the electric field is repeatedly switched on and off the spatial patterns of different morphologies are formed, changing between semiconductor/insulator bilayers and lateral (quasi-2-dim) structures or between lateral droplet-like morphologies dominated by continuous semiconductor or insulator phase.

Figure 1. Schematic presentation of the coating process, the polymer solution is placed between bar and the substrate. An electric field can be applied during film formation to locally modify polymer layer structure.

The described method and equipment is patent pending (number P.418951, filing date 2016-10-01)

Acknowledgements

This work was supported by the Polish Ministry of Science and Higher Education within the Iuventus Plus Program realized in the period 2015–2017 (Grant No. 0001/IP3/2015/73).

References

[1] J. Rysz, M. Josiek, M.M. Marzec, E. Moons, J. Polym. Sci. Part B Polym. Phys. **51** (2013) 1419–1426

 ISBN: 978-80-8152-530-8

Properties of biodegradable Fe materials modified by MgO and ZnO nanoparticles.

Andrea Morovská Turoňová[a*], Monika Hrubovčáková[b], Miriam Kupková[b]

[a]*Institute of Chemistry, Faculty of Science, P. J. Šafárik University, 040 01 Košice, Slovakia*
[b]*Institute of Materials Research, Slovak Academy of Sciences, 040 01 Košice, Slovakia*

andrea.morovska.turonova@upjs.sk

A new generation of metallic biodegradable materials are used in the preparation of various medical implants. To change the properties of such material is possible by a various additives. An addition of nano-inorganic metal oxides as MgO and ZnO to pure iron material leads to control of corrosion resistance. These specific nanoparticles cause also the reduction a bacterial contamination [1, 2]. Attention is focused on the biodegradability and biocompatibility of materials.

The samples were prepared by a powder metallurgy from powdered carbonyl iron with amounts 0.5, 1.0 wt.% of nanoparticles MgO or 0.5, 1.0, 5.0 wt.% of nanoparticles ZnO. The powders were mixed in a turbula mixer, compressed and sintered. Some samples were also modified by spark plasma sintering (SPS). Corrosion of samples in the Hank`s solution was investigated. Using the chronometrical potentiometry, the open-circuit potential (OCP) was recorded. Immediately after the determination of OCP, potentiodynamic measurements were performed. The samples were examined in more detail using a scanning electron microscope.

The corrosion potential of a freely corroding Fe sample (OCP) decreased with time, the OCP of Fe-ZnO and Fe-MgO samples exhibit a relatively constant course. The nanoparticles are uniformly dispersed in the iron particles, therefore corrosion is largely uniform. Addition of nanoparticles causes a negative shift in corrosion potential. Samples modified by SPS have OCP values shifted more positively. During the sintering in the presence of plasma, the partial homogenization of the nanoparticles in Fe was occurred. The materials have different porosity and therefore are more resistant to corrosion electroless process.

From the polarisation measurements is evident, that the addition of MgO or ZnO shifts the corrosion potential negatively, compared to the pure Fe sample. The negative shift indicates the increased tendency of these samples to corrode. It is probably caused the samples disorder and less homogenous character of the porosity. The corrosion rate is not affected by the overall porosity, rather the pore dimensions and their character, which can significantly accelerate and promote pitting and crevice corrosion. In the case of samples treated by SPS, the addition of nanoparticles causes an insignificant shift of corrosion potential. The corrosion rate of the mentioned samples is lower. The material is more compact, the surface is more homogeneous.

In the further research, it is interesting to investigate degradation processes in the real environment of body fluids and to observe the effect of the presence of different nanoparticles in iron samples on biocompatibility and hemocompatibility.

a b

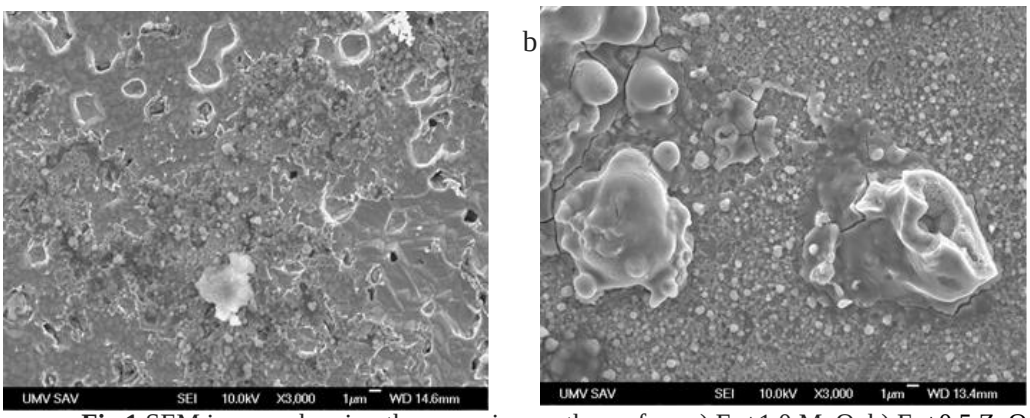

Fig.1 SEM images showing the corrosion on the surface a) Fe+1.0 MgO, b) Fe+0.5 ZnO

 ISBN: 978-80-8152-530-8

Acknowledgement

This work was supported by the Slovak Grant Agency VEGA under project VEGA 1/0074/17, VEGA 2/0100/15 and by the project APVV-16-0029.

References

[1] Tang, Z.-X., Lv, B.-F.: MgO nanoparticles as antibacterial agent: preparation and activity. Brazilian Journal of Chemical Engineering 2014, vol. 31, 3, 591 – 601.

[2] Vaseem M., Umar A., Hahm Y.: ZnO Nanoparticles: Growth, Properties, and Applications, In book: Metal
Oxide Nanostructures and Their Applications, chapter 4, American Scientific Publishers, 2010, 1-36.

 ISBN: 978-80-8152-530-8

Corrosion resistance of structurally complex phases in Al–Co alloys

M.Palcut[a]*, P. Priputen,[a] L. Ďuriška,[a] I. Černičková,[a] J. Janovec[b]

[a] *Slovak University of Technology in Bratislava, Faculty of Materials Science and Technology in Trnava, J. Bottu 25, 917 24 Trnava, Slovakia*
[b]*Slovak University of Technology in Bratislava, University Science Park, Vazovova 5, 812 43 Bratislava, Slovakia*

**marian.palcut@stuba.sk*

Al–TM alloys (TM = transition metal) with compositions close to 75 at. % Al constitute an important group of complex metallic alloys (CMA). These materials are composed of structurally complex intermetallic phases with large unit cells, inclusive of quasicrystals [1–4]. First quasicrystalline phases were described by Shechtman et al. [5]. Their discovery was awarded by Nobel Prize in chemistry in 2011 [1]. Because of the specific crystal structure, the structurally complex intermetallic phases are suitable for different applications. The Al–based CMAs have been utilized as scratch–resistant coatings [6]. Furthermore, possible applications of these materials in catalysis [7], hydrogen generation [8], metal–matrix and polymer–matrix composites have been reported [9].

In the present work, the phase constitution and corrosion behavior of as–solidified and as-annealed Al–Co CMAs have been studied. Six Al–Co alloys (Al–24Co, Al–25Co, Al–26Co, Al–27Co, Al–28Co, Al–29Co, composition given in atomic percents) were prepared by arc–melting from high purity Al and Co granules. The melting was performed in high purity Ar. After melting the alloys were solidified on a water-cooled Cu mold. Two of the alloys, Al–26Co and Al–29Co, were further annealed at 1050 °C for 330 h to reach near-equilibrium conditions. The microstructure of the as-solidified and as-annelaed alloys was studied by field emission gun scanning electron microscope JEOL JSM–7600F coupled with an Oxford Instruments energy dispersive X–ray spectrometer. Furthermore, the alloys phase constitution was investigated by X–ray Panalytical Empyrean PIXCel 3D diffractometer working with a CoKα1,2 radiation beam. Each alloy was composed of different microstructure constituents. The observed phase constitution was interpreted based on previously published Al–Co phase diagram and non–equilibrium processes taking place during casting. The as–solidified and as-annelaed alloys were subjected to corrosion testing at 21±2 °C in three different aqueous solutions: 0.6 M NaCl, 0.01 M HCl and 0.01 M NaOH. Open circuit potentials of the alloys were measured immediately after sample immersion in the electrolyte. Furthermore, an electrochemical polarization of the alloys was performed in a standard 3–electrode cell controlled by potentiostat (PGU 10V–1A–IMP–S, Jaissle Electronic Ltd., Germany). The alloys corrosion potentials and corrosion current densities were determined by Tafel extrapolation of the experimental polarization curves. A pitting corrosion in 0.6 M NaCl and 0.01 M HCl was found and some of the constituent phases were preferentially attacked by this type of local corrosion. The electrochemical nobility of individual intermetallic compounds is discussed. Finally, the conclusions towards the alloys corrosion resistance in acidic, saline and alkaline environment are provided.

Acknowledgements

Work presented in this paper was jointly supported by the European Regional Development Fund project ITMS:26220120048, the Grant Agency VEGA projects 1/0068/14, 1/0018/15 and 1/0465/15, and the Slovak Research and Development Agency project APVV–15–0049.

References

[1] J. M. Dubois, Chem. Soc. Rev. 41 (2012) 6760–6777.
[2] M. Palcut, P. Priputen, M. Kusý, J. Janovec, Corros. Sci. 75 (2013) 461–466.
[3] M. Palcut, P. Priputen, K. Šalgó, J. Janovec, Mater. Chem. Phys. 166 (2015) 95–104..
[4] P. Priputen, M. Palcut, M. Babinec, J. Mišík, I. Černičková, J. Janovec, J. Mater. Eng. Perform., 26 (2017) 3970-3976.
[5] D. Shechtman, I. Blech, D. Gratias and J. W. Cahn, Phys. Rev. Lett., 53 (1984), 1951-1954.
[6] T. Duguet, S. Kenzari, V. Demange, Th. Belmonte, J. M. Dubois, V. Fournee, J. Mater. Res., 25 (2010) 764-772.
[7] M. Armbrüster, R. Schlögl, Y. Grin, Sci. Technol. Adv. Mater., 15 (2014) 034803.
[8] L. Soler, J. Macanás, M. Muñoza, J. Casado, Int. J. Hydrogen Energy, 32 (2007) 4702 – 4710.
[9] S. Kenzari, D. Bonina, J. M. Dubois, V. Fournée, Sci. Technol. Adv. Mater., 15 (2014) 024802.

 ISBN: 978-80-8152-530-8

Scanning ion selective electrode technique as a sensitive method for probing buffer activity of polyelectrolyte layers

H. M. Maltanava,[a] S. K. Poznyak,[a] D. V. Andreeva,[b] M. C. Quevedo,[c] A. C. Bastos,[c] J. Tedim[c] and E. V. Skorb[d,e]

[a] *The Research Institute for Physical Chemical Problems, Belarusian State University, Minsk 220030, Belarus*
[b] *Center for Soft and Living Matter, Institute of basic science Ulsan, National Institute of Science and Technology, Ulsan 44919, Republic of Korea*
[c] *CICECO, Department of Materials and Ceramic Engineering, University of Aveiro, Aveiro 3810-193, Portugal*
[d] *Laboratory of Solution Chemistry of Advanced Materials and Technologies (SCAMT), ITMO University, St. Petersburg 197101, Russian Federation*
[e] *Department of Chemistry and Chemical Biology, Harvard University, 12 Oxford Street, Cambridge 02138, MA, United States*

**annamaltanova@gmail.com*

The polyelectrolyte multilayer films formed by the layer-by-layer (LBL) technique are attractive materials with large scale potential applications in the fields of surface modification, sensors, separation membrane for gases as well as supporting layers in biomaterials [1]. The morphology and chemical properties of polyelectrolytes alter significantly depending on such parameters as molecular weight, charge density, pH, temperature, and others [1, 2]. Despite the extensive research efforts for governing of the LBL formation and modification under any external stimuli, certain aspects still remain unclear. In our study we focused on measuring the buffering capacity of pH-sensitive poly(ethyleneimine) (PEI) – poly(sodium-4 styrenesulfonate) (PSS) assembly. Nanostructured TiO_2 films were used as a light-sensitive substrate, producing a local change in the pH when UV-stimulated photocatalytic reactions take place on the semiconductor surface [3]. In order to monitor local pH changes near the surface, we applied scanning ion selective technique (SIET). This technique provides measuring the concentration of specific ions (here, H^+ ions) at a nearly constant microdistance. SIET maps were recorded sequentially in 0.05 M Na_2SO_4 solution 100 μm above the TiO_2 surface before, during and after UV irradiation. In the dark, the pH is not changed appreciably over the bare titania surface and is about 5.8. After applying the local UV illumination of the surface the pH decreases significantly over the light spot. Local acidification of solution up to pH 3.8 occurs in the center of the irradiated zone. The pH decreases more rapidly after starting the illumination, reaches a limiting value for the period of 3-4 min and then relaxes to the initial value during appr. 40 min, indicating that the UV-triggered acidification process is reversible. PEI-PSS layers were deposited on the TiO_2 surface for studying the buffer activity of polyelectrolytes. During irradiation of polymer-covered titania films, the pH decreased from initial 7.0 to final 4.5. In comparison with bare TiO_2, the region of local pH change is significant wider and spreads outside the irradiated zone, which can be related to protons accumulation and spreading in the LBL layer owing to their binding to amine groups of PEI. Furthermore, the pH relaxation near the LBL-coated TiO_2 surface slows down after light switching off.

In conclusion, we have demonstrated successful application of SIET technique for mapping of H^+ ions activity over the bare and LBL-covered nanostructured TiO_2 films under the local UV irradiation. Generation of protons during photocatalytic reactions on the TiO_2 surface leads to a local acidification in the irradiation zone. Spreading of H^+ ions and slower pH relaxation near the TiO_2 surface modified by PEI-PSS layers in comparison with the bare TiO_2 have proved the high buffer activity of polyelectrolyte layers.

Acknowledgements

We acknowledge funding from SMARCOAT project. This project has received funding from the European Union's Horizon 2020 research and innovation programme under the Marie Skłodowska-Curie grant agreement No 645662. E.V.S. thanks the RSCF grant no. 17-79-20186.

References

[1] G. Decher, J. B. Schlenoff, Eds. *Multilayer Thin Films-Sequential Assembly of Nanocomposite Materials*; Wiley-VCH: Berlin, Germany, 2003.
[2] R. von Klitzing, Phys. Chem. Chem. Phys. 8 (**2006**) 5012–5033.
[3] H. M. Maltanava, S. K. Poznyak, D. V. Andreeva, M. C. Quevedo, A. C Bastos, J. Tedim, M.G.S. Ferreira, E. V. Skorb, ACS Applied Materials & Interfaces 9 (**2017**) 24282−24289.

 ISBN: 978-80-8152-530-8

Silver nanowires – synthesis, modification and use to obtain multifunctional fabrics

E. Mackiewicz[a]*, P. Giesz[a,b], M. Cieślak[b], J. Grobelny[a], G. Celichowski[a]

[a] *Department of Materials Technology and Chemistry, Faculty of Chemistry, University of Lodz, Pomorska 163, 90-236 Lodz, Poland*

[b] *Scientific Department of Unconventional Technologies and Textiles, Textile Research Institute, Brzezinska 5/15, 92-103 Lodz, Poland*

**ewelina.mackiewicz@chemia.uni.lodz.pl*

Silver nanowires (AgNWs) are widely investigated and used material in different fields of science and industry such as optoelectronics, biomedicine and textronics. By controlling their length and chemical structure of their surface (the presence of stabilizers, organic modifiers or oxide coatings), we can form the properties of the resulting nanomaterial. Thus, the properly prepared and well characterized AgNWs can be used to obtain multifunctional fabrics with relevant from the application point of view properties, such as antimicrobial activity or conductivity [1-3].

Work presents the controlled synthesis of uniform in size and shape silver nanowires via the chemical reduction method and their modification by covering their surface with metal oxide (e.g. tin oxide, titanium oxide), obtaining so called core-shell structures. The prepared materials were characterized by UV-Vis, FT-IR and Raman spectroscopy techniques and were depicted using transmission scanning electron microscopy (STEM). The diameter of AgNWs was 46 ± 2 nm and length 8 μm, whereas the oxide shell thickness was about 15 nm, providing high stability and protection against silver degradation. In the next step, nanowires were used to modify the cotton fabrics and obtain multifunctional hybrid systems. For this purpose NWs were deposited on the fabrics by the dipping technique and proper tests to investigate the properties of the final product were conducted. The results showed the high conductivity of the material, even after many washing cycles, the high antimicrobial activity against two model bacteria *Staphylococcus aureus* and *Klebsiella pneumoniae*, and the photocatalytic activity confirmed by the nicotine decomposition experiment.

Silver nanowires show great potential in multifunctional fabrics preparation. Cotton modified with AgNWs and metal oxide is highly conductive, antibacterial and photocatalytically active which allows us to consider it as the promising material in terms of future applications [2,3].

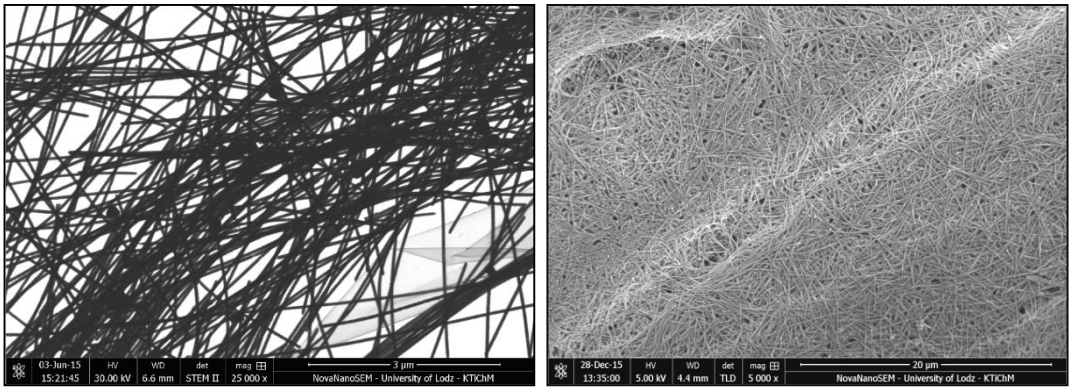

STEM images of silver nanowires (left) and cotton fabric modified with AgNWs (right).

Acknowledgements

This work was supported by University of Lodz, Subsidy for scientific research contributing to the development of young researchers and PhD students, project number: B1711100001603.02.

References

[1] K. Zilberberg, F. Gasse, R. Pagui, A. Polywka et al., *Adv. Funct. Mater.* **24** (2014) 1671-1678.

[2] P. Giesz, E. Mackiewicz, A. Nejman, G. Celichowski, M. Cieślak, *Cellulose* **24** (2017) 409-422.

[3] P. Giesz, E. Mackiewicz, A. Nejman, G. Celichowski, J. Grobelny, M. Cieślak, *Carbohydrate Polymers* (2017) – article in press

 ISBN: 978-80-8152-530-8

Silver nanowires modified with metal oxides for conductive materials preparation

E. Mackiewicz[a]*, P. Giesz[a,b], M. Cieślak[b], G. Celichowski[a]

[a] *Department of Materials Technology and Chemistry, Faculty of Chemistry, University of Lodz, Pomorska 163, 90-236 Lodz, Poland*

[b] *Scientific Department of Unconventional Technologies and Textiles, Textile Research Institute, Brzezinska 5/15, 92-103 Lodz, Poland*

**ewelina.mackiewicz@chemia.uni.lodz.pl*

Silver is the material with the highest conductivity among metals, hence with its use inks and paints for conductive paths and electronic components are prepared. Combining this feature with the properties of the material structure, silver nanowires (AgNWs) are extremely important material for electronic and optoelectronic applications. Commonly used material in the manufacture of transparent electrodes, that are necessary for the production of flat screens and photovoltaic modules, is still indium tin oxide, but due to its disadvantages intensive research on its replacement is being conducted. AgNWs seem to be an excellent candidate in this case. But it is important not only to produce the material itself but also to provide its protection against possible degradation that can be achieved by the efficient modification of the silver surface [1-3].

The study included controlled synthesis of AgNWs colloid by chemical reduction method, surface modification of obtained nanowires with metal oxide (e.g. SnO_2, TiO_2) with the core-shell structure formation and their spectroscopic and microscopic characteristics (UV-Vis, STEM, FT- IR, Raman). AgNWs with a diameter of 46 ± 2 nm and a length of approximately 8 μm were obtained and the resulting metal oxide shell was 15 nm thick. Then deposition of the material on various substrates was carried out and the final systems were characterized to determine their physicochemical properties, especially conductivity. The recorded surface resistance of 20 Ω confirmed that the prepared nanomaterial has a high application potential.

The results show the enormous potential of combining the properties of nanomaterials containing silver with metal oxides for conductive materials preparation.

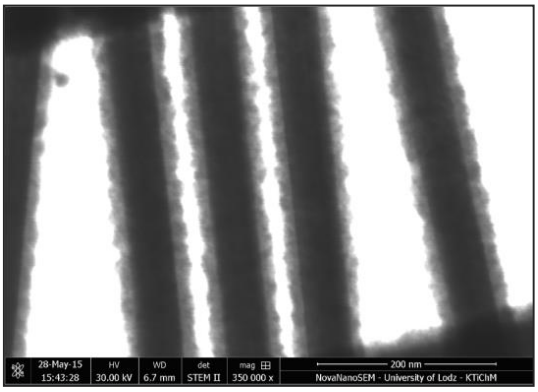

STEM image of silver nanowires modified with tin oxide.

Acknowledgements

This work was supported by University of Lodz, Subsidy for scientific research contributing to the development of young researchers and PhD students, project number: B1711100001603.02.

References

[1] K. Zilberberg, F. Gasse, R. Pagui, A. Polywka et al., *Adv. Funct. Mater.* **24** (2014) 1671-1678.
[2] P. Giesz, E. Mackiewicz, A. Nejman, G. Celichowski, M. Cieślak, *Cellulose* **24** (2017) 409-422.
[3] P. Giesz, E. Mackiewicz, A. Nejman, G. Celichowski, J. Grobelny, M. Cieślak, *Carbohydrate Polymers* (2017) – article in press

 ISBN: 978-80-8152-530-8

Acidity of Nanostructured Zr/Al Oxide Based Catalysts for Conversion of C_2-C_4 Alcohols to Olefins Based on the Data of EPR Spectra of Adsorbed Spin Probes

N.Aliyeva[a]*, A.Aliyeva[a] . S.Osmanova[b], E.Mammadov[a], E.Ismailov[a]

[a]*Institute of petrochemical processes, Azerbaijan National Academy of Sciences, 30, Khojaly Ave., Baku, AZ1025, Azerbaijan*

[b]*Institute of Catalysis and Inorganic Chemistry, Azerbaijan National Academy of Sciences, 29, Huseyn Javid Ave., Baku, AZ1143, Azerbaijan*

**nusabaaliyeva2007@gmail.com*

Nano-structured aluminum oxide based systems are used as catalysts for many chemical processes [1,2]. Since the intermediate chemical interactions of the reactants with the catalyst take place on the surface of the catalyst, it is necessary to obtain the information about the active centers of the catalyst surface to understand the role of the modifiers in these processes. The method of IR spectroscopy is widely used to determine the concentration and strength of acid sites on the surface [3,4]. However, the concentration of such centers in many cases may be small and the sensitivity of the IR spectroscopy method for many systems is insufficient. In such cases, EPR spectroscopy of adsorbed spin probes is often used [5,6]. In the presented report the results of the study of acid sites of catalysts based on Zr / Al oxide system for the conversion of C_2-C_4 alcohols to hydrocarbons using EPR spectroscopy of the nitroxide radicals (NR) are given. The structures of the used spin probes are shown below and the values of EPR parameters of these radicals in a benzene solution are given in the Table.

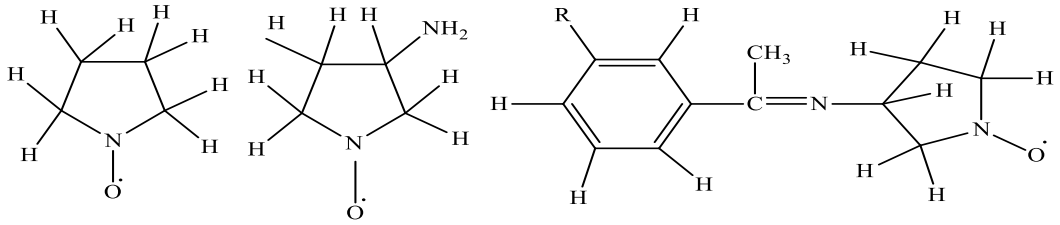

I II

R = Cl, Br, CH_3

III, IV, V

Table. The values of the EPR parameters of nitroxide radicals in a benzene solution*.

Nitroxide radicals					±0,2mT			
	g_1	g_2	g_3	g_{izo}	A_1	A_2	A_3	A_{izo}
I	2,00223	2,00638	2,00995	2,00619	0,60	0,60	3,45	1,55
II	2,00216	2,00634	2,00964	2,00598	0,58	0,58	3,44	1,53
III	2,00212	2,00635	2,00992	2,00613	0,56	0,56	3,40	1,51
IV	2,00215	2,00638	2,00974	2,00609	0,54	0,54	3,40	1,49
V	2,00215	2,00638	2,00981	2,00611	0,54	0,54	3,42	1,50

*The given values are determined in comparision of experimental and calculated EPR spectra

It was shown the formation of stable at room and more higher temperature surface paramagnetic complexes [A_s*NR] during the adsorbtion of these nitroxide radicals onto the Zr/Al oxide based catalysts. Based on the EPR spectra of nitroxide radicals adsorbed from benzene solutions on the surface of catalysts, the number of acceptor centers is determined and the nature of the complexes of adsorbed nitroxide radicals with the catalyst surface depending on the composition of the catalysts is studied.

References

[1] T. Mallat, A. Baiker, Chem. Rev**. 104 (** 2004) 3037–3058.

[2] T. Zaki, J. Colloid and Interface Sci. **284 (**2005) 606-613.

 ISBN: 978-80-8152-530-8

[3] M.E. Malyshev, E.A. Paukshtis, L.V.Malysheva, A.V. Toktarev, L.A Vostrikova. Kinetics and Catalysis. . **46 (** 2005) 10-106.
[4] M.R. Gafurov, I.N.Mukhambetov, B.V. Yavkin, G.V. Mamin, A.A. Lamberov, S.B. Orlinskii. J. Phys. Chem. C. **119** (2015) 27410-27415
[5] A.F. Bedilo, E.I.Shuvarakova, A.A.Rybinskaya, D.A. Medvedev. J. Phys. Chem. C. **118** (2014)15779-15794.

 ISBN: 978-80-8152-530-8

Development of Complex Fluoro Aluminates *via* Fluorolytic Sol-Gel Synthesis

F. Schütz[a], M. Bäthge, K. Scheurell[a], G. Scholz[a], M. Feist[a], E. Kemnitz[a*]

[a] *Department of Chemistry, Humboldt-Universität zu Berlin, Brook-Taylor-Straße 2, 12489, Germany*

**erhard.kemnitz@chemie.hu-berlin.de*

Introduction

For many decades, the modern industry of applied optics and antireflective coatings has special demands regarding the properties of the applied materials [1, 2]. Often, thin films of established compounds, like MgF_2 or SiO_2, respectively, exhibit a low reflectance but still suffer from environmental impacts like moisture or abrasion [3-5]. Thus, exceptional materials, which provide a low refractive index and insolubility, are needed.

Along these issues, complex fluoroaluminates, $MgAlF_5$, $MgAlF_5 \cdot 2H_2O$, and $MgAl_2F_8 \cdot 2H_2O$ seem to comply with these challenges [6]. Already in existence as the mineral Leonardsenite ($MgAlF_5 \cdot 2H_2O$) [7] or obtained by hydrothermal syntheses ($MgAlF_5$, $MgAl_2F_8 \cdot 2H_2O$) [8, 9], the chosen compounds provide low refractive indexes and poor solubility.

Methods

Fluorolytic Sol-Gel Synthesis

The fluorolytic sol-gel synthesis is the method of choice to obtain colloidal dispersions of metal fluorides [10]. Treating metal alkoxides with anhydrous HF in an alcoholic solvent (Fig. 1), the process allows producing several liters of sol, which can be subsequently used for dip coating [11].

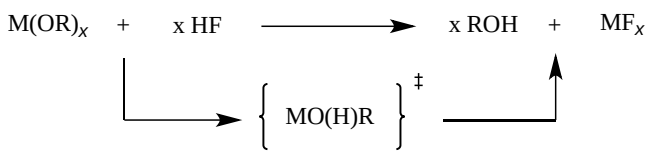

Fig. 1: General reaction scheme of the fluorolytic sol-gel synthesis.

Superposition Model

Although many articles about $M^{II}AlF_5$ structures have been published yet, there are no NMR data about corresponding Mg containing analogues [12-15]. Thus, all experimental ^{19}F NMR data were compared with simulations of the ^{19}F superposition model by BUREAU et *al*. [16], in which all calculations were referred to pure fluorides. Influences of protons in hydrate containing analogues $MgAlF_5 \cdot 2H_2O$ and $MgAl_2F_8 \cdot 2H_2O$ have been neglected concerning missing availability of deshielding tensor S_l. Moreover, the deshielding effects of the cations in structures like $A^{II}B^{III}X_{2A+3B}$ depend on both the electronic overlap as well as the cation-cation interaction [17] and, therefore, lead to variations in experimental and calculated chemical shifts. For a better graphical depiction, calculated spectra were shifted in a range of 20-22 ppm.

Dip Coating and Layer Validation

All layers were fabricated on float glasses by dip coating. For this purpose, glass slides were put into the sol and extracted consistently with defined extraction speed (40 cm • min^{-1}). After thermal treatment (T = 450°C, t = 15 min) layers were investigated with transmission spectroscopy, longtime water bath test (14 days), and crock meter test (steel wool, $F_{Pressure}$ = 4 N, 25 strokes).

 ISBN: 978-80-8152-530-8

Results

In addition to the compounds known from the literature, fluorolytic sol-gel synthesis was extended and applied with different molar ratios (1:1, 1:2, 2:1; Mg:Al, Fig. 2).

$$0.7x\ Mg(OEt)_2 + 0.3x\ MgCl_2 + y\ Al(O^iPr)_3 \xrightarrow[\substack{MeOH \\ -\ 0.7x\ EtOH \\ -\ y\ ^iPrOH \\ -\ 0.3x\ HCl}]{(x+y)\ HF_{MeOH}} Mg_xAl_yF_{(2x+3y)} \left| \begin{array}{l} 1.)\ x;\ y = 1;\ 1 \\ 2.)\ x;\ y = 1;\ 2 \\ 3.)\ x;\ y = 2;\ 1 \end{array} \right.$$

Fig. 2: Reaction scheme for different molar ratios.

It can be seen that a defined amount of metal chloride is needed to end up with a clear sol. This is caused by the catalytic cycle of produced HCl, which was discussed in a previous paper [18]. Sols of all molar ratios were obtained water clear, longtime stable, and with low viscosity. Static ^{19}F solid state NMR measurements show the existence of pure fluorides AlF_3 [-170 ppm; -155 ppm], MgF_2 [-198 ppm; -192 ppm], and fluorine sites surrounded by both Mg and Al [-185 ppm; -172 ppm] (Fig. 3). A tiny signal of adsorbed HF molecules can additionally be found at -186.4 ppm. Despite the appearance of those fluorine sites in strongly disordered environments, the formation of $MgAlF_5$ within the sols can be denied concerning the comparability towards simulations. To get a more precise insight of structural information, xerogels were obtained by evaporation of the solvent and were subsequently thermally treated.

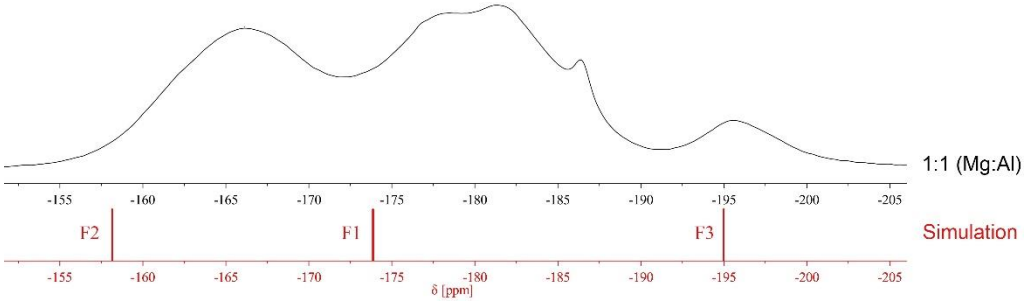

Fig. 3: Comparison of static ^{19}F solid state NMR (sol, molar ratio 1:1, Mg:Al) and calculated spectra of $MgAlF_5$.

In line with the situation mentioned above, xerogels of molar ratios 1:1 and 1:2 (Mg:Al) are not comparable to the calculated spectra of $MgAlF_5$ as well, but $MgAlF_5 \cdot 2H_2O$ and $MgAl_2F_8 \cdot 2H_2O$. The measured and calculated spectra of xerogels with molar ratios 1:1 and 1:2 show good agreement with the different fluorine sites within the structure (Fig. 4: a) $MgAlF_5 \cdot 2H_2O$, F2: light green, F1: dark green; b) $MgAl_2F_8 \cdot 2H_2O$, F3: light green, F2: medium green, F1: dark green, $[BF_4]^-$: purple). In addition, XRD data match with their corresponding powder diffraction files. In contrast to this, data of the xerogel of molar ratio 2:1 (Mg:Al) indicate the formation of MgF_2 and $MgAlF_5 \cdot 2H_2O$.

 ISBN: 978-80-8152-530-8

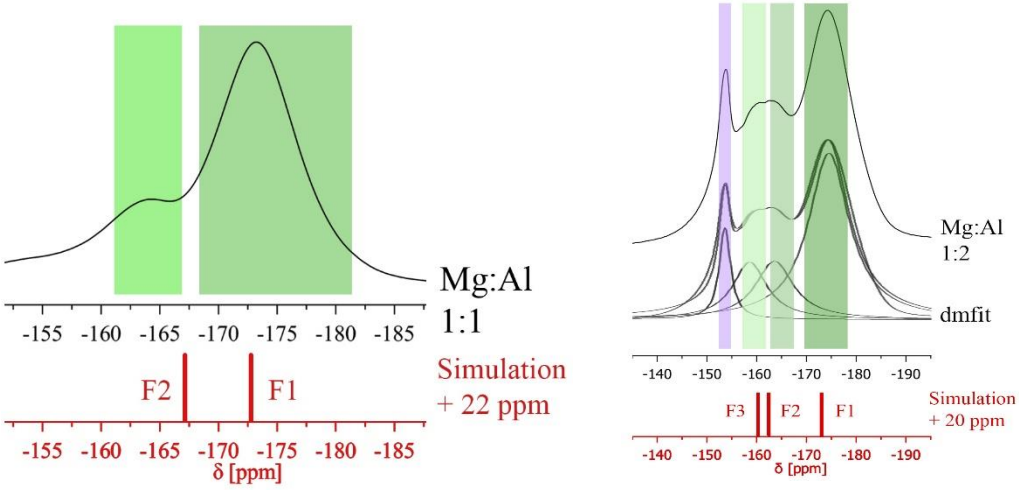

Fig. 4: a) ^{19}F MAS NMR of Xerogel **1** (Mg:Al = 1:1) and simulated spectra of $MgAlF_5 \cdot 2H_2O$. b) ^{19}F MAS NMR of Xerogel **2** (Mg:Al = 1:2) , dmfit analysis, and simulated spectra of $MgAl_2F_8 \cdot 2H_2O$.

Heading back to our initial aim, to access antireflective layers with improved stability, sols of all molar ratios were applied for coating of glass slides (Tab. 1). It can be seen, that all layers provide antireflective behavior with a reflectance of almost less than 1%. In addition to this, stability towards mechanical abrasion and longtime water bath test is extremely enhanced. Although glasses were exposed to water for 14 days, layers just show tiny scratches after repeating crock meter test (Fig. 5a-c).

Tab. 1: Overview of layer properties.

Layer	Ratio (Mg:Al)	T [°C]	t [min]	dT [°C/min]	d [nm]	R [%]	T[%]	$n_{632,8nm}$
1	1:1	450	15	10	111.4	1.02	97.51	1.32
2	1:2	450	15	10	172.3	0.93	93.20	1.30
3	2:1	450	15	10	171.2	0.39	96.96	1.27

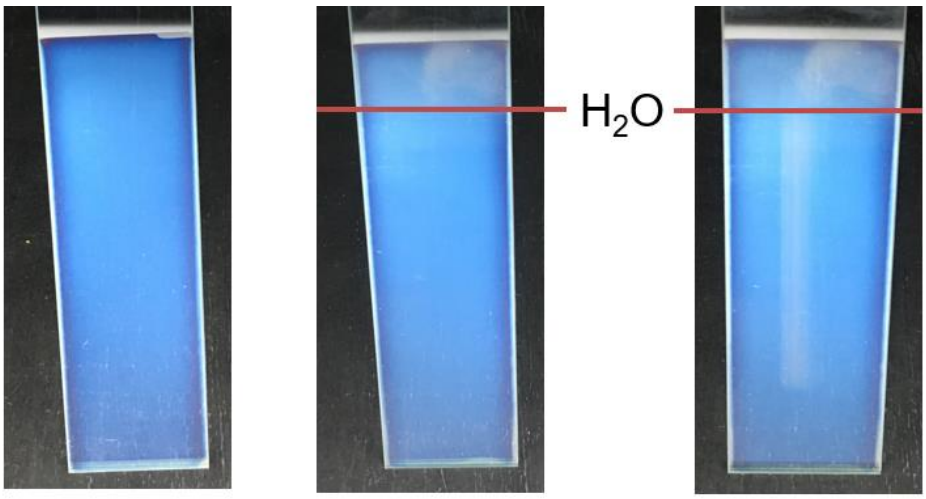

Fig. 5 a) freshly prepared Layer **3**. b) Layer **3** after 14 days of water bath test. c) Layer **3** after 14 days of water bath test and 25 strokes of steel wool.

 ISBN: 978-80-8152-530-8

References

[1] N. Ozer, in, North-Holland, 1996.

[2] B.E. Yoldas, Appl. Opt., **19** (1980) 1425-1429.

[3] C. Ballif, J. Dicker, D. Borchert, T. Hofmann, Solar Energy Materials and Solar Cells, **82** (2004) 331-344.

[4] I.M. Thomas, Appl. Opt., **27** (1988) 3356-3358.

[5] B.E. Yoldas, D.P. Partlow, Thin Solid Films, **129** (1985) 1-14.

[6] M.J. Weber, in, CRC Press, Boca Raton, USA, 2003.

[7] D. Mitolo, A. Garavelli, T. Balić-Žunić, P. Acquafredda, S.P. Jakobsson, The Canadian Mineralogist, **51** (2013) 377.

[8] M. Weil, F. Werner, Monatshefte für Chemie / Chemical Monthly, **132** (2001) 769-777.

[9] M. Weil, F. Werner, F. Kubel, Monatshefte für Chemie / Chemical Monthly, **133** (2002) 267-275.

[10] S. Rüdiger, E. Kemnitz, Dalton Transactions, (2008) 1117-1127.

[11] H. Krüger, E. Kemnitz, A. Hertwig, U. Beck, Thin Solid Films, **516** (2008) 4175-4177.

[12] M. Body, C. Legein, G. Silly, J.Y. Buzaré, Journal of Non-Crystalline Solids, **353** (2007) 2231-2236.

[13] T.J. Kiczenski, J.F. Stebbins, Journal of Non-Crystalline Solids, **306** (2002) 160-168.

[14] C. Martineau, C. Legein, J.-Y. Buzaré, F. Fayon, Physical Chemistry Chemical Physics, **11** (2009) 950-957.

[15] M. Weil, E. Zobetz, F. Werner, F. Kubel, Solid State Sciences, **3** (2001) 441-453.

[16] B. Bureau, G. Silly, J.Y. Buzaré, J. Emery, Chemical Physics, **249** (1999) 89-104.

[17] M. Gerken, J.A. Boatz, A. Kornath, R. Haiges, S. Schneider, T. Schroer, K.O. Christe, Journal of Fluorine Chemistry, **116** (2002) 49-58.

[18] T. Krahl, D. Broßke, K. Scheurell, B. Lintner, E. Kemnitz, J Mater Chem C, **4** (2016) 1454-1466.

 ISBN: 978-80-8152-530-8

Structural Peculiarities of Silver nanoparticles containing Barium Borate Glass and Effects of Gamma Irradiation

A.M. Abdelghany[a*], H.A. ElBatal[b]

[a]*Spectroscopy Department, National Research Center, 33 ElBehouth St., Dokki, 12311, Cairo, Egypt.*
[b]*Glass Research Department, National Research Center, 33 ElBehouth St., Dokki, Dokki, 12311, Cairo, Egypt.*

Combined UV/Vis optical absorption and FT infrared spectral measurements were carried out for synthesized barium borate glasses of the nominal composition (55%B_2O_3. 45% BaO) and glasses of the similar composition containing additional 0.3, 0.6, 1.0, 1.5% AgBr before and after subjecting for specific gamma ray dose (8Mrad). The optical spectrum of the undoped barium borate reveals two strong charge transfer UV absorption bands which are attributed to generate from unavoidable trace iron (Fe^{3+} ions) impurities which are contaminated within the chemicals used for the preparation of this glass. The silver-doped glasses show an additional visible band with its position varying with the form in which silver ions are introduced. Gamma irradiation produces variable changes in the optical spectra between the undoped and Ag-doped glasses. The differences may be correlated with the assumption of shielding of heavy Ba^{2+} ions with higher percent and the possible contribution of silver ions.

UV/Vis optical absorption spectra shows the presence of surface plasmon resonance band (SPR) with variable intensity at about 520 nm and supported by transmission electron micrscopic image (TEM). FT infrared absorption spectra of the undoped and silver-doped glasses reveal extended and characteristic vibrational bands due to the sharing of modes due to triangular and tetrahedral borate groups. Scanning electron microscopic studies show few small microcrystals of silver scattered in the landscape of the micrograph. The origin of the formation of such microcrystals is assumed to be due to the reduction of silver ions by traces of Fe^{2+} ions present as impurities and to the contribution of high temperature at melting.

Keywords:

Barium borate glass; Silver ions; FTIR; UV-Vis. spectra; Gamma irradiation; SEM.

Acknowledgements

We thank Prof. Dr. F.M. Ezz El-Din (national center for radiation technology) for assistance with gamma ray irradiation and for his critical comments that greatly improved the manuscript.

References

[1] H.A. El Batal, F.H. ElBatal FH, A.M. Abdelghany, The Open Spectroscopy Journal, 8(2014)1-8.
[2] S. Ibrahim, F.H. ElBatal, A.M. Abdelghany, Journal of Non-crystalline Solids 453(2016)16-22.
[3] A. Okasha, S.Y. Marzouk, A.H. Hammad, A.M. Abdelghany, Optik - International Journal for Light and Electron Optics, 142(2017)125–133.

 ISBN: 978-80-8152-530-8

Novel reactor design for removal of heavy metals from industrial wastewater by biomass of Cu and Co-doped alginate-coated chitosan nanoparticles: Application of RSM for process optimization

A. Esmaeili* and N. Khoshnevisan

Department of Chemical Engineering, North Tehran Branch, Islamic Azad University, PO Box 19585/936, Tehran, Iran

**akbaresmaeili@yahoo.com*

In this study, the efficiency of alginate-coated chitosan nanoparticles (Alg-CS-NPs) for removal of heavy metals from industrial effluents was investigated. A reactor containing biomass was constructed using response surface methodology (RSM) for process optimization. Reactor tests were carried out with both synthetic and industrial effluents containing nickel. The optimum conditions to achieve maximum removal efficiency (RE) rates for both synthetic and industrial effluents were specified for contact time (0–120 min), pH level (1–9), biomass dose (0.1–0.9 gr), and initial metal ion concentration (10–90 mg/L). It was determined that 94.48% of the nickel could be removed at pH = 3, 70 mg/L initial nickel concentration, a dose of 0.3 gr biomass, and 30 minutes contact time. The kinetic data fit well to a pseudo second-order model and the equilibrium data of the metal ions could be described well with Freundlich isotherm models.

Keywords: Chitosan nanoparticles; Alginate; Cu and Co-doped; Reactor design; Heavy metals

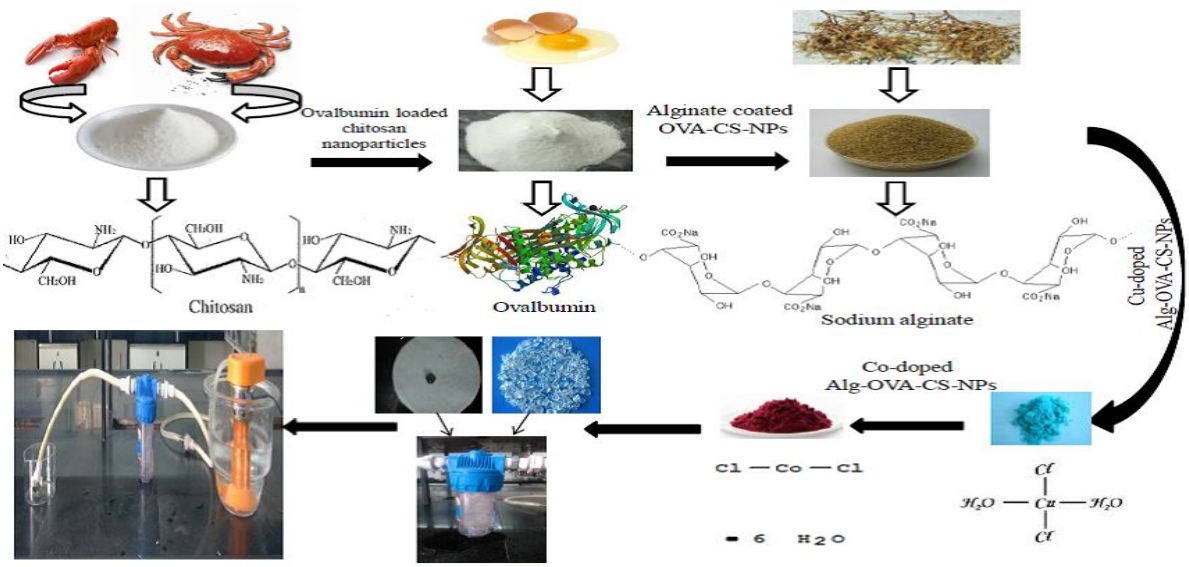

 ISBN: 978-80-8152-530-8

Short characteristic and applications of chosen natural nanomaterials

M.W. Malko[a]*, A. Wróblewska [a], P. Miądlicki [a]

[a] *West Pomeranian University of Technology Szczecin, Department of Chemical Engineering and Technology, Institute of Organic Chemical Technology, Pulaskiego 10,70-322 Szczecin*

**mariuszmalko@gmail.com, agnieszka.wroblewska@zut.edu.pl*

Clay belongs to a wider group of minerals, however, in chemistry, all clay minerals may simply be described as hydrous silicates. In terms of their natural locations, clay minerals can be divided into two classes: residual clays and transported clays (or sedimentary clays). Residual clays are produced from the surface weathering of rock or shale (a dark fine-grained sedimentary rock composed of layers of compressed clay, silt, or mud) through various methods, and they are generally found in the place of origin. Residual clays could be produced by the chemical decomposition of rocks, i.e., granite containing silica and alumina; by the solution of rocks, i.e., limestone; and by the disintegration and solution of shale. The transported clay, the second type, is removed from the original deposit through erosion and deposited to a distant place.

A common characteristic of clay minerals is their finegrained natural structure with sheetlike geometry. The sheet-structured hydrous silicates are generally referred to as phyllosilicates. Individual natural clay particles are smaller than 0.004 mm in diameter - they can ranged from 0.002 to 0.001 mm in diameter for quartz, mica, feldspar, iron, and aluminum oxides. Colloidal clay particles are finer (<0.001 mm in diameter) and are found in layered silicates.

Clay minerals may be divided into four major groups, mainly in terms of the variation in the layered structure. These include the kaolinite group, the montmorillonite/smectite group, the illite group, and the chlorite group. The kaolinite group has three members, including kaolinite, dickite, and nacrite, each with a formula of $Al_2Si_2O_5(OH)_4$. The same formula indicates that the members of this group are polymorphs – it means that they have the same formula but differing structures. Each member is composed of silicate sheets (Si_2O_5) bonded to aluminum oxide/hydroxide layers ($Al_2(OH)_4$); the two types of layers are tightly bonded. These clays are used as fillers in ceramics, paint, rubber, paper, and plastics. In organic catalysis kaolinite was used as catalyst in transformations of (-)-myrtenal epoxide to new optical active compounds [1].

Montmorillonite, talc, pyrophyllite, saponite, and nontronite are a few members of the larger smectite clay group. The general formula for the chemical structure of this group is as follows: $(Ca,Na,H)(Al,Mg,Fe,Zn)_2(Si,Al)_4O_{10}(OH)_2*H_2O$. The important difference among the members of this group is seen in the chemical characteristics. The layer structure of these materials contains silicate layers oraz an aluminum oxide/hydroxide layer $Al_2(OH)_4$). These materials are used as fillers in paints, rubbers, as plasticizer in molding sands, in drilling muds, and as electrical, heat, and acid-resistant porcelain. One of the members, talc, is used in powders for face. On the other hand, montmorillonite clays were used as good catalysts in isomerisation of α-pinene [2] or in oxidation pinene [3] and limonene [4], and in production of camphene and limonene from pinene over acid di- and trioctahedral smectite clays [5].

The illite group is represented by the mineral, illite, the only common clay type. The general formula of this material is as follows: $(K,H)Al_2(Si,Al)_4O_{10}(OH)_2*H_2O$. It is an importantrock-forming mineral and a main component of shales. The structure of this group is similar to the montmorillonite. Mineral illite is used as filler in some drilling mud, and it is a common constituent in shales. The chlorite group is relatively large and not necessarily considered as clays; therefore, it is placed as a separate group in phyllosillicate. Amesite, chamosite and daphnite are some members of this group; however, they are different in formulas and structures. These clays do not possess a general formula.

Bentonite is an important source of montmorillonite in nature. It is a rock formed from highly colloidal and plastic clays mainly composed of montmorillonite. Bentonite particles are indistinguishable from kaolin clay minerals viewed under scanning electron microscope (SEM); however, the main difference indicated is thickness. Sodium or potassium salts of bentonite exfoliate into thin plates that could be 1 nm in thickness, theoretically. In addition to montmonillonite, bentonite may contain crystalline quartz, cristobalite, and feldspar. In general, the clay minerals based on bentonite may exhibit the properties of thixotropic-gel formation with water, high water absorption, and high cation-exchange capacity. These properties could be varied in clay minerals depending upon the nature of interstitial water, and exchangeable cations in the interlayer space.

Montmorillonite was discovered in 1847 in Montmorillon in the Vienne prefecture of France. Montmorillonite used for medicinal purposes may have occurred in over 200 cultures, including the ancient Egyptians, pre-Aztec Amargosians, natives of Mexico, South Americans, and North Americans. An important

 ISBN: 978-80-8152-530-8

behavior of clay mineral is the ionic substitution in the sheet structure, resulting in useful modifications. Ions, i.e., Fe^{3+} and Al^{3+}, are small enough to enter the tetrahedral coordination with oxygen and substitute Si^{4+}. Similarly, cations, i.e., Mg^{2+}, Fe^{2+}, Fe^{3+}, Li^{+}, Ni^{2+}, and Cu^{2+} can be substituted for Al^{3+} in the octahedral sheet. Large sized cations, i.e., K^{+}, Na^{+}, and Cs^{+}, can be located between the layers and, therefore, are referred to as interlayer cations. Anionic substitution is also possible, and the hydroxyl ion (OH^{-}) can be substituted by F^{-} ion. Chemical composition, ionic substitution, layer structure, and particle size of natural clay minerals have important roles in creating a variety of minerals with specific characteristics. However, sheet structure was used to classify the clay minerals, and chemical composition was used for nomenclature.

References

[1] I. V. Il'ina, K. P. Volcho, D. V. Korchagina, V. A. Barkhash, and N. F. Salakhutdinov, Russ.J. Org. Chem., 46 (2007), 56-59.
[2] J Mukesh Kr. Yadav, Chintansinh D. Chudasama, Raksh V. Jasra, J. Mol. Catal. A.Chem, 216 (2004) 51–59.
[3] E. P. Romanenko, E. A. Taraban, A. V. Tkacheva, 55, Russ. Chem. Bull (2006) 993—998.
[4] C. Fernandes, C. Catrinescu, P. Castilho, P.A. Russo, M.R. Carrott, C. Breen, Appl. Catal., A , 318 (2007) 108–120.
[5] C.Volzone, O. Masini, N. A. Comelli,L. M.Grzona, E.N. Ponzi, M. I. Ponz,i Appl. Catal., A, 214 (2001) 213–218

 ISBN: 978-80-8152-530-8

Studies on the properties of montmorillonite used as the catalyst in the oxidation of R-(+)-limonene with hydrogen peroxide

M.W. Malko[a]*, A. Wróblewska [a], P. Miądlicki [a]

[a] *West Pomeranian University of Technology in Szczecin, Department of Chemical Engineering and Technology, Institute of Organic Chemical Technology, Pulaskiego 10,70-322 Szczecin*

**mariuszmalko@gmail.com, agnieszka.wroblewska@zut.edu.pl*

Montmorillonite is a material that rises in the composition of rocks called bentonites, also found in Poland. It was found in the mid-19th century in Montmorillon, France. It is a mineral of volcanic origin with density ranging between 1.9-2.7 g / cm³ [1 - 3]. The general chemical formula of montmorillonite is written below [1-2]:

$$M_x\ (Al_4\text{-}xMg_x)\ Si_8O_{2O}\ (OH)_4$$

where: M - metal cation; x - amounts 0.5 ÷ 1.3.

Montmorillonite is a layered aluminosilicate with a lamellar structure (lamellar is composed of three layers: two outer tetrahedral, comprising between them octahedral layer). The thickness of the montmorillonite plate is 0.96 nm, the remaining dimensions are in the range of 200 to 1000 nm, while the number of packages per unit crystallographic cell varies from several to several thousand. It depends on external factors, among which we distinguish the type of layered mineral, the origin of its creation, the geological environment in which it was formed, and the mechanical forces acting on its particles. Between the layers are located cations metal, mainly sodium (Na^+) or calcium (Ca^{2+}) and water molecules. Because of interstitial cations that have "loose" character, sodium montmorillonite (Na MMT) and calcium montmorillonite (Ca MMT) are distinguished. Montmorillonite is a highly hydrophilic mineral, used as a nanopillifier (polymer matrix product in approx. 5 wt%). A small amount of this aluminosilicate introduced into the polymerization improves gas permeability, thermal resistance and flammability.

Due to the availability and low price, montmorillonite has been widely used in food, ceramic, rubber, paper, pharmaceutical, chemical and metallurgical industries. It is used as a thickener in emulsions, for the clarification of beverages, to produce mineral fertilizers, drilling rigs, and for the reclamation of areas contaminated with heavy metals. Because of its high water and nutrient storage capacity, it also plays a very important role in agriculture. Montmorillonites are used in various industries as catalysts or catalyst carriers. Raw bentonites can also serve as adsorbents, such as decolourizers, filtering systems, ion exchangers, or they can be used as drilling fluids. In the form of a granular filter, montmorillonite is used for the purification and decolorization of drinking water, mineral and vegetable oils, as well as wines and other beverages. In addition, bentonites are used as geomembranes, serving as seals under tanks that store substances harmful to the environment [3-7].

In our studies montmorillonite was used.

Montmorillonite clays were generally the most popular catalyst for pinenes isomerization process [8], although kaolinitic clay was also successfully used for this purpose. Preliminary acid treatment of clays had a considerable effect on the conversion of pinenes and the product ratio depends on the amount of acid used and on its concentration and the temperature of acid treatment. The data about the dependence of the catalytic activity of acidic clays and isomerization selectivity on the nature of acid centres, obtained in these works indicated that the transformations of pinenes in to camphene occurred predominantly on the Bronsted acid centres. This material was previously prepared by bentonite purification by the method of sedimentation. The catalyst in the form of montmorillonite was characterized by the following instrumental methods: XRD, SEM, BET and EDX. Catalytic tests were performed with limonene.

References

[1] W. Królikowski, Z. Rosłaniec, Composites, 4 (2004) 3-15.

[2] J. Gołębiewski, Przem. Chem., 83 (2004) 15-20.

[3] M. Olejnik, Techniczne wyroby włókiennicze (2008) 67-74.

[4] M. Kacperski, Polim., 47(2002) 801-807.

[5] M. Malesa, Elastomers, 3 (2004) 12-17.

[6] M. Kacperski, Composites, 3 (2003), 225-231

[7] A. Kunert, M Zaborski, Przem. Chem., 1 (2010) 1510-1517.

[8] N. Comelli, Maria C. Avila, C. Volzone, M. Ponzi, Cent. Eur. J. Chem., 11 (2013) 689-697.

 ISBN: 978-80-8152-530-8

Annealing duration effect on optical, structural and morphological properties of ultrasonic sprayed Cu_2ZnSnS_4 films

S. Kermadi*, S. Sali, L. Zougar, M. Boumaour

[a] *Laboratoire des Modules Photovoltaïques, Centre de Recherche en Technologie des Semi-conducteurs pour l'Energétique, 2 bd. Frantz Fanon, B.P. 140 7 Merveilles, Algers*

**kermadisalim@yahoo.fr*

General participation rules

Ultrasonic sprayed Cu_2ZnSnS_4 (CZTS) were successfully deposited on microscopic glass substrates from an aqueous solution of $CuCl_2$ $2H_2O$, $ZnCl_2$, $SnCl_2$ and thiourea. The deposited films at substrate temperature of 310 °C were heat treated up to 550 °C under N_2 gas flows with sulfurization process (under sulfur vapor flow). The effect of annealing time from 30 to 90 min on optical, structural and morphological properties was investigated using a combination of Raman spectroscopy, scanning electronic microscopy and Ultraviolet visible near infrared absorbance spectroscopy. Raman studies confirm the formation of Kesterite type CZTS with CuS as a secondary component. All the deposited films show an optical absorption coefficient higher than 10^4 cm^{-1} and an optical band gap between 1.55 and 1.58 eV. By increasing sintering duration, the optical band gap was slightly influenced while the grain size increased strongly up to 2 µm.

Keywords: CZTS, thin film solar cells, crystal growth, structural properties

References

[1] S. Schorr, The crystal structure of kesterite type compounds: a neutron and Xray diffraction study, Sol. Energy Mater. Sol. Cells 95 (2011) 1482-1488

[2] P.A. Fernandes, P.M.P. Salom e, A.F. da Cunha, A study of ternary Cu2SnS3 and Cu3SnS4 thin films prepared by sulfurizing stacked metal precursors, J. Phys.D. Appl. Phys. 43 (2010) 215403.

 ISBN: 978-80-8152-530-8

Electrochemical detection of glucose on gold microelectrodes

Jana Hovancová[a*], Ivana Šišoláková[a], Renáta Oriňaková[a], Andrej Oriňak[a]

[a]*University of*

Pavol Jozef Šafárik, Faculty of Science, Institute of Chemistry, Department of Physical Chemistry, Moyzesova 11, Košice 040 01

**jana.hovancova@student.upjs.sk*

Gold is consider to be an eligible candidate for development of nonenzymatic glucose sensors, due to its excellent electrocatalytical properties [1]. Moreover, gold nanoparticles show enhanced current response, biocompatibility and ability to detect glucose in neutral and alkaline solution in comparison with another materials [2]. Gold microelectrodes (with diameter 1 mm) were used because of its application as nonenzymatic sensors. Miniaturisation of system could be achieved due to its small size. Mechanism of electrochemical oxidation of glucose on gold surface was studied with an effort to create optimal condition. The results were compared with literature. Effect of pH change was studied too and optimal condition was propounded. The electrode surface was modified by gold nanoparticles to achieve more active sites and better sensor properties. Modified gold microelectrodes were able to detect glucose in linear range 0.5 – 40 mM. It meets commercialised glucose sensors requirements, where the linear range is 1 – 30 mM.

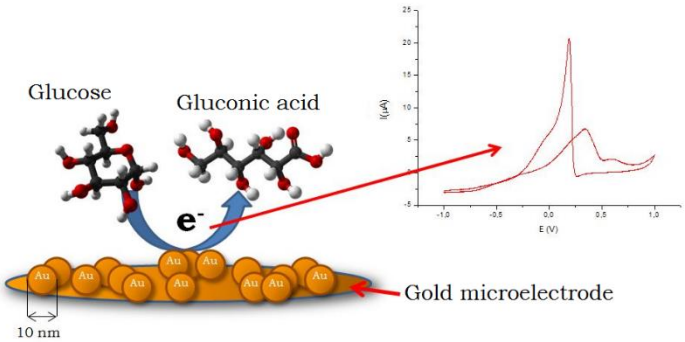

Fig. 1 Schematic illustration of gold electrode modified with gold nanoparticles.

Acknowledgements

This work was supported by the Project APVV-16-0029 of the Slovak Research and Development Agency and Project VEGA 1/0074/17 of the Slovak Scientific Grant Agency.

References

[1] K.E. Toghill, R.G. Compton, J. Electrochem. Sci. **5** (2010) 1246–1301.
[2] S. Karra, M. Wooten, W. Griffith, W. Gorski, Electrochim. Acta. **218** (2016) 8–14.

 ISBN: 978-80-8152-530-8

Low cost preparation of slow-release fertilizer of natural clinoptilolite by ammonia enrichment

J. Macko[a*], A. Oriňak[a] , F. Mihok[a]

[a] *Department of Physical chemistry, P. J. Šafárik University in Košice, Moyzesova 11, 041 54 Košice, Slovakia*

**jan.macko@upjs.sk*

Clinoptilolite has been found very effective in ammonia adsorption from its solution by means of its excellent ion exchange capacity since the 1970s of last century [1]. Zeolites possess a net negative structural charge resulting from isomorphic substitution of cations in the crystal lattice. Minerals from the zeolite group differ from one another in the content of Si and Al. Clinoptilolite is the most common and abundant high-siliceous zeolite. The ratio of Si/Al in clinoptilolite is 5.7. Clinoptilolite belongs to the heulandite group. It has a two-dimensional channel system that allows the mineral to act as a molecular sieve. Moreover, this kind of zeolite shows high sorption and ion-exchange capacity, ion exchange selectivity, catalytic activity and structural temperature stability up to 700-750°C [2]. Zeolite is a well-known material for its abilities to preferentially remove ammonium ions from surrounding solution. Unlike systematic ion exchange resins, zeolite is known to possess a better selective ion-exchange capability for ammonium ion than Ca^{2+} and Mg^{2+}. Natural zeolites are low cost ion-exchangers and after ammonia enrichment can be used as slow-release fertilizers with possibility of slow ammonia release [3]. The pretreatment of natural zeolites by acids, bases, surfactants, etc., is an important method to improve their ion-exchange capacity. Practically, the result of any pretreatment operation is the increase of the content in a single cation, what is called homoionic form. Therefore, prior to any ion-exchange application, certain ions from the structure of the material are removed by pretreatment and more easily removable ones are located [4]. Here we present an easy and low cost way of slow-release fertilizer preparation using natural clinoptilolite, which is common in nature. Mentioned kind of slow-release fertilizer has premised possibility of nutrient slow release. As the source of ammonia can be used wastewater and sewages. Where decrease of ammonia concentration is necessary. The presence of ammonium ion in water causes some problems, such as reducing the concentration of dissolved oxygen in water, accelerating the growth of algae and finally coating the surface of water resources which leads to decrease of water qualities [5].

Acknowledgements

This work was supported by VEGA 1/0074/17, APVV-16-0029. Authors also wish to thank Duslo, a.s. for financial support.

References

[1] M. M. Jafarpour, A. R. Fooland, M. K. Mansouri, Z. Nikbakhsh, H. Saeedizade, International Journal of Environmental, Chemical, Ecological, Geological and Geophysical Engineering. 4 (2010) 481-487.

[2] M. Zabochnicka-Swiatek, K. Malinska, Global NEST Journal. 12 (2010) 256-261.

[3] P. Sopa, P. Pungpo, 37th Congresson Science and Technology of Thailand. (2011) 1-6.

[4] I. Tosun, Int. J. Environ. Res. Public Health. 9 (2012) 970-984.

[5] Z. B. Mokhtari-Hosseini, E. Kazemian, R. Tayebee, T. Shenavaei-Zare, Hem. Ind. 70 (2016) 21-29.

 ISBN: 978-80-8152-530-8

Role of Dissociation in Evaluation Quality of Fertilizers

F. Mihok[a], A. Oriňak[a*] , O. Petruš[a], J.Macko[a]

[a] *Department of Physical chemistry, P. J. Šafárik University in Košice, Moyzesova 11, 041 54 Košice, Slovakia*

**andrej.orinak@upjs.sk*

Aggressive urbanization, which started last century, caused even further decrease to area available to agriculture. Aforementioned situation led to extensive use of fertilizers to keep yield up with the ever-increasing demand for produce by ever increasing population, even as the total area decreased. Agriculture started looking for innovative solutions how to keep up with ever increasing demand. On the other hand, Fertilizers with controlled release became the most appealing option. This new kind of fertilizer is still based on Nitrogen, but in its case Nitrogen part is stored within membrane. These membranes are made to withstand huge changes in temperatures in just matter of hours which usually happen in buildings where they are stored during summer. Temperature resistance is just additional feature, the key role of the membrane is to adjust the release of Nitrogen to the soil according to the plant which is currently being grown there. Additionally, usage of controlled release fertilizer can reduce the amount of cycles in which fertilizer is being added to the soil reducing the total fuel costs as well. Membrane is made specifically from degradable materials not to cause further stress for the soil. The most used substance to start dissociation through the membrane is water. Water passes into the membrane. Fertilizer then passes out of the membrane dissolved in water. This process slowly causes the membrane to dissolve as well, but at a much slower rate. Properties of fertilizer, especially their membrane, are affected by many factors, but mainly by used materials and production process. Common differences in membranes are their porosity, thickness, resistance to changes in temperature, resistance to acidic or basic soils and more. This work studies how different production and different materials affect the controlled release fertilizer. Dissociation was measured with electrode that was measuring electric resistance of studied solution. Only clean water with 18 $M\Omega.cm^{-1}$ was used to prevent distortions that could be created by presence of different particles in regular tap water. With increase of particles which dissociated from fertilizer electrical resistance rose. The speed of the dissociation was then obtained as linear directive of function of electrical resistance of water at a time. Ways to accurately and effectively measure dissociation of fertilizer were also explored and tested by this work.

Acknowledgements

This work was supported by VEGA 1/0074/17, APVV-16-0029. Authors also wish to thank Duslo, a.s. for financial support.

 ISBN: 978-80-8152-530-8

The 3rd International Conference on Nanomaterials: Fundamentals and Applications
Book of Abstracts

Edited by: Doc. RNDr. Andrea Fedorková, PhD.
RNDr. Ondrej Petruš

Publisher: Pavol Jozef Šafárik University in Košice
Year: 2017
Pages: 122
Author's sheets: 6,5
Edition: first
Available at: https://unibook.upjs.sk
Publication date: October 2017

ISBN 978-80-8152-530-8